ERROR QUANTIFICATION IN CRACK MEASUREMENT OF BUILDING MATERIALS USING TERRESTRIAL LASER SCANNING (TLS)

A THESIS SUBMITTED TO
THE GRADUATE SCHOOL OF NATURAL AND APPLIED SCIENCES
OF
MIDDLE EAST TECHNICAL UNIVERSITY

BY

MERT OYTUN

IN PARTIAL FULFILLMENT OF THE REQUIREMENTS
FOR
THE DEGREE OF MASTER OF SCIENCE
IN
CIVIL ENGINEERING

DECEMBER 2020

Approval of the thesis:

ERROR QUANTIFICATION IN CRACK MEASUREMENT OF BUILDING MATERIALS USING TERRESTRIAL LASER SCANNING (TLS)

submitted by **MERT OYTUN** in partial fulfillment of the requirements for the degree of **Master of Science** i**n Civil Engineering Department, Middle East Technical University** by,

Prof. Dr. Halil Kalıpçılar
Dean, Graduate School of **Natural and Applied Sciences** _____

Prof. Dr. Ahmet Türer
Head of the Department, **Civil Engineering** _____

Assist. Prof. Dr. Güzide Atasoy Özcan
Supervisor, **Civil Engineering, METU** _____

Examining Committee Members:

Prof. Dr. M. Talat Birgönül
Civil Engineering Dept., METU _____

Assist. Prof. Dr. Güzide Atasoy Özcan
Civil Engineering Dept., METU _____

Prof. Dr. Irem Dikmen Toker
Civil Engineering Dept., METU _____

Assist. Prof. Dr. Aslı Akçamete Güngör
Civil Engineering Dept., METU _____

Assist. Prof. Dr. Saman Aminbakhsh
Civil Engineering Dept., Atılım University _____

Date: 30.12.2020

I hereby declare that all information in this document has been obtained and presented in accordance with academic rules and ethical conduct. I also declare that, as required by these rules and conduct, I have fully cited and referenced all material and results that are not original to this work.

Name, Last name : Mert Oytun

Signature :

ABSTRACT

ERROR QUANTIFICATION IN CRACK MEASUREMENT OF BUILDING MATERIALS USING TERRESTRIAL LASER SCANNING (TLS)

Oytun, Mert
Master of Science, Civil Engineering
Supervisor: Assist. Prof. Dr. Güzide Atasoy Özcan

December 2020, 158 pages

Cracks are the most common and crucial indicators giving clues about the as-is condition of structures. Moreover, they have always been a major concern for public safety, as they are pioneers that point to issues in buildings and have been sought to be identified and analyzed. Today, the most common way of deformation analysis highly depends on manual inspection methods, mostly criticized for being highly subjective, time-consuming, and error-prone. Accordingly, perpetual improvement has been observed in the building inspection and damage assessment using different tools and methods until today. Nevertheless, in the last decade, 3D Terrestrial Laser Scanners (TLSs) usage in deformation analysis has gained considerable popularity among other remote sensing tools due to its high accuracy and reliability rates. However, the change in scan data quality based on changes in scanning and material settings has limited the use of TLS and has shown the necessity of research on this subject. The main purpose of this research is to compare data sets of various building materials captured with different scan settings of TLS (scanning distance, resolution, and incidence angle) and to evaluate dimensional measurement accuracy in the

context of crack detection. In this study, the error quantification in the crack measurement of the three most commonly used building materials (reinforced concrete, wood, and masonry brick) using TLS is performed. The proposed framework includes laboratory experiments, data processing, comparative analyses, and derivation of error estimation equations of scan data quality as a function of scanning distance, crack width, and incidence angle for each material type. The findings contributed to the literature both theoretically and practically by (1) empirically addressing the level of combined effects of the scan settings on scan data quality and (2) providing outcomes that would facilitate the optimization of laser scan planning.

Keywords: Crack Measurement, 3D Terrestrial Laser Scanning, Point Cloud, Structural Health Monitoring, Error Quantification

ÖZ

KARASAL LAZER TARAMA (TLS) KULLANARAK YAPI MALZEMELERİNDEKİ ÇATLAKLARIN ÖLÇÜMÜNDE HATA TAYİNİ

Oytun, Mert
Yüksek Lisans, İnşaat Mühendisliği
Tez Yöneticisi: Dr. Öğr. Üyesi Güzide Atasoy Özcan

Aralık 2020, 158 sayfa

Çatlaklar, yapıların güncel durumu hakkında ipuçları veren en yaygın ve en önemli göstergelerdir. Ayrıca, binalardaki sorunlara işaret eden öncüler olduğundan, kamu güvenliği için her zaman büyük bir endişe kaynağı olmuş ve tanımlanıp analiz edilmeye çalışılmışlardır. Günümüzde, deformasyon analizinin en yaygın yolu büyük ölçüde manuel inceleme yöntemlerine bağlıdır ve bu yöntemler çoğunlukla son derece öznel, zaman alıcı ve hataya açık oldukları için eleştirilmektedir. Bu doğrultuda, farklı araç ve yöntemler kullanılarak yapı denetim ve hasar tespitinde bugüne kadar sürekli gelişme gözlemlenmiştir. Bununla birlikte, son on yılda, deformasyon analizinde 3D Karasal Lazer Tarayıcıların (TLS'ler) kullanımı, yüksek doğruluk ve güvenilirlik oranları nedeniyle diğer uzaktan algılama araçları arasında önemli bir popülerlik kazanmıştır. Ancak, tarama ve malzeme ayarlarındaki değişikliklere bağlı olarak tarama verisi kalitesindeki değişiklik, TLS kullanımını sınırlandırmış ve bu konuda araştırma yapılması gerektiğini göstermiştir. Bu araştırmanın temel amacı, farklı TLS tarama ayarları (tarama mesafesi, çözünürlük ve geliş açısı) ile yakalanan çeşitli yapı malzemelerinin veri setlerini karşılaştırmak ve çatlak tespiti bağlamında boyutsal ölçüm doğruluğunu değerlendirmektir. Bu

çalışmada TLS kullanılarak en çok kullanılan üç yapı malzemesindeki (betonarme, ahşap ve tuğla) çatlakların ölçümünde hata tayini yapılmıştır. Önerilen çalışma, laboratuvar deneylerini, veri işlemeyi, karşılaştırmalı analizleri ve her malzeme türü için tarama mesafesi, çatlak genişliği ve geliş açısının bir fonksiyonu olarak tarama verisi kalitesinin hata tahmini denklemlerinin türetilmesini içerir. Bulgular, (1) tarama ayarlarının tarama veri kalitesi üzerindeki müşterek etkilerinin düzeyini deneysel olarak ele alarak ve (2) lazer tarama planlamasının optimizasyonunu kolaylaştıracak sonuçlar sağlayarak literatüre hem teorik hem de pratik olarak katkıda bulunmuştur.

Anahtar Kelimeler: Çatlak Ölçümü, 3B Karasal Lazer Tarama, Nokta Bulutu, Yapı Sağlığı İzleme, Hata Ölçümü

Dedicated to my beloved family and nephew, Ayaz Gümüş…

ACKNOWLEDGMENTS

Before anything else, I am proud to be part of an inspiring environment, the Middle East Technical University. I have always felt the privilege of being a part of this institution. For this reason, I would like to express my sincere appreciation to all the administrative staff of the university and to Graduate School of Natural and Applied Sciences. I would also like to thank the Civil Engineering Department's academic and managerial staff, which has always been of great importance in my life, for their assistance throughout my studies.

First and foremost, I would like to express my deepest gratitude to my precious supervisor Dr. Güzide Atasoy Özcan, for her invaluable contributions such as guidance, advice, constructive criticism, encouragement, and insights that she has provided to me at every point of my graduate studies. Regardless of the time of day, she endeavored to be always with me with sincere enthusiasm, patience, and determination.

Secondly, I would like to express my thankfulness to the thesis defense jury's esteemed members for reviewing my thesis, providing feedback, and dedicating their valuable time on the day of the presentation.

Besides, I am thankful to the Scientific and Technological Research Council of Turkey since the institute financially supports this study under the coverage of the TUBİTAK-BİDEB National Excellence Scholarship Programme for MSc Students (2210-A).

Furthermore, I appreciate our great leader Mustafa Kemal Atatürk, whom I admire for his ceaseless efforts, strong determination, and undeniable foresight.

Finally, I would like to thank my dear family members Ayten Oytun, Meriç Oytun Gümüş, and Atila Yavuz for their lifelong support and their efforts to motivate me under all circumstances.

TABLE OF CONTENTS

LIST OF TABLES

TABLES

LIST OF FIGURES

FIGURES

LIST OF ABBREVIATIONS

ABBREVIATIONS

AEC – Architecture, Engineering and Construction

AEP – Average Error Percentage

ANOVA – Analysis of Variance

ASTM – American Society for Testing and Materials

BIM – Building Information Modeling

CAD – Computer-Aided Design

DI – Digital Imaging

FEMA – Federal Emergency Management Agency

FISP – Façade Inspection Safety Program

FOV – Field of View

LIDAR – Light Detection and Ranging

METU – Middle East Technical University

MLR – Multiple Linear Regression

NIST – National Institute of Standards and Technology

PS – Phase Shift

RC – Reinforced Concrete

RFID – Radio-frequency identification

TLS – Terrestrial Laser Scanner

TOF – Time of Flight

UAV – Unmanned Aerial Vehicle

UAG – Unmanned Ground Vehicle

USDOC – U.S. Department of Commerce

VI – Visual Inspections

CHAPTER 1

INTRODUCTION

1.1 Introduction

Earthquakes are among the most destructive and costly natural hazards humanity has ever faced (U.S. Geological Survey, 2006). Unfortunately, their impacts on the built environment have not been fully resolved yet. They affect all products of the Architecture, Engineering and Construction (AEC) industry at different levels. In other words, depending on their magnitude, they can cause slight damages to structural components (e.g., cracking, spalling, and fragmentation) or cause more major damages that result in more severe consequences (e.g., the sudden collapse of structures, hence fatalities). Consideringly, researchers conducted studies on the effects of earthquakes on structures. They concluded that the severity of earthquakes in buildings depends on the building-earthquake source distance and the soil layer's characteristics beneath buildings. Moreover, they claim that fatalities and material damages occur due to incorrect or incomplete engineering practices, design errors, the use of low-quality materials, and poor-quality crafts (Yon et al., 2017).

The earthquake statistics tables announced by the United States Geology Survey (USGS) clearly show that millions of people have died, and billions of dollars in financial losses have happened due to severe earthquakes in history until today. Furthermore, according to as study by the Federal Emergency Management Agency (FEMA) (2000), earthquake losses in the U.S. are up to $4.4 billion a year. Therefore, there have been many developments in the construction industry, especially in application techniques and building materials. However, the severity of the damages in the built environment due to recent earthquakes reveals that these developments are still inadequate. Besides, the high rates of earthquake zones in the world disclose the danger that humanity faces in this context (Benz et al., 2010).

Among all the engineering structures, buildings have become one of the essential built structures in human history. Since buildings are people's living spaces, they need to be robust, durable, and functional under varying loads and environmental effects throughout their lifespans. Hence, they must be correctly designed, built, and maintained. Among these three phases, maintenance becomes more vital than others considering a lack of standardization in this phase.

Damages in buildings are the most significant signs in evaluating their existing health condition. For this reason, especially the maintenance of buildings after earthquakes in line with the changes in dynamic environments becomes highly crucial. Structural health should be monitored first to determine the need for maintenance because structural health monitoring findings can be used directly to decide whether maintenance is required or not and to develop maintenance strategies.

The most common way to provide maintenance to buildings is the structural damage assessment. To understand their environment better, people have wondered remote sensing technologies dating back to the invention of photography (G. K. Moore, 1979). People have invented tools and gadgets and carried out a wide variety of experiments in their journeys to satisfy their curiosity. As a result, they have achieved substantial progress in this field, especially during the Second World War, due to the advances in radar, sonar, and thermal infrared technologies. Today, remote sensing and 3D imaging technologies continue to evolve faster than ever before, and they are started to be prevalently used for structural damage assessment.

Unlike these emerging technologies, the current prevailing method used in structural damage assessment, namely manual inspection, highly relies on the experts' engineering judgments (Hirosawa et al., 1994; Kempton et al., 2001). In these methods, experienced specialists are expected to inspect the damaged structures by physically examining the damage indicators (e.g., cracking, spalling, fragmentation, crushing, tilting), taking corresponding measurements, and analyzing the health condition of structural components (Menches et al., 2008). Consequently, they

decide on the damage modes, damage severities, and whether structures can further be serviceable or not.

The most challenging part of these assessments is that they are highly subjective, time-consuming, and error-prone (Yamaguchi & Hashimoto, 2010). Hence, researchers have concentrated on more automated remote sensing technologies to identify and assess the damages in structures in more secure, fast, and accurate ways (Abdel-Qader et al., 2003; Gavilán et al., 2011; Salvatore Cafiso & Battiato, 2006; Z. Zhu et al., 2011). Consequently, laser technologies, one of the most versatile 3D imaging technologies, have attracted great attention compared to others recently. These technologies owe their popularity mainly to the ability to provide almost precise results to their users. There is a wide variety of tools, which use this technology for different purposes, such as 3D x-ray imaging, 3D Structured Light, 3D laser imaging, and computed tomography. Among all the tools and methods, Terrestrial Laser Scanner (TLS) has been used in practice and studied in literature based on its benefits, such as providing remarkably high qualified point cloud data among laser technologies (Liang et al., 2018; P. Wang et al., 2019) and being one of the oldest applications of 3D imaging technologies. TLS works with one of the two different principles in distance measurements: (1) the Time of Flight (TOF), which uses the time of flight of a laser beam to calculate the distances, or (2) Phase-Shift (PS) TLS, which measures the phase shift of the reflected laser energy to calculate the distances.

The capabilities of TLS have not been fully discovered yet since devices' measurement sensitivity varies according to many different parameters such as scan settings and environmental conditions. Moreover, since it takes a considerable amount of time to test each parameter and evaluate the results, a standard for the data acquisition process with these devices has not been established yet. To develop a research area and fill these gaps, The National Institute of Standards and Technology (NIST) organized several workshops. Eventually, the American Society for Testing and Materials (ASTM) E57 3D imaging systems committee of standards and procedures was established in 2006. Soon after, the characteristics of laser scanners

began to be explored in detail. Accordingly, researchers have started to explore these parameters' effects on scan data quality in previous decades. They have achieved some clarifications on some parameters' effects; however, they have not clearly explained how different building material types affect the scan data quality yet. Still, various studies mention that the type of target material considerably affects the scan data quality, and this issue should be further studied (Boehler & Marbs, 2003; Clark & Robson, 2004; Thomas Voegtle et al., 2008).

Consideringly, the materials from which the buildings are built have become more crucial than ever before. Among all building materials, concrete is one of the most common building materials due to its durability, economy, safety, formability, and sustainability. Furthermore, its usage exceeds individual water consumption rates with three tonnes per year per capita (Gagg, 2014). Despite the excessive use of concrete, the latest building census conducted in 2000 by the State Institute of Statistics in Turkey reveals that only 48% of the buildings in the country are composed of Reinforced Concrete (RC) framed skeletons while 51% of buildings are composed of masonry or stone stacks (TCBDİE, 2001). Today, although there is a decrease in masonry buildings' construction rate, they are still in use, especially in rural areas (Donduren & Kollu, 2018). Apart from these, wood is also preferred as a building material. Especially in the U.S., wooden structures are thought to be even stronger than reinforced concrete buildings, and therefore, they are used at high rates in building constructions (Ramage et al., 2017).

Hence, researchers have focused on identifying structural damage types of RC, masonry, and wooden structures after earthquakes in a more automated and unconventional way. For this reason, they used TLS extensively in their studies and received promising results on the effects of different parameters on scan data quality (Alkan & Karsidag, 2012; Boehler & Marbs, 2003; D D Lichti et al., 2000). They have mainly tried to comprehend the relationship between the damage levels and the structural health status. However, none of them focuses explicitly on exploring the effects of different building materials on laser scan data quality from the crack identification point of view.

1.2 Problem Statement

As mentioned in the previous part, there are several disadvantages of current methods used for structural damage assessments. Furthermore, with the rapid development of technology, these methods are considered outdated since they are carried out manually, are time-consuming, and have high subjectivity levels (Hirosawa et al., 1994; Kempton et al., 2001). Hence, several studies are underway to transform into more automated and modernized smart systems to develop more reliable structural health monitoring methods and tools.

Today, Terrestrial Laser Scanner (TLS) utilization is prevalent due to their high-efficiency rates in data collection (Olsen et al., 2010). TLS has been used for a wide range of engineering applications, assuming that laser scanners' technical information given in user manuals is accurate (Bernardini et al., 2002; M Tsakiri et al., 2006). Many scholars believe that TLS is superior to other 3D imaging systems because TLS has several benefits on data acquisition for various study fields, including damage assessments and structural health monitoring (Liang et al., 2018; Wilkinson et al., 2016). Some of these benefits are as follows:

- Effectiveness in the determination of several damage indicators such as cracks, concrete-plaster spalling, and reinforce deflection-buckling
- Robustness in creating 3D models of large surfaces by processing data acquired with TLS (cloud-to-cloud registration)
- Flexibility in operations such as comparing as-is conditions with the as-designed conditions or generating building information models from the data obtained by TLS
- Independency on the illuminance conditions leading to the ability of long-distance data collection

On the other hand, some researchers are in doubt with the technical information given in user manuals of devices due to the following reasons:

- Variation of the measurement results depending on how carefully the calibration and measurement processes are performed
- Insufficient number of tests performed in the process of producing technical data and related user catalogs
- Variations in the scan data quality depend on different parameters, such as environmental conditions, scan settings, and targets' intrinsic properties.

Therefore, a few studies carried out experiments with different parameters to test the accuracy rates of the scan data (Alkan & Karsidag, 2012; Boehler & Marbs, 2003; D D Lichti et al., 2000).

While there is still controversy about the accuracy of the values presented by the instruments, in order to use laser scanning technology for damage assessment and structural health monitoring; (1) the limitations of this technology should be identified, (2) it should be ensured that the quality of the data obtained matches the measurement accuracy given in the user manuals.

As a result of the scientific studies carried out over the years, the major limitation of TLS has been claimed to be mixed pixels. Mixed pixels mainly occur when the laser beam hits the edge of the objects, splits into parts, and falls on two different surfaces located at different distances from the source. One of these two surfaces is called the foreground, and the other one is called the background. Signals reflected from both surfaces are perceived by the source but cannot be overlaid. As a result, the erroneous measurement, called mixed pixels, occurs at the scanned point (Q. Wang, Sohn, et al., 2016). Since this is the most crucial obstacle that reduces the accuracy of geometric measurements, several studies are conducted to find solutions. As a result, the field is developed by the minimization of the measurement error.

As noted, the effects of several parameters on the scan data quality have been studied by researchers over the years, but the effects of them on the scan data quality obtained specifically from crack identification in structures, have only been investigated by a limited number of studies. Nevertheless, in the same studies, it is

mentioned that cracks are the most critical indicators in structural damage assessment, and they need to be assessed in future works.

Moreover, it is stated that different building materials can significantly affect the quality of the scan data. For example, Maria Tsakiri et al. (2002) mentioned that the material from which the target is made can significantly affect the laser scan data quality and pointed out that this phenomenon may cause severe problems, especially in geometric measurements. They addressed the main reason as the differences in both texture and transmittance-reflectivity rates of the scanned surface. In their studies, Derek D. Lichti & Harvey (2002) worked on reflecting surface properties of scanned objects by observing the effects of the samples of building materials having various surface roughness and mineral compositions over Time of Flight (TOF) laser scanner measurements. The study was carried out by measuring entire surface areas of objects rather than measuring certain dimensions, as in deformation analysis. All in all, it was concluded that the difference in the target material does not constitute a significant error; however, the study may be missing the fact that the large areas are less error-prone than crack like small surfaces in terms of measurement accuracy. To achieve a conclusion as mentioned in their studies, it is necessary to obtain similar results for small dimensions such as cracks.

None of the available studies focused on examining scan data quality from the crack identification point of view. In particular, the exploration of both the individual and the combined effects of several scan parameters and different building materials on the scan data quality acquired by the crack identification and dimensioning purpose is still a missing point in this field.

These findings reveal an urgent need to investigate the effect of different building materials on scan data quality from the crack identification point of view in detail.

1.3 Research Motivation

One of the most substantial research questions that have not yet been answered on Terrestrial Laser Scanner (TLS) is how data collection processes can be standardized. Besides, the accuracy rates of the scan data and geometric structures generated from the data (e.g., 3D models, volumes, surfaces, and meshes) are still uncertain. Considering these needs, the National Institute of Standards and Technology (NIST), a natural sciences laboratory as an agency of the U.S. Department of Commerce (USDOC), organized several workshops to find remedies. Eventually, the American Society for Testing and Materials (ASTM) E57 3D imaging systems committee of standards and procedures was established in 2006. Although the committee was set up to work on all issues related to 3D imaging systems, they mostly concentrate on the ones related to (1) laser scanners and (2) optical range cameras.

In NIST's first publication, Cheok et al. (2006) presented two pre-standards and discussed the terminology of 3D imaging. In the following years, in their NIST TN1695 test Cheok et al. (2011) reported that the most concerned topic in all workshops was the range error. Moreover, it was pointed out that the most studied scan parameters were (1) target reflectivity, (2) target material type, (3) scanning distance between the target and the instrument, (4) angle of incidence, and (5) surrounding conditions. Among them, the effects of the second, third and fourth ones are explored in this study, while the first one was left for future studies, and the last one was excluded by conducting experiments in a controlled indoor environment.

In literature, it has been clearly stated that the type of target material affects the error rate of the data obtained (Kaasalainen et al., 2010; Pfeifer et al., 2007; T Voegtle & Wakaluk, 2009). However, there has been no study on the effects of the target material type on scan data quality from the crack assessment perspective, including tests performed under NIST up to date.

Therefore, in this thesis, it is decided to explore the effects of different scan and material (building materials) settings on the scan data quality of crack identification and measurement process. The study's promising nature and the belief that the findings will take the field one step further form the research motivation.

1.4 The Objective of the Thesis

The ultimate objective of this study is to calculate the Absolute Error Percentages (*AEP*s) that occur when scan data from damaged structural elements of the three most common building materials are used in crack determination and measurements. In this way, several conclusions will be drawn about the effects of different building materials on scan data quality and accuracy, which have not been mentioned in literature yet. In this context, it is crucial to know the details of data collection and processing methods. Hence, it has become necessary to conduct some preliminary experiments while reaching the ultimate objective.

Based on these preliminary experiments, the following sub-goals have been established:

- To explore the damage modes and severity classifications in the world
- To visualize, measure, and calculate the *AEP*s of the cracks on different testbeds with several scan settings
- To explore the individual and combined effects of different scan parameters on scan data quality
- To identify the overall trends between different scan settings and their corresponding calculated *AEP*s

In line with the experiments' findings, accomplishing these goals can enable this study to contribute to the American Society for Testing and Materials (ASTM) E57 committee of the National Institute of Standards and Technology (NIST) in their studies on 3D imaging systems standards and procedures.

1.5 Research Questions and Hypotheses

Terrestrial Laser Scanner (TLS)'s error performance analysis on detecting and measuring the cracks in the building components requires a comprehensive study because these measurements' accuracy depends on several scan parameters. These parameters can be divided into two groups: (1) parameters that depend on the scan settings of TLS and (2) environmental parameters involving environmental conditions, scanning distance, and target characteristics.

Exploring these different parameters' effects on crack identification error is a challenging task because it requires carrying out too many experiments. Therefore, this process is considered to be quite time-consuming and costly. Moreover, it is challenging for only one person to conduct numerous experiments on all different parameters. Even so, researchers have studied this subject and have contributed to the development of the field. However, it can be thought that studies have not reached complete results because there are still parameters whose effects have not been understood yet.

For this reason, more experimental studies should be conducted, and the scan data should be evaluated. To conduct these experiments properly, sufficient information should be obtained about the application areas of TLS, their features, limitations, and methods of analyzing the scan data.

All in all, three research questions have been proposed to address them:

1. What are the salient parameters that affect scan data quality?
2. What is the combined effect of several scan parameters on scan data quality?
3. What is the effect of building material type on scan data quality?

In line with the research questions, the following hypotheses are proposed.

H1. Scan data quality variation based on a change in scanning distance, resolution, incidence angle, sensitivity settings, and target material type

could be represented numerically in the context of crack identification and dimensioning.

H2. Normal sensitivity setting usage in laser scanning operations will be inadequate for studies where the measurement accuracy is the primary concern.

H3. Crack shape regularity and width size affect the crack edge detection process.

H4. *AEPs* are independent of the positioning method used to achieve the desired incidence angle during laser scanning, provided the same scanning settings are used.

H5. Identical crack edges on flat surfaces are easier to detect than rougher ones, as point cloud data are visualized according to the variation in-depth on the scan surface.

H6. *AEP* estimation equations could be derived for each building material type as a mathematical function of crack width, scanning distance, and incidence angle.

The hypotheses mentioned above are discussed in Chapters 4 and Chapter 5 based on the corresponding experiments' results. The relevant hypothesis's numbering is indicated at the end of the sentences where it is discussed. In this way, it becomes easier to understand the discussions' contributions in the relevant sections to the hypotheses.

1.6 Scope, Limitations, and Organization

In this study, (1) the effects of different scan parameters on the scan data quality, and (2) the error rates in crack width measurement of different building materials are investigated.

In more detail, this study mainly focuses on determining the effects of the three most commonly used building materials on the laser scan data quality. While achieving the proposed goal in the study, (1) extensive literature review on data collection and

data quality via TLS is carried out, (2) several scan parameters are tested using two different materials (e.g., asphalt and foam board), and (3) three sets of experiments are conducted using the three different building materials, namely, reinforced concrete, wood, and masonry brick.

In literature review chapter, the scan parameters affecting scan data quality, various methods used in structural health monitoring, and different damage assessment codes and standards worldwide are explored. In the case studies, the cracks in the target objects are scanned, and the acquired data is processed via Leica Cyclone Register 360 point-cloud processing software. The aim is to comprehend the effects of different scan parameters on scan data quality by calculating the dimensional measurement error of the cracks in the target objects. Lastly, in the experiments, the effects of the three most commonly used building materials on the scan data quality is assessed, and a parametric formulation of the scan data quality based on the error values is obtained.

All in all, this study develops an understanding of the objective, fast, and accurate acquisition and analysis of scan data from the perspective of evaluating cracks caused by seismic actions in structural elements made of reinforced concrete, wood or masonry brick.

The scope of the study is limited to the evaluation of the performance of TLS on the identification of cracks in post-earthquake damaged structural elements of different building materials for the following three reasons:

1. In literature, it is stated that TLS is the most accurate measuring devices among remote sensing technologies to identify the damage in the building components
2. TLS usage for data acquisition is in line with the research goals of this thesis
3. The lack of information in literature about the identification of cracks in damaged structural elements of different building materials with TLS and the effects of these materials on scan data quality

There are various brands of TLS that works either with the principle of Phase Shift (PS) or Time of Flight (TOF). Throughout the study, a TOF based TLS, Leica Scan Station P40, is used to obtain data. Focusing on one scanner is considered as one of the limitations of the study. However, it is one of the most commonly used and studied types of TLS (Costa-Jover et al., 2019; Indirabai et al., 2019); hence, the results are expected to represent other scanners. One other limitation is that crack depth analysis is excluded from the scope of the study. The crack depth is valuable information on structural damage assessment in practice because deep cracks in structural elements may indicate that the load-bearing capacity has been exceeded. In contrast, superficial cracks such as plaster cracks show that the limit has not been exceeded yet, so the structural element is still safe. However, crack depth assessment highly relies on expert judgment and is expressed by insights rather than numbers in practice. Therefore, all discussions are made according to the experiments' findings based solely on the cracks' width measurements.

Given the information in previous sections, the rest of the study is organized as follows:

In Chapter 1, a brief introduction has been made so that the reader can obtain general information about the content of the thesis work. Subsequently, the problem statement, the research motivation, the thesis's objectives, and the research questions are discussed.

In Chapter 2, within the literature review scope, the tools and methods used in the post-earthquake structural damage assessment up to date are introduced and compared. In this chapter, the first research question is tried to be answered.

In Chapter 3, the methodological details of the thesis work are discussed based on the research questions. More specifically, the details regarding the data acquisition and the data processing for the experiments conducted in this thesis are explained.

In Chapter 4, the details of the preliminary experiments that aim to (1) explore the correlation between different scan settings and the quality of the scan data and (2)

verify the TLS before using it for core experiments are specified. Moreover, in this chapter, (1) experiments' findings are evaluated, and (2) their contributions to the design of the core experiments carried out in Chapter 5 are discussed. The results of this chapter are used on the elucidation of the second research question.

In Chapter 5, the details of the core experiments are given. In these core experiments, the effects of different building materials on the scan data quality are investigated. This chapter is composed of the details about (1) the design of the experiments, (2) execution of the experiments, (3) the evaluation of the findings, and (4) making inferences in light of these findings. The findings of this chapter are used in answering the third research question.

Lastly, in Chapter 6, the presented study's critical findings are summarized, the study's contributions are revealed, and possible future research directions are discussed.

CHAPTER 2

LITERATURE REVIEW

2.1 Introduction

In recent years, technological advances in remote sensing tools have attracted more attention than ever due to the growing need to inspect engineering structures. In this context, buildings are more subject to research than other engineering structures, as they are one of the most common types of structures in a built environment and can easily be damaged in earthquake conditions. For this reason, it is understood that earthquake-damaged buildings must be inspected for the identification of the damage types and severities in their elements. In this way, it is envisaged that decisions can be made about the buildings' structural health and serviceability.

Today, manual inspection is the most common method of structural damage assessment. In this method, a specialist with advanced structural engineering knowledge (1) visually inspects the damaged components of buildings, (2) fill out the assessment forms, (3) make necessary calculations, and (4) decide on the damage mode and damage severity of the buildings (Applied Technology Council (ATC), 1989; Lizundia et al., 2014).

This method is mostly criticized since it is highly subjective, time-consuming, and error-prone (Graybeal & Washer, 2015; LeBoeuf & Shafir, 2006). Moreover, this method's geometric measurements may not provide sufficiently accurate results since the execution steps highly rely on manual operations (Graybeal & Washer, 2015; Rens et al., 1997).

The recent advancements in technology and the aspiration to find solutions to the problems above have driven both the academics and practitioners to search for other methods for inspecting engineering structures. Thus, they have concentrated on

developing remote sensing technologies to provide more accurate, reliable, and automated structural damage assessment methods. Hence, they conducted several studies on utilizing these technologies through various data collection and analysis tools (Ajmar et al., 2011; Dominici et al., 2017; Kerle, 2015; Kersbergen, 2018; Mitomi et al., 2001).

Structural damage may appear in various forms, namely damage indicators. The most common types of them are cracks, spalling, displacements, and inclinations. Cracks are considered the most important ones since they are considered the main signs indicating damage types (Altan et al., 2001; The Applied Technology Council, 1998). Moreover, the measurable crack properties (e.g., widths, orientations, depth of penetration) in the structural components involve much information about structural health conditions. For this reason, cracks that occur in the post-earthquake period in structural components must be determined and assessed.

Nowadays, Terrestrial Laser Scanner (TLS) has gained considerable popularity due to its broad usage capability in various engineering fields and high accuracy and reliability rates, among other remote sensing tools. It has several benefits in terms of its usability for damage indicator identification in damage assessment processes in particular (Anil & Akinci, 2013; Olsen et al., 2010).

On the other hand, TLS has strong and weak sides, like every measuring device. The most challenging part with the TLS is that the collected scan data greatly affected by the scan parameters such as scanning distance, resolution, and incidence angle (Q. Wang & Kim, 2019a). Moreover, other factors, including the target's surface reflectivity, weather conditions, illuminance conditions, and target's material type, also affect the scan accuracy (Dai et al., 2013).

To date, researchers have investigated the effects of these parameters on scan data quality. However, none of them have explored the combined effects from the perspective of identifying cracks in different building materials in detail. Furthermore, several professional organizations like the American Society for Testing and Materials (ASTM) E57 Committee on 3D imaging systems, VDI/VDE

2634, and ISO Technical Committee (TC)/172 are endeavoring to understand the impact of these parameters on scan data quality and standardize the related processes.

In this context, this section poses the current literature on (1) the crack characteristics suggested in different post-earthquake damage assessment guidelines in the world and (2) the various tools and methods used in data collection and data processing in structural damage assessment processes.

2.2 Crack Characteristics

Post-earthquake damage assessment plays a crucial role in understanding the current conditions of buildings. In order to make a sound damage assessment, it is necessary to examine the damage indicators in the structural members and report accordingly. These damage indicators can develop in many different ways (e.g., cracks, spalling, displacements, and inclinations). Cracks are the most crucial ones since they are considered the main signs indicating damage types (Altan et al., 2001; The Applied Technology Council, 1998).

This thesis consists of experimental studies conducted to explore the combined effects of scan parameters on the quality of scan data obtained from cracks in different building materials. The investigation of the crack characteristics suggested in literature is necessary to obtain consistent and practical results from these experiments. This is because the crack characteristics are commonly used in post-earthquake structural damage assessment to determine the structural elements' damage modes and severities. In this way, the capabilities of TLS in crack identification can be evaluated objectively.

In this context, researchers have been working on post-earthquake damage assessment in buildings for decades. Over the years, several approaches have been developed worldwide and gained into the literature. In each of these approaches, the relationship between crack characteristics and building damage condition is defined differently. In other words, since the most common building materials of each

country are different, post-earthquake damage assessment guidelines and specifications also vary country wise.

In Japan, the Guideline for Post-earthquake Damage Evaluation and Rehabilitation was developed in 1991. The guideline aims to provide nationwide damage identification and rating criteria for the inspectors. It includes investigation methods of damages in three typical structural systems used in Japan, such as reinforced concrete, wooden, and steel buildings. In the broadest sense, this guideline identifies damage in five main classes by considering the physical observations and measurements of crack widths on structural elements (Maeda et al., 2014). As a result, the buildings are placarded with color codes such as inspected and safe (green), limited use only (yellow), and unsafe (red) (Japan Council for Quick Inspection of Earthquake Damaged Buildings, 2002; Sunohara, 2018).

In the U. S., Federal Emergency Management Agency (FEMA)'s 306 "Evaluation of Earthquake Damaged Concrete and Masonry Wall Buildings: Basic Procedures Manual" and 307 "Evaluation of Earthquake Damaged Concrete and Masonry Wall Buildings: Technical Resources" have been published. The purpose of these guidelines is to propose criteria for assessing earthquake damage and guiding this action. Furthermore, they contain detailed visuals and explanations about the classification of damage in structural elements. In these guides, the component damage classification is defined in five different levels (e.g., Insignificant, Slight, Moderate, Heavy and Extreme) by observing the size of the cracks on the components (Maffei et al., 2000; The Applied Technology Council, 1998).

As in other countries, "Field Manual for Post-Earthquake Damage and Safety Assessment and Short Term Countermeasures (AEDES)" has been published on this subject in Italy (Baggio et al., 2007). This manual's primary purpose is to standardize damage assessment and analysis processes and ensure rapid reaction after the earthquake. To this end, the componentwise damage levels for Reinforced Concrete (RC) and Masonry buildings are given in six different grades based on varying crack

widths (e.g., D0-no damage, D1-slight damage, D2-medium damage, D3-severe damage, D4-very heavy damage, and D5-collapse).

In Greece, Anagnostopoulos et al. (2004) have also published an extensive report on buildings' post-earthquake damage and usability assessment. The report provides details on four typical building types (RC, masonry, steel, and wood). The criteria for damage assessment in elements (i.e., load-bearing and non-bearing) are set, and damage severities are categorized for them. These damage severity classes are; (1) None, (2) Slight, (3) Moderate to Heavy, and (4) Severe to Total. In addition, a color posting system (Green, Yellow, and Red) is created based on the damage severities.

Lastly, in Turkey, the book Union of Chambers of Turkish Engineers and Architects (2016) mentions the details regarding damage detection in RC and Masonry buildings affected by an earthquake. In this book, the damage detection procedures are described, damage severities are labeled with codes (O, A, B, C, and D), classified as undamaged, slightly damaged, moderately damaged, heavily damaged, and very heavily damaged.

Although all guidelines and specifications vary in content, they agree on particular points:

1) Cracks are the primary indicators in the assessment of the buildings' health status.
2) The dimensions of the cracks, which indicate the same damage status, vary for different materials.
3) The directions, widths, and depths of the cracks are the main dimensions used to evaluate the damages.

According to their orientations, cracks are classified into four different types (e.g., horizontal or shear, diagonal, flexural or vertical, and splitting). This classification process, namely the damage mode's determination, is the first structural damage assessment step. Such cracks may occur alone or together in structural members.

The dimensional analysis of cracks becomes essential because the information collected is used to assess damage severity. Moreover, it is noted in all guidelines that different types of cracks with the same crack size can indicate different levels of damage severity. For example, it has been stated that a more severe earthquake is needed for a shear crack to occur compared to a flexural crack of the same width. Eventually, the diagonal types are indicated as the most critical ones among them.

As mentioned above, there is no common understanding of the crack widths' boundaries, indicating the severity of damage for different building materials.

Accordingly, "Post-earthquake damage and usability assessment of buildings: Further development and applications. The final report" and "Field Manual for Post-Earthquake Damage and Safety Assessment and Short Term Countermeasures (AEDES)" published by Anagnostopoulos et al. (2004) and Baggio et al. (2007) respectively, are used as references in designing the test setups in this study since they present the most detailed explanations.

In the documents mentioned above, the details regarding the assessment parameters to be considered and the methodological approaches to be employed while conducting the post-earthquake structural damage assessment are comprehensively explained. However, within this thesis's scope, studies are conducted only at the focus of crack widths.

The corresponding suggested crack widths intervals of different building materials are given below in Table 2.1.

Table 2.1. Material Based Suggested Crack Widths

Material Type	**Crack Width**	**Damage Severity Level**
Reinforced Concrete (RC)	No signs of any distress	None
	$d < 3$ mm	Slight
	3 mm $< d <$ 10 mm	Moderate – Heavy
	$d >$ 10 mm	Severe – Total Collapse

Table 2.1 (cont'd)

Material Type	Crack Width	Damage Severity Level
Wood	Hairline cracks in the plaster of interior walls	None – Slight
	d < 2 mm	Slight
	2 mm < d < 4 mm	Moderate – Heavy
	d > 4 mm	Severe – Total Collapse
Masonry Brick	Cracks in the plaster caused by shrinkage or damages occurred in the past	None
	d < 2 mm	Slight
	2 mm < d < 10 mm	Medium – Severe
	d > 10 mm	Very Heavy – Total Collapse

2.3 Data Collection and Analysis Methods for Crack Identification

As stated at the beginning of this chapter, there is an increasing momentum towards developing remote sensing technologies. For this purpose, numerous studies using various data collection and analysis methods have been done and will continue to be carried out in the future. These methods can be studied in three classes; manual or visual inspection methods, image-based systems, and laser scanning.

2.3.1 Manual-Visual Inspection Methods

Visual inspection (VI) methods are the most common and traditional way of structural damage assessment (The Applied Technology Council, 1998). The purpose of these methods is; to determine the extent or severity of damage and make the necessary preliminary assessments. VI methods have widely been used for structural damage assessment and health monitoring in several transportation structures (e.g., roads, highways, airports, and tunnels)(Fu, 2005). Moreover, it has

also been preferred for the same purpose in other infrastructures and superstructures such as buildings, dams, coastal structures, water supply, and sewage treatment systems. However, the most common use of these methods is in structural damage assessment of buildings after an earthquake since these structures form a large portion of the built environment and are earthquake sensitive structures.

In these methods, it is expected from the practitioner to be familiar with the damage indicators and damage types and to have a high degree of interpretation ability. Furthermore, an adequate amount of knowledge on the relationship between the built structure and the soil conditions of local terrain and construction materials' behavior under the applied loads is essential for a more accurate assessment (Anil, 2015). Thus, specialists with a structural engineering background are the perfect matches for this purpose.

In practice, these specialists physically visit structures, inspect damage indicators in building components with naked eye, and gathers observational and quantitative data (The Applied Technology Council, 1998)(Figure 2.1) and (Figure 2.2 (a), and (b)).

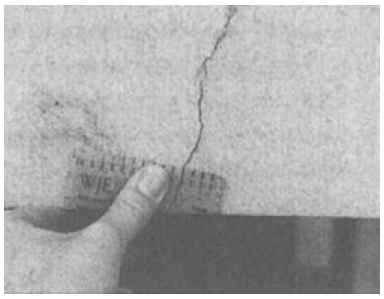

Figure 2.1. Manual Crack Measurement Using a Width Gauge (Farmer, 2004)

(a) Crack Width Measuring

(b) Visual Observation

Figure 2.2. Visual Inspection Processes (Becker et al., 2016; E. Moore, 2018)

The use of these methods has been addressed in several studies in literature. Nakano et al. (2004) introduced structural damage severity analysis procedures based on visual inspections and residual seismic capacity of load-bearing elements. In these procedures, damage assessment is addressed from two aspects: foundation and superstructure damage assessment. While the level of foundation settlement and leaning determines a foundation's damage, the crack widths measured as a part of the visual inspection are used for the structural members' damage classification. They correlate their observations and measurements with the structural elements' seismic capacity, considering that visual inspection is not sufficient alone for damage severity analysis. The health condition of a building is determined by the joint analysis of the foundation and superstructure damage assessments.

In another study Dandoulaki et al. (1998) pointed out the importance of post-earthquake building inspection by discussing the Konitsa earthquake's details in 1996 in Greece. In the article, the historical development of post-earthquake building inspection is discussed in chronological order. It is noted that, despite the high frequency of devastating earthquakes in Greece, there were no post-earthquake building usability assessment procedures until 1984. After the Konitsa earthquake, the building usability assessment is carried out in two steps, where both rely on the visual observations (i.e., first-degree and second-degree evaluations). The first-degree evaluation is that teams of two persons (at least one is a structural engineer) visually inspect buildings to classify their usability in three categories (usable, temporarily unusable, and unusable).

In the first-degree evaluation, buildings are assessed in several aspects as follows:

- The details of a building for easy identification such as its address, owner info, corresponding municipality, and other similar information
- Building description (number of stories, year of construction, occupancy, and type of structure)
- Building usability classification (usable, temporarily unusable, and unusable/dangerous).

- Need for safety measures (barricades around power, water, and gas outputs, and immediate support need).
- Corresponding expert comments.

In the second-degree evaluation, damage indicators are examined in more detail, and related measurements are taken manually.

Although these methods are still commonly used in practice, they are highly criticized for being highly unreliable, risky, expensive, and time-consuming (Abdel-Qader et al., 2003; Anil et al., 2011; Yu et al., 2007). Accordingly, both practitioners and academics have sought more innovative, standardized, and reliable structural damage assessment methods in recent years. As a result, it is realized that remote sensing technologies deployment in these processes can be a powerful method of solving these problems. Hence, image and point-cloud-based solutions are developed, which eliminate the deficiencies of visual inspection methods.

2.3.2 Image-Based Systems

Due to the rapid development of sensor technologies, alternatives to traditional manual inspection methods for crack detection have been sought. This quest aims to minimize the drawbacks of manual inspection methods. As a result of all these efforts, the concept of remote sensing and machine vision, which have become very popular, especially in recent years, have begun to be discussed by broad audiences (Shanmugamani et al., 2015; Spencer et al., 2019). These methods' main concern includes but is not limited to the flaw detection in structures (Schabowicz, 2019).

Ultimately, in the engineering communities, Digital Imaging (DI), the digital representation of a physical object or its characteristics, has begun to be commonly used for structural damage identification, analysis, and health monitoring in infrastructure and superstructure projects (e.g., bridges, highways, dams, and buildings). Image-based systems consist of two stages: data collection and analysis.

In the data collection step, besides the most traditional and straightforward method as manually obtaining images with handheld cameras, various other systems are used to automate data collection, such as mounting digital imaging devices like digital cameras and x-ray devices on mobile robots, trucks, or Unmanned Aerial Vehicles (UAVs). These systems automatically record and store every information displayed on their lenses into a storage area. However, the collected data needs to be processed and interpreted.

For this purpose, a scientific field called computer vision that seeks to develop a semantic understanding of digital contents such as photographs and videos for computers has emerged. Several computer vision techniques and algorithms such as image classification, object detection, tracking and identification, semantic and instance segmentation, and image reconstruction are promoted in time.

With these developments, analysis and manipulation to increase digitalized image quality that enables feature and defect extraction from the digitalized data have become possible. Like other approaches, DI has several advantages and disadvantages in structural damage detection, assessment, and health monitoring.

Some of its main advantages are that it enables contactless measurements via cheap, easily accessible, and portable hardware (Laefer et al., 2010; Sharma & Mehta, 2016). Moreover, image-based methods are considered more objective, reliable, safe, and rapid in data collection than manual methods (Koch et al., 2014).

On the other hand, these methods have their challenges and drawbacks. Sharma & Mehta (2016) summarizes these challenges as the need for some provisional parameters before the application, hardness of real-time intermittent data flow and insufficient memory of digital cameras to store the data during the applications, and software related issues.

Consequently, the immense advances in machine vision have attracted the attention of civil engineering communities (Fraser, 1998; S. W. Kim & Kim, 2011; Mandriota et al., 2004). Ye et al. (2016) reviewed machine vision usage in structural health

monitoring by discussing the cutting edge methods. Accordingly, up to now, numerous image-based systems have been developed and studied for structural damage assessment, health monitoring, and inspection purposes in literature.

Barazzetti & Scaioni (2009) proposed an image-based approach for structural crack assessment capable of extracting the crack profile and measuring its dimension from the digital images. Hutchinson & Chen (2010) introduced an image-based framework to monitor and quantify concrete surface cracks where digital cameras are utilized in image acquisition. The proposed scheme involves determination, localization, and geometric quantification of damages. Likewise, Yamaguchi et al. (2008) presented an image-based approach for detecting cracks in concrete surfaces.

One of the image-based approaches is the use of digital cameras in mobile robots. Yu et al. (2007) used digital camera mounted mobile robot to detect and acquire the image data of concrete cracks in a tunnel and analyzed it via an image processing routine. Similarly, in Phillips & Narasimhan (2019), the use of an Unmanned Ground Vehicle (UGV) with integrated visual sensors for data collection in automated bridge inspection is presented.

One other approach is the image-based 3D reconstruction. In these methods, 3D surfaces are reconstructed from multiple images. Zheng (2014) demonstrated this approach's application on the RC specimens and compared the results with the actual crack measurements from the crack detection and analysis perspective. The study's findings revealed that digital crack identification and measurement via image-based 3D reconstruction is as successful as manual inspection with the advantage of being safer, especially in post-disaster reconnaissance. Torok et al. (2014) proposed a system for post-earthquake damage assessment on buildings based on the image-based 3D reconstruction and crack detection algorithms.

Another approach is to install digital cameras on UAVs or drones. UAVs are air vehicles that do not have a crew on board (Figure 2.3). These devices may be either fully automated or remotely controlled. They were used for military reconnaissance during the First World War for the first time in history. Since then, it has been used

in many other industrial areas such as search and rescue, storage and inventory management, forestry, agriculture, mining, oil, and construction (Irizarry et al., 2012; Nisser & Westin, 2006).

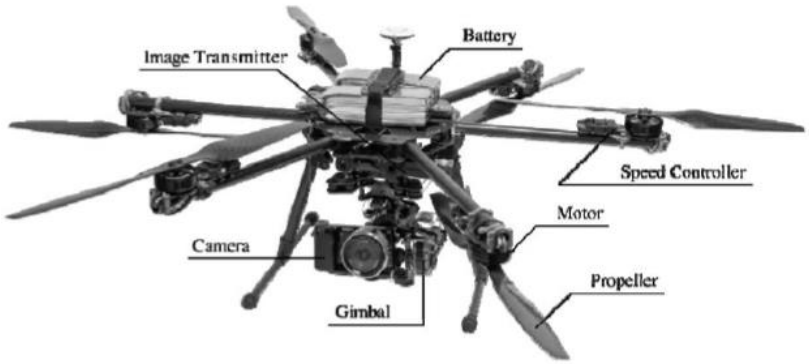

Figure 2.3. A representative Digital Camera Mounted UAV (Liu et al., 2014)

In the last decade, UAVs' utilization, especially in the construction industry, has garnered great popularity due to its potential of enhancing work quality while reducing the cost and time of construction tasks (Motawa & Kardakou, 2018). In the construction industry, these air crafts are used for numerous purposes such as safety and quality inspection (Gheisari et al., 2014; Obradović et al., 2019), site logistics (Bryan et al., 2015), mapping and surveying (Mancini et al., 2013; Zulkipli & Tahar, 2018), progress and health monitoring (Ahmed et al., 2018; Sankarasrinivasan et al., 2015), and post-disaster structural damage assessment (Adams et al., 2010; Kerle et al., 2019; Meier & Soesilo, 2015).

In his thesis study on UAV-based pavement crack identification system development supported by Artificial Intelligent, Ersöz (2016) stated that before the adoption of UAVs into the industry, spaceborne photography was the only way of field data acquisition; however, UAVs offer cheaper and more accurate solutions for similar purposes now. Furthermore, in his study, he emphasized UAVs' benefits over the post-disaster assessment of engineering structures compared to other image-based systems. Similarly, Bendea et al. (2008) showed that it is possible to develop a low-cost drone that could be used to detect damage in structures after hazardous events.

Ellenberg et al. (2014) introduced an application of UAV usage for image-based crack detection in masonry walls. H. Kim et al. (2015) presented a prototype of the UAV-based image processing in identifying concrete cracks since cracks are important clues regarding the existing condition of structures (Figure 2.4). Likewise, Hyunjun Kim et al. (2017) suggested a hybrid system composed of image processing with UAV technology for concrete crack identification.

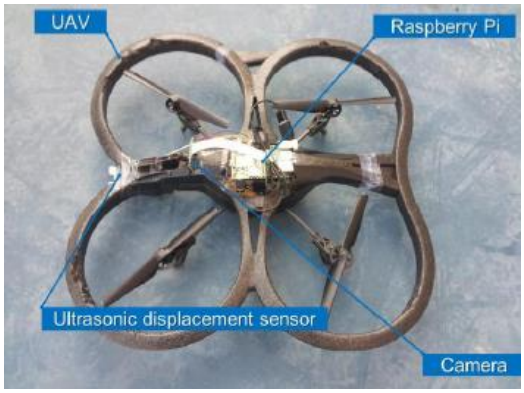

Figure 2.4. UAV-Based Prototype for Crack Identification (H. Kim et al., 2015)

Dai et al. (2013) compared image-based and laser scanning technologies regarding the level of accuracy, data quality, time-efficiency, and investment cost. Based on the experiments' results with different settings on two bridges and a building, the authors revealed that image-based systems could be cost-effective, but their data accuracy and quality are lower than of laser scanning. Furthermore, Golparvar-Fard et al. (2011) compared the accuracy and usability of image-based technologies with laser scanning for performance monitoring. The authors concluded that although image-based technologies are more user-friendly, cheaper, and do not require expertise, laser scanning is more accurate in studies where precision is a priority, such as a deformity, fault, or failure detection.

Several researchers attempted to fuse image-based technologies with laser scanning in their research since laser scanning has better accuracy, data quality, and efficiency (Alshawabkeh & Haala, 2004; Forkuo & King, 2004; Rönnholm et al., 2007). The aim was to eliminate each technology's particular weaknesses and obtain more

realistic, accurate, and qualified 3D models of surroundings. Indeed, these approaches are extremely promising, but in order to obtain better results from similar studies, it is necessary to determine the capabilities and characteristics of laser scanners, which is the main subject of this work.

2.3.3 Laser Scanning

In recent years, 3D point cloud data acquisition with laser scanners has gained popularity alongside manual and image-based methods due to its benefits over data accuracy and data acquisition speed. Therefore, laser scanners have been investigated in numerous studies, as stated in the systematic review of the fifteen years between 2004 and 2018 (Q. Wang & Kim, 2019b). The 197 research papers review revealed that laser scanners are adopted in various purposes and fields such as (e.g., 3D semantic modeling, landslide analysis, safety, progress monitoring, health monitoring, and quality and damage assessment) in the construction industry.

For 3D semantic modeling, existing studies have covered a broad spectrum of applications, including detection and visualization of structural (beams and columns) and non-structural (doors, windows, piping, cable trays, and ducting) elements. For example, Valero et al. (2016) presented a framework for 3D modeling of indoor spaces using point cloud data acquired by TLS and Radio-frequency identification RFID technology. Yokoyama et al. (2010) developed a new technique to rebuild Computer-Aided Design (CAD) representations of point clouds. Similarly, Xiong et al. (2013) concentrated on creating as-is building information models from laser scan data. The proposed approach successfully identifies and models interior structural elements, even in the presence of occlusions. The authors noted that this method would facilitate especially the renovation planning and building maintenance related processes. Moreover, in their research, the authors explored the 3D reconstruction of pipelines from laser scan data since they play a crucial role in the maintenance of a building (Lee et al., 2013; Son et al., 2015; Son & Kim, 2016).

For safety, existing studies include laser scanner utilization for the site and worker monitoring and safe equipment design. Cheng & Teizer (2013) proposed a framework for real-time visualization and tracking of construction sites. A laser scanner was used in the study due to its high accuracy for visualization of site resources (workers, equipment, and materials). The authors concluded that it is possible to obtain critical data regarding the onsite activities, which increase the personnel's construction safety and situational awareness, based on case studies' findings. Moreover, Teizer et al. (2010) pointed out that blind spots are the most common cause of equipment-related fatalities on construction sites. Therefore, they developed a tool for blind spot identification of construction equipment and alert workers by processing laser scan data. Similarly, a technique to improve equipment design by identifying equipment's blind spots was introduced in Marks et al. (2013).

Various studies exist in which laser scanners were used to monitor construction progress in different engineering structures such as dams, bridges, highways, and buildings, in literature. For example, Shih et al. (2007) used laser scanner based point cloud data in comparing as-planned and as-is conditions of a historical temple in Taiwan. Turkan et al. (2011) presented an approach that fuses Building Information Modeling (BIM) and laser scan data to monitor concrete structure erection processes. Puri & Turkan (2020) applied quite a similar approach in a bridge construction project in Albany, OR. Chengyi Zhang & Arditi (2013) also acquired promising findings regarding the calculation of progress completion of a construction work via 3D laser scanning technology.

The findings of the systematic review studies M. K. Kim et al. (2019); Q. Wang & Kim (2019b) revealed the existing research on laser scanner utilization for structural health monitoring and quality and damage assessment. The reviewed articles cover surface defects inspections (crack, spillage, flatness, and deformation), dimensional quality inspections (including pipes, facade elements, columns, and post-disaster building damage), and displacement analysis of retaining walls, dams, bridges, and landslides. M. K. Kim et al. (2014; Q. Wang, Kim, et al. (2016) concentrated on dimensional quality inspection of precast concrete elements based on laser scan data.

Safa et al. (2015) proposed a quality inspection system that employs laser scanning technology for defect detection in piping construction. González-Aguilera et al. (2008); Oskouie et al. (2016); Park et al. (2007) demonstrated successful applications of TLS-based structural health monitoring of different types of superstructures. Others worked on structural damage detection, classification, quantification, and assessment. Olsen et al. (2010) presented a comprehensive guide on the use of TLS in structural damage assessment. Kashani et al. (2015); Zhou et al. (2016) explored the ways of using TLS for damage assessment of hurricane-affected superstructures. M. K. Kim et al. (2015) developed a technique for real-time localization and quantification of spalling on concrete surfaces with TLS. Similarly, Guldur Erkal & Hajjar (2017) introduced a surface extraction based method for surface defect identification and measurement, including cracks and spalling. Moreover, several approaches for damage detection and assessment for various contexts were proposed by Kashani & Graettinger (2015); Monserrat & Crosetto (2008); Teza et al. (2009).

Ultimately, the benefits and barriers of laser scanner implementation in the construction industry were identified in Sepasgozar et al. (2016). The findings testified that although laser scanner usage in indoor and outdoor applications provides advantages on the 3D visualization of environments, the high number of indoor objects and variation of scan data quality based on scan parameters limit their utilization. Liang et al. (2018); P. Wang et al. (2019) stated that laser scanners can provide a high level of accuracy. Dai et al. (2013), on the other hand, mentioned that the data quality acquired by laser scanners is highly sensitive to various scanning parameters (e.g., angle of incidence, scanning range, and resolution) and environmental factors (e.g., humidity, illumination conditions, temperature and color, surface roughness, and reflectivity of target objects).

At an institution level, laser scan data's sensitivity to several parameters and the lack of information on 3D imaging systems' performance, including laser scanners, was first realized by the National Standards and Technology Institute (NIST) in 2003. Subsequently, four workshops were organized to evaluate the current situation and plan 3D imaging systems' future.

The establishment of the American Society for Testing and Materials (ASTM) E57 3D imaging systems committees of standards and procedures in 2006 motivated researchers in this field to contribute to the establishment of standards by further exploring the laser scanning characteristics. Consequently, a document of standards describing the terminology to be used in the 3D imaging industry was presented in light of the workshops' findings (Cheok et al., 2006). The studies carried out in the following years provided the report's presentation Cheok et al. (2011) suggesting the scanning parameters to be investigated for laser scanner characterization.

Several researchers have discovered the effects of scanning distance, angle of incidence, scanning resolution, object color, object surface properties, ambient temperature, light, and other parameters, on laser scan data quality over the years.

Boehler & Marbs (2003) extensively explored the quality of the scan data acquired by laser scanners via conducting a series of experiments. The authors, aiming to compare several laser scanner brands' performance, examined the data obtained from large-scale objects or details in terms of resolution, surface reflectivity, edge effect, range, and angular accuracy in the experiments. The findings revealed that laser scanners might cause significant errors under certain conditions; thus, their performance should be further investigated, especially for the cases where small details need to be determined (i.e., when the accuracy is the primary concern).

Kaasalainen et al. (2011) researched the effects of scanning range and angle of incidence on scan data quality and correction techniques for them. In their study, authors compared the newly obtained data set of sand forms as target materials with those existing in literature acquired with different TLSs. The authors observed that changes in the scan data quality due to scanning distance are based on the laser scanner characteristics, but the target material's surface properties mainly cause the changes regarding the angle of incidence. Despite the study's valuable results, scan data quality was interpreted depending on the data intensity rather than dimensional accuracy measurements, and only individual effects of tested scanning parameters on scan data quality were discussed instead of concentrating on combined effects.

T Kersten et al. (2008) tested the range measurement accuracy for multiple laser scanners with three different target types and investigated the effect of incidence angle on scan data quality.

Soudarissanane et al. (2007) scanned a fiberboard and white-coated plywood to explore the influence of the incidence angle on scan data quality. A rotating plate was used throughout the experiments to provide incidence angles between -90° and +90°, and scan data were obtained from three different distances. The scan data quality was analyzed in terms of point cloud density to correlate it with the scanning range and incidence angle. Although information about the level of impacts of scanning distance and incidence angle in scan data quality were obtained in the study, no information was provided about other parameters having significant effects on scan data quality, such as the color, surface texture, and type of the scanned object.

Clark & Robson (2004) referred to the variation in the laser scan data quality concerning the surface reflectivity based on several experiments in literature. Therefore, the researchers explored a laser scanner's performance, namely Cyrax 2500, over certain surfaces of different colors via performing laboratory experiments with a color-checker chart. During the experiments, a systematic correlation among surface color and scanning range measurements was observed. Accordingly, the authors proposed a mathematical correction factor that works effectively in the range of 4 to 5.5 m and aims to increase scan data accuracy. Moreover, the effect of incidence angle on scan data quality was discussed based on variations in the number of points captured due to changes in the incidence angle. The findings showed that the effect of the incidence angle on the scan data quality varies depending on whether the surface is matte or reflective. Especially, the data obtained from an angle between 20° and 40° on matte surfaces was less noisy than the one obtained with 0°. Consequently, the authors emphasized that similar experiments should be performed with real objects having various surface characteristics and colors at varying distances and incidence angles to validate the findings.

Similarly, TP Kersten (2005) studied the effects of object surface characteristics and various scan parameters over the 3D distance measurement accuracy of the data acquired by a laser scanner Mensi GS100. The researcher discussed the general trends in the individual effect of each surface characteristics and scan parameters, based on the findings of the experiments with varying test setups. Nevertheless, in the end, it is concluded that there is a complex interaction between scan data quality and variables such as the angle of incidence, and target material's type, surface properties, and color. Considering, examining each parameter's individual effects on scan data quality may be misleading; therefore, scan data variation based on this combined influence needs to be investigated.

Anil & Akinci (2013) discussed the performance of laser scanners for post-earthquake crack identification in RC structures and identified some scan parameters (e.g., scanning resolution and scanning range) that affect the scan data quality. The authors conducted a series of experiments and concluded that crack detection via TLS is possible, provided the scan parameters are appropriately set depending on the crack characteristics. Accordingly, Shi & Ergan (2019) conducted a series of controlled experiments in the context of laser scanners' usage for building façade inspection. In their study, the authors simulated cracks in different widths, lengths, and orientations on a foam board and tested a laser scanner's crack identification performance by changing scanning resolution and distance. The authors provided valuable insights regarding the level of impact of the observed scan parameters on scan data quality, however, the natural crack forms, and the effect of different building materials were not examined. In this sense, the study provides limited information about laser scanners' performance for crack identification.

Hassan et al. (2017) pointed out that the TLS data of different materials vary in terms of reflectance intensity and RGB patterns. Hence, in the study, they scanned concrete and clay brick samples to explore the feasibility of identifying material type from the TLS data based on reflectivity and RGB dispersion. Although this study shows that it is possible to determine different construction materials by TLS, it does not explain the accuracy of the surface properties to be obtained from these data.

Thomas Voegtle et al. (2008) discussed the effect of several materials and their corresponding colors on the scan data quality based on data intensity measurements in the context of scanning range accuracy. A broad spectrum of building materials commonly used on building façades such as wood, metal plate, and plaster was examined in the experiments. Although the study provided helpful general statements, the findings cannot be representative because it was conducted based on scanning range accuracy, where lower measurement error was expected than in studies examining smaller-scale details. Moreover, the scan data driven defect detection in brick surfaces was considered in Suchocki & Katzer (2018). In the study, both laboratory and field tests were performed to detect discontinuities such as cavities and cracks. The experiments conducted in the study only provide information about damage detection in brick walls and in this context, it has been overlooked that the quality of the scanning data varies depending on the different materials. In addition, the effect of scanning resolution on data quality was not taken into account, and the error quantification of TLS was not mentioned.

Finally, Yuan et al. (2020) developed a method to classify common building materials from TLS data based on the determination of object features (e.g., material reflectance, color, and surface roughness). Furthermore, the performance of different construction materials on scan data quality was analyzed by observing the materials' classification success rates. As a result of the research, it was found that commonly used construction materials could be determined through TLS data with adequate accuracy, but no explanation was made about the parameters affecting data quality other than scanning distance. The proposed system also raises doubts that it can produce results with the same efficiency on damaged surfaces and detect superficial defects since it is tested only on smooth surfaces.

CHAPTER 3

METHODOLOGY

3.1 Introduction

The quality of point cloud data acquired by 3D Terrestrial Laser Scanners (TLSs) highly varies depending on the scan settings and numerous other parameters such as wind and illumination conditions, target material type, and target reflectivity. Therefore, different error rates occur in measurements taken from scan data with different data quality. Until today, many researchers have wondered how the measurement accuracy is affected based on the changes in these parameters (Boehler & Marbs, 2003; Reshetyuk, 2006). Hence various researchers, both in literature and in practice, explored this field. As a result of these studies, it has been understood that the scan data quality varies in different settings, but no precise analysis or trend has been revealed in the context of crack identification and analysis. Nevertheless, the effects of different building materials on data quality have not yet been discovered from the crack identification point of view. Moreover, only individual effects of different scan parameters on scan data quality were discussed in studies; therefore, it was concluded that there is an urgent need to examine the combined effects of these parameters on scan data quality in a comprehensive study.

Before introducing the details of this study's methodological approach, one of the first steps of any research work should be discussed. This step, deciding on the research method and scientific research type, is carried out independently from the rest of the methodological approaches. There are several methods of scientific research, such as quantitative, qualitative, mixed, and exploratory. These methods should be chosen based on two terms: (1) the purpose of the study and (2) the characteristics of the acquired data. In this direction, the following criteria are taken into consideration when determining the research method.

- The characteristics of the obtained data such as being measurable or inferable (i.e., quantitative, or qualitative)
- The suitability of the data obtained to carry out a systematic study with statistical, mathematical, and computational techniques

Among the research methods, quantitative research methods are either descriptive or experimental. In the descriptive methods, the subject was measured only once. In the experimental methods, the researcher is empowered to examine the causalities of modifications on the subject of interest.

Since this study is iterative and progressive research where numerical, precise, and mathematically manipulative scan data groups are analyzed, the experimental quantitative research method was considered appropriate.

Based on the information discussed in the first and second chapters and the fact given above, the methodology within this study's scope is carried out in two iterative steps: data acquisition and data processing (Figure 3.1). These steps are composed of two sets of experiments that are named preliminary experiments and core experiments. The purpose of these experiments is to explore the following two research questions in depth.

1. What are the salient parameters that affect scan data quality?
2. What is the level of individual and combined effects of the scan parameters, including building material type, on scan data quality?

The first research question is designed to identify the general characteristics of 3D TLS and comprehend their limitations in practice. The following steps are taken to shed light on the question.

- A comprehensive literature review is conducted, and the conceptual foundations of the study have been established.
- Two experimental setups are designed with varying scanner configurations to scan an asphalt sample with cracks.

- The scan data is processed, and corresponding experiments are performed to assess the variation in the dimensions of the cracks in each test setup.
- The findings of these experiments are compared with the suggestions in literature, parameters that affect scan data quality are determined, and inferences are made.

The second research question is designed to determine the degree of effect of the determined parameters on the laser-scanned point cloud data quality. Therefore, the focus of this question is the experimental measurement of parameter sensitivity. Accordingly, the following steps are carried out.

- The findings of the experiments that are performed in the preliminary experiments are compared with similar studies in literature, and parameters used in the conducted experiments to answer the second research question are determined accordingly.
- To explore the error rates of 3D TLS on identifying post-earthquake damages in buildings constructed with different materials, three sets of experimental test setups are designed and performed.
- Crack patterns of three different building materials (e.g., RC, wood, and masonry) are scanned by changing the scan settings (e.g., scanning distance, resolution, and angle of incidence) of the TLS.
- Following the data acquisition, each scan data is analyzed separately in the point cloud processing software.

In experimental research, it is essential to provide sufficient details for another researcher to reproduce the obtained results. Hence, in the rest of this chapter, further details of the methodology are given in section 3.2, 3.3. and 3.4. Moreover, a schematic representation of the workflow of the methodology is given below in Figure 3.1.

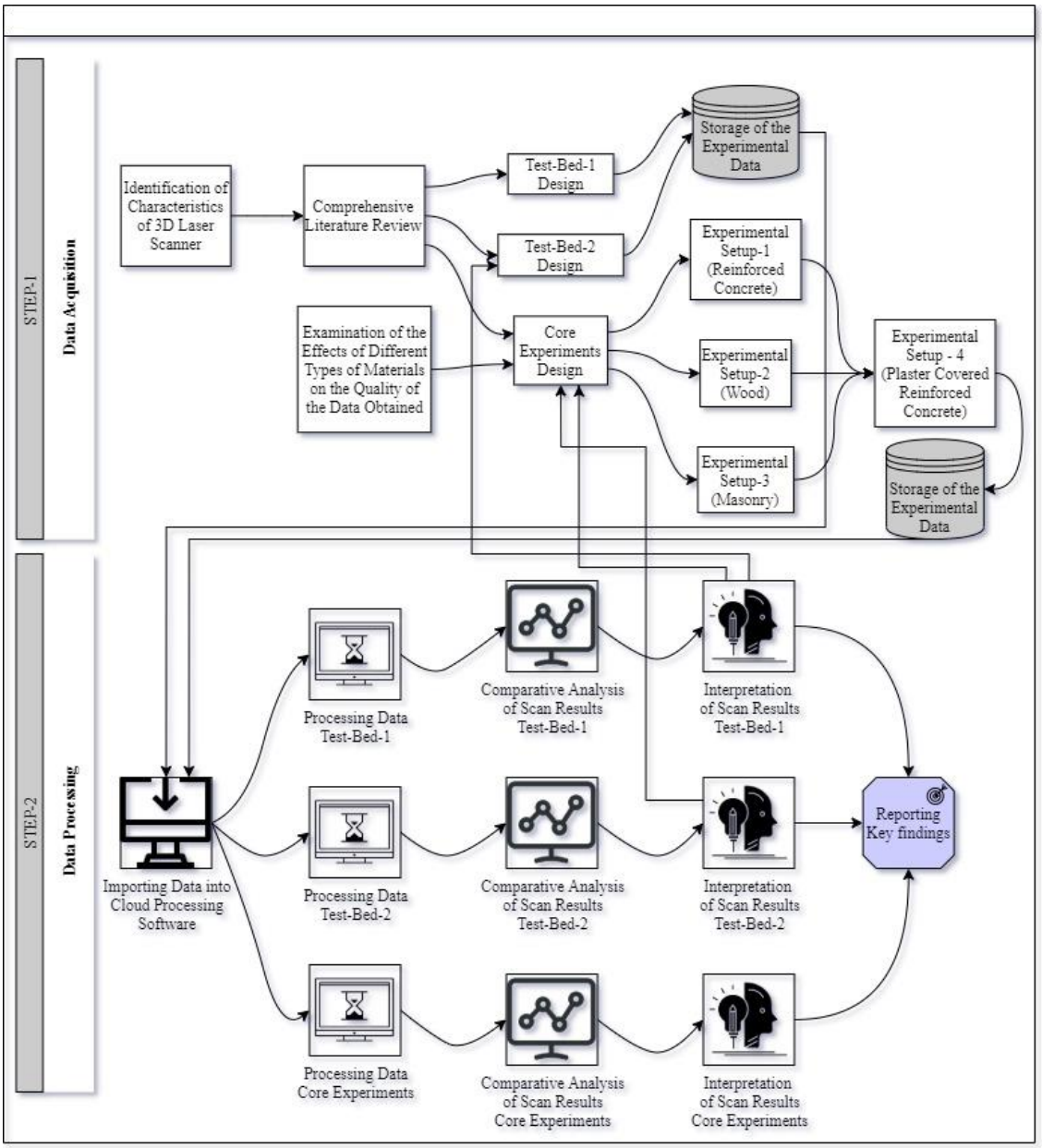

Figure 3.1. Methodological Framework

3.2 Data Acquisition Equipment and Data Processing Software

As a point-cloud data acquisition tool, TLS works with one of the two different principles in distance measurements: (1) the Time of Flight (TOF), which uses the time of flight of a laser beam to calculate the distances, or (2) phase-shift (PS) TLS

which measures the phase shift of the reflected laser energy to calculate the distances. PS scanners are known to have more accurate distance measurement capability than TOF scanners (Suchocki, 2020). However, it is thought that TOF scanners can challenge PS scanners and even give better results, so it has been recognized that they can be used for similar purposes with PS scanners (San José Alonso et al., 2012).

Throughout this thesis, one of the most robust remote sensing instruments, Leica Scan Station P40 3D TLS, is used for data acquisition (Figure 3.2). The device operates on the principle of TOF, as shown in Figure 3.3.

Figure 3.2. Leica ScanStation P40 (Leica Geosystems AG, 2018)

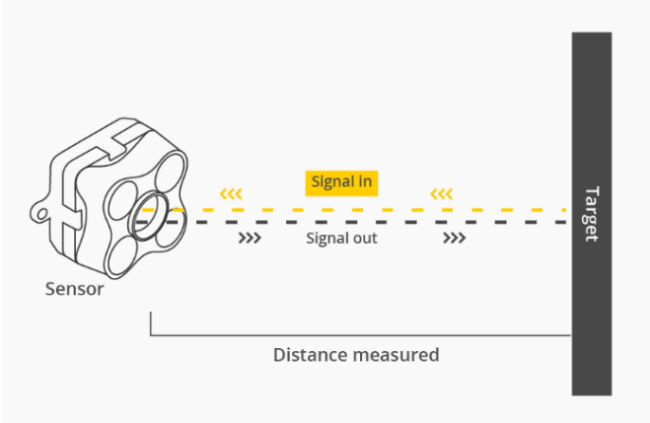

Figure 3.3. Time of Flight (TOF) Principle Representation (Terabee, 2019)

ToF is a technology used to measure the linear distance between a sensor and the target. The operation takes place in three main steps;

1. A signal is emitted from the laser ray source (Laser Scanner).
2. The linear laser beam hits the target surface and is reflected by the target.
3. Signal returns to its primary source.

All distance measurements are calculated considering the signal "release-reflection-receive" time interval. The device can perform these measurements at an ultra-high-speed, gathering 1 million point data per second, up to 270 meters range. Moreover, the device has an integrated 4-megapixel high-resolution digital camera with the white balancing feature. This laser scanner can be used in extreme temperature conditions such as -20°C to +50°C and can be stored between -40°C and +70°C. The device can also be used in rough terrain conditions without recharging since it has a range of more than 1 km and is equipped with two high capacity rechargeable li-ion batteries. These batteries can provide up to 5.5 hours for indoor measurements and up to 7.5 hours for outdoor measurements. Further technical details of the instrument are shown in Table 3.1.

Table 3.1. Laser Scanner Specifications (Leica Geosystems AG, 2017)

System Accuracy	
Accuracy of a single measurement	
Range accuracy	1.2 mm + 10 ppm over a full range
Angular accuracy	8" horizontal; 8" vertical
3D position accuracy	3 mm at 50 m; 6 mm at 100 m
Target Acquisition	2 mm standard deviation at 50 m

Table 3.1 (cont'd)

Distance Measurement System	
Type	Ultra-high-speed time-of-flight enhanced by Waveform Digitizing (WFD) technology
Wavelength	1550 nm (invisible) / 658 nm (visible)
Laser class	1 (in accordance with IEC 60825:2014)
Range and reflectivity	The minimum range of 0.4 m Maximum range at the reflectivity 120 m 180 m 270 m 8% 18% 34%
Scan rate	Up to 1'000'000 points per second
Range noise	0.4 mm rms at 10 m 0.5 mm rms at 50 m
Field-of-View Horizontal Vertical	 360° 290°
Power	
Power supply	24 V DC, 100 – 240 V AC
Physical	
Scanner Dimensions (DxWxH) Weight	 238 mm × 358 mm × 395 mm / 9.4" × 14.1" × 15.6" 12.25 kg / 27.0 lbs, nominal (w/o batteries)
Battery (Internal) Dimensions (DxWxH) Weight	 40 mm × 72 mm × 77 mm / 1.6" × 2.8" × 3.0" 0.4 kg / 0.9 lbs
Mounting	Upright or inverted

For the data processing, Leica Cyclone Register 360-point cloud processing software is used. Leica Cyclone Register 360 is chosen as the processing tool due to its user-friendly interface, extreme speed, superior capacity, and robustness in its operations.

3.3 Procedures of Preliminary Experiments

Within the preliminary experiments' scope, two case studies are planned following the problem statement, research questions, and objectives of this thesis. The experiments are designed considering the existing conditions such as laboratory and equipment capacity, material diversity, and technical specifications of the computers used for data processing. Comprehensive information about the design and testing procedures of these case studies is provided in the following paragraphs.

The first case study, which is the scanning of an asphalt sample, is carried out in two parts. In data acquisition and processing steps, the following tasks are performed: (1) scanning the cracked cylindrical asphalt sample multiple times with different scan settings, (2) digitally storing the data obtained from these scans for later evaluation, (3) analyzing the scan data in the processing software, and noting the findings, and (4) comparing the findings with each other, and making inferences.

In the second case study, the steps similar to those followed in the first one are carried out for a foam board sample. This case study is a comparison study in which one of the existing studies in literature is chosen, "Leveraging Point Cloud Data for Detecting Building Façade Deteriorations Caused by Neighboring Construction." (Shi & Ergan, 2019). This study is conducted in the Department of Civil and Urban Engineering of New York University. It is particularly preferred based on its high repeatability rates and the ability to answer this thesis's research questions.

In this context, the same test setup used in the study is designed and prepared to replicate it. The established test setup is scanned using the chosen study's methodology with a different data collection tool. Finally, to verify the device's

representativeness, this study's findings are compared to the chosen study's findings before using it in the core experiments.

Ultimately, these preliminary experiments are carried out to achieve the two objectives presented below.

1. Exploration of how different scanning parameters affect the quality of the data obtained by scanning cracks in buildings
2. Verification of the Leica Scan Statin P40 laser scanner before conducting the studies in the core experiments

In this context, the most important step among the others is calculating and comparing the scan data measurements' error rates. Further details of these procedures are explained in Chapter 4 of this study.

3.4 Procedures of Core Experiments

Following the previous studies, core experiments are planned using the inferences made from the preliminary experiments and information gathered from the literature. These experiments aim to investigate the direct effects of different building materials on measurement accuracy.

In these experiments, the three most common building materials' specimens are used to scan the cracks in their surfaces. Accordingly, three different experiment setups are established.

In the first setup, a cracked reinforced concrete sample is used, while in the second and third setups, a cracked wooden sample and a cracked masonry brick sample are used, respectively.

In all test setups, (1) the specimens are scanned several times with the different scan settings, (2) the respective distances in these scans are measured using two different measurement methods, (3) the Absolute Error Percentages of these measurements

are calculated, and (4) these calculated error rates are compared with each other to make inferences.

The procedures performed within the scope of the experiments in this part are given below;

- The determination of the building materials to scan
- The determination of the scan settings
- Storage and processing of the scan data
- The comparison of the findings and making inferences

Further details of these procedures are explained in Chapter 5 of this study.

CHAPTER 4

PRELIMINARY EXPERIMENTS ON CRACK IDENTIFICATION

4.1 Introduction

Buildings, which are the living spaces of people, should be closely monitored since they are highly vulnerable to sudden shocks such as earthquakes. During an earthquake, buildings can experience destructive forces due to the momentary dissipation of massive amounts of energy on the ground. These forces cause deformations on building components at different rates, depending on the material in which the components are produced. The deformations can occur in two main components of buildings: structural elements (e.g., beams, columns, foundation, footings, and floors) or non-structural elements (e.g., architectural elements, utility/mechanical systems, and building contents). Structural elements are the ones that form the skeleton of the buildings and provide support to the structure, and non-structural elements are the other components in a building. Structural elements are responsible for carrying the load on buildings and keeping buildings standstill. Therefore, severe deformation in them can cause permanent property damages, severe injuries, and even fatalities. On the other hand, deformations or failures in non-structural elements do not cause severe damages or building collapse.

The deformations mentioned above can occur in structures in various forms such as cracks, plaster spills, displacements, fractures, and even collapses, but cracks are the most critical indicators in determining the level and severity of the damages. Thus, cracks formed in structures after earthquakes must be examined to evaluate the type and severity of damages.

Today, structural health monitoring methods highly rely on visual inspection techniques. These methods are usually based on highly manual approaches of an expert. Commonly experienced specialists visit the structures where the damage has

occurred to assess the damage and report their observations. Although this method seems extremely easy and feasible initially, it is highly criticized because of its high subjectivity, time-consuming, and error-prone nature. Hence, most researchers have concentrated on more automated remote sensing technologies to identify and assess the deformed structures in more secure, fast, and accurate ways.

Terrestrial Laser Scanners (TLSs) have been stated to provide sensitive measurement to its users (Liang et al., 2018; P. Wang et al., 2019). However, the measurement sensitivity of devices varies according to many different parameters. Hence, the degree of error-proneness of TLS has not been fully discovered yet. Moreover, since it is a very long process to test each parameter and evaluate the results, a standard for the data acquisition process with these devices could not be established yet.

To that end, in this chapter, it is intended to explain the details of the design, analysis, and evaluation steps of the preliminary testbeds. Two experimental setups were designed for this purpose, and data was collected by performing numerous laser scans. Then, the acquired data were analyzed using point cloud processing software, and the results were compared with each other. Cracked asphalt specimen was scanned in the first setup while in the second, simulated cracks on a foam board were scanned. In the first experimental setup, a cracked asphalt specimen is consciously selected since it is one of the most problematic materials in terms of reflectivity which significantly affects laser scan data quality. In the second experimental setup, the performance of this study's data acquisition device, Leica Scan Station P40, was verified by benchmarking of the experiments conducted in this study with one of the chosen studies from the literature.

All in all, this chapter's findings were later used to achieve a better understanding of two issues; (1) determining the parameters affecting the quality of the scan data obtained, (2) obtaining information about the effects of these parameters on crack identification processes.

4.2 Case Study-1 (Cracked Asphalt Specimen)

This case study is conducted in two stages. In both stages, the cracked pavement specimen given below in Figure 4.1 is scanned.

Figure 4.1. Cracked Asphalt Specimen

Before the sample is marked with white chalk, an initial scanning is carried out without markings; however, it is observed that it is not easy to make any measurements along the cracked line due to the absence of a contrast on the surface of the object. For this reason, first, the surface is marked with white chalk to create a contrast, then the rest of the experiments are carried out.

As the first step in this case study, some testable variables are selected from all possible parameters proposed in literature to test the direct effects of different scan settings on the quality of the data acquired. Hence, the quality of the scan is considered as a function of a set of variables:

$$Q_s = f(S, W, \theta, R, D) \qquad (Eq.1)$$

Where,

- *Q_s stands for the quality of the scan*
- *S stands for the sensitivity settings*
- *W stands for the crack width (mm)*
- *θ stands for the angle of incidence (Figure 4.2) (°)*
- *R stands for the resolution settings*
- *D stands for the scanning distance between laser scanner and object (m)*

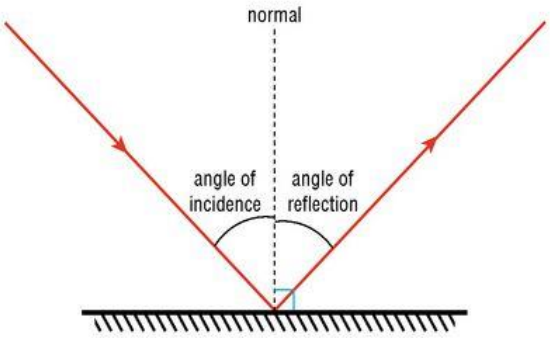

Figure 4.2. The Angle of Incidence Representation (Adam-Carr, 2010)

4.2.1 Stage One

In the first stage, the parameters' values are determined after reviewing the literature and evaluating the capacity of the laser scanner. For example, in line with the values suggested in literature, it is decided to conduct the experiments at three different scanning distances as D_1 = 1, D_2 = 3, and D_3 = 5 m and three different incidence angles: $\theta_1 = 0°$, $\theta_2 = 30°$, and $\theta_3 = 45°$.

The laser scanner offers resolution settings in seven different options defined in mm at 10 m. These options are 50, 25, 12.5, 6.3, 3.1, 1.6, and 0.8. When deciding on the optimal resolution setting for the experiments, the cracks' size, and the maximum acceptable percentage error rate is considered. To be more specific, the crack's actual size at the point of interest is known to be 11 mm, and for the experiments, it is assumed that the maximum acceptable percent error rate must be in the range of 10%. Based on this, it is concluded that the lowest resolution setting should be 3.1 mm. In addition to this option, 0.8 mm, which is the best resolution setting that the machine can offer, is selected as a second resolution alternative.

When deciding on the sensitivity preferences, the features of the two different options in Table 4.1 are evaluated.

Table 4.1. Notable Differences Between Sensitivity Options

	Sensitivity Level	
	High	**Normal**
Rate of Receiving Valid Measurements (e.g., away from the object, low reflective surfaces)	More	Less
Return Signal Type	Low	High
Sample Rate	Higher	Lower/Reduced
Duration	High	Less

These tests are carried out in both sensitivity options because of the notable differences between the scan durations of them. The study focuses on low resolution and low sensitivity and high resolution and high sensitivity pairs, which can be considered as two extremities.

The details of all selected parameters for this stage are summarized in Table 4.2 below.

Table 4.2. Design Parameters in Case Study-1, Stage-1

Scanning Distance (m)	$D_1 = 1$, $D_2 = 3$, $D_3 = 5$
Scanning Resolution (mm at 10 m)	$R_1 = 0.8$, $R_2 = 3.1$
Incidence Angle (°)	$\theta_1 = 0$, $\theta_2 = 30$, $\theta_3 = 45$
Sensitivity	S_1 = High, S_2 = Normal

After the parameters are decided, a test environment is designed based on the needs, and the test setup is established. While deciding on the test environment, particular attention is paid to the conditions of accessibility to the planned maximum data acquisition distance and the stability of the ambient light of the atmosphere. Consequently, the tests are carried out in an isolated room with a 6x6 m settlement area, illuminated by constant lights.

The corresponding test atmosphere and the experimental setup are demonstrated in Figure 4.3 (a), (b), and (c) and Figure 4.4, respectively.

(a) View from the Room Entrance

(b) View from the Other Edge

(c) View Through the Entrance

Figure 4.3. Test Atmosphere in Case Study-1, Stage-1

Figure 4.4. Experimental Setup in Case Study-1, Stage-1

After the necessary adjustments are made and the test parameters are determined, the rest of the study is carried out in two steps: data collection and data processing.

In the data acquisition part, (1) the instrument is calibrated/leveled up by tightening or loosening the screws to center the bubble indicator on it to increase the data accuracy, (2) the exact distance to the center of the target object is measured using the device's distance measurement feature to check whether the measured value is the same as the intended value, (3) the parameters given in Table 4.2 are changed one by one keeping the relevant distance constant, and (4) a scan is performed after each modification. At the end of the experiments, a total of 9 sets of point clouds are obtained: 6 from 1 m, 1 from 3 m, and 2 from 5 m. The details of the used parameters of each scan are shown in Table 4.3 below.

Table 4.3. Parameters Used in Case Study-1, Stage-1

Scan #	**Scanning Distance (m)**	**Align**	**Angle of Incidence (°)**	**Scanning Resolution (mm at 10 m)**	**Sensitivity**	**Scan Durations (s)**
1	1	Front	0	0.8	High	1799
2	1	Front	0	3.1	Normal	92
3	1	Side	45	0.8	High	1500
4	1	Side	45	3.1	Normal	150
5	1	Top	30	0.8	High	1829
6	1	Top	30	3.1	Normal	115
7	3	Front	0	0.8	High	814
8	5	Front	0	3.1	Normal	66
9	5	Front	0	0.8	High	465

The data processing part is conducted by selecting the edges of the cracked region manually to measure the distance between the two chosen points in the Leica Cyclone Register 360-point cloud processing tool. Leica Cyclone Register 360 is

chosen as the processing tool due to its user-friendly interface, extreme speed, superior capacity, and robustness in its operations. The data processing procedures are as follows:

1. Importing of each scan data in Leica Cyclone Register 360
2. Optimization of the cloud color by changing the color setting to the Hue/Intensity map. This modification regulates the visual representation of the points according to their normal directions, with different colors. Thus, it eases the selection of the edge points and increases the accuracy of the measurement. The representative change in the view is shown in Figure 4.5 (a) and (b)
3. Selection of crack edges by providing the maximum amount of zoom-in view
4. Measurement of the distances between the chosen points using the software's distance measuring tool

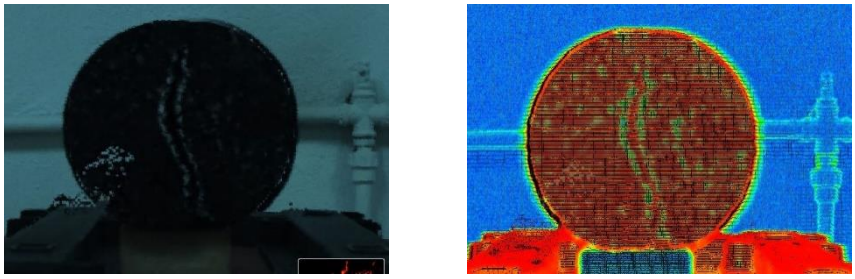

(a) Color from Scanner (b) Hue/Intensity Map Color

Figure 4.5. Representative Change in Colors in Case Study-1, Stage-1

The abovementioned stepwise procedure is followed for each scan data, and the results are noted for later evaluation.

The Absolute Error Percentage (*AEP*) of the measurements are calculated by employing Equation 2:

$$AEP = \frac{|\,Measured\ Value - Exact\ Value^{*}\,|}{Exact\ Value^{*}}\ x\ 100 \qquad (Eq.2)$$

*: Exact value of the crack width is constant as 11 mm, on the point of interest.

The calculated *AEP*s of all scans are tabulated in Table 4.4.

Table 4.4. *AEP*s in Case Study-1, Stage-1

Scan #	**Scanning Distance (m)**	**Angle of Incidence (°)**	**Scanning Resolution (mm at 10 m)**	**Measured Width (mm)**	**Absolute Error Percent (*AEP*) (%)**
1	1	0	0.8	11	0.00
2	1	0	3.1	11	0.00
3	1	45	0.8	11	0.00
4	1	45	3.1	14	27.27
5	1	30	0.8	11	0.00
6	1	30	3.1	11	0.00
7	3	0	0.8	11	0.00
8	5	0	3.1	12	9.09
9	5	0	0.8	11	0.00

The findings of the experiments conducted in this part are promising. Therefore, these results are used as a guide in designing the second stage of the Case-1 experiments. The corresponding results are given in Table 4.5 below.

Table 4.5. Results of Case Study-1, Stage-1

Compared Scans	**Findings**
3, 4	• Incidence angle affects the error rate (H1).
1, 2, 6, 7, 9	• If the sample aligns on axes perpendicular to the laser scanner's line of sight, the sensitivity level and resolution settings do not affect error rates up to 5 m.

Table 4.5 (cont'd)

Compared Scans	Findings
1, 2, 5, 6, 7, 8, 9	• If scanning is carried out directly across the object, neither resolution nor sensitivity settings cause an error in measurements.
1, 2 3, 4	• Although scanning with the normal sensitivity setting saves significant amount of time (reduce the scan duration at least by 85.8%) on data acquisition, it should not be preferred since it causes measurement error even at relatively close distances (H2).

4.2.2 Stage Two

In the second stage of this case study, the same specimen is scanned with a different experimental setup. The findings of the first stage are assessed to decide on the parameter settings of the second stage. In the experiments carried out at this stage, the focus was on examining the effects of relatively long distances and arrival angles larger than 0° on the measurement error rates. After all, the following parameters are selected to be tested:

- The scanning distance between the laser scanner and the object (D)
- The angle of incidence (Figure 4.2) (θ)
- The resolution settings (R)

Unlike the experiments conducted in the first stage, the following changes, summarized in Table 4.6, are made while designing these experiments.

1. In the experiments conducted in the first stage, D_1, D_2, and D_3 scanning distances are tested. When the findings are examined, it is noted that the error rates are relatively low. Therefore, in this stage, the scanning distances are updated as D_3, D_4 = 7 m, and D_5 = 10 m, and the experiments are carried out accordingly.

2. Findings from the experiments performed in the first stage and the suggested incidence angles in literature are assessed. Accordingly, the incidence angles values are kept constant at θ_1, θ_2, and θ_3. As mentioned before, in the experiments in the first stage, the target's repositioning is preferred to fulfill the designed angle of incidence conditions. The target is required to be moved laterally in the repositioning method, as illustrated in (Figure 4.6 (a)). That this method requires experiments to be carried out in wide areas due to the need to move the sample laterally poses a significant problem in conducting experiments. Therefore, a modified method which is verified in Chapter 5 in section 5.1.1, is used in the experiments this time to meet the designed incidence angle conditions. In this modified method, the target is rotated in the required angles instead of the relocation, while the laser scanner device is held stationary as illustrated in (Figure 4.6 (b)). Details regarding these methods are further discussed in the next chapter.

In the experiments performed in the first stage, it is revealed that the higher resolution settings of the machine should be tested since the calculated error rates in the scans carried out with the S_2 resolution setting are relatively high. Thus, the experiments in this stage are carried out with the resolution settings of S_3 =1.6 mm and S_1.

(a) Sample position in Case Study-1, Stage-1

(b) Sample position in Case Study-1, Stage-2

Figure 4.6. Sample Positions in Case Study-1

Table 4.6. Design Parameters in Case Study-1, Stage-2

Scanning Distance (m)	$D_3 = 5$, $D_4 = 7$, $D_5 = 10$
Scanning Resolution (mm at 10 m)	$S_1 = 0.8$, $S_3 = 1.6$
Incidence Angle (°)	$\theta_1 = 0$, $\theta_2 = 30$, $\theta_3 = 45$
Sensitivity*	S_1 = High

*: As inferred from the first stage experiments' results, the normal sensitivity option led to a substantial dimensioning error. Thus, throughout the experiments in this stage, only the high-resolution option is used.

After deciding on the parameters, the test setup is established. The need for a wide area to scan the object is eliminated by the modified method on the incidence angle. A long and relatively narrow corridor with fixed lighting is chosen as the experiment environment to reach up to the maximum scanning distance easily.

The corresponding test atmosphere and the experimental setup are demonstrated in Figure 4.7 (a), (b).

(a) View from the Laser Scanner (b) View from the Object

Figure 4.7. Test Atmosphere in Case Study-1, Stage-2

Following the preparations, data acquisition and data analysis processes are performed.

The data acquisition is executed by following the procedures below:

1. Calibration of the laser scanner and adjustment of the scanning distance.
2. Scanning of the test setups that are designed based on the parameters given in Table 4.6.

In this stage's experiments, a total of 18 scans are performed, 6 for each of the 5 m, 7 m, and 10 m scanning distances. The parameter details of each scan are shown in Table 4.7 below.

Table 4.7. Parameters Used in Case Study-1, Stage-2

Scan #	**Scanning Distance (m)**	**Angle of Incidence (°)**	**Scanning Resolution (mm at 10 m)**
1	5	0	0.8
2	5	0	1.6
3	5	45	0.8
4	5	45	1.6
5	5	30	0.8
6	5	30	1.6
7	7	0	0.8
8	7	0	1.6
9	7	45	0.8
10	7	45	1.6
11	7	30	0.8
12	7	30	1.6
13	10	0	0.8
14	10	0	1.6
15	10	45	0.8
16	10	45	1.6
17	10	30	0.8
18	10	30	1.6

After receiving the scan data, data processing procedures are executed. In this context, (1) the data is imported to the data processing software, (2) the image color settings option of the data processing software is changed from "Color from Scanner" to the "Hue/Intensity Map" to detect the edges of cracks easier (Figure 4.5), (3) two points are selected from the endpoints of the cracked area for each scan, and (4) the distance between each selection is measured through the software's distance measurement tool and noted for evaluation purposes (Figure 4.8).

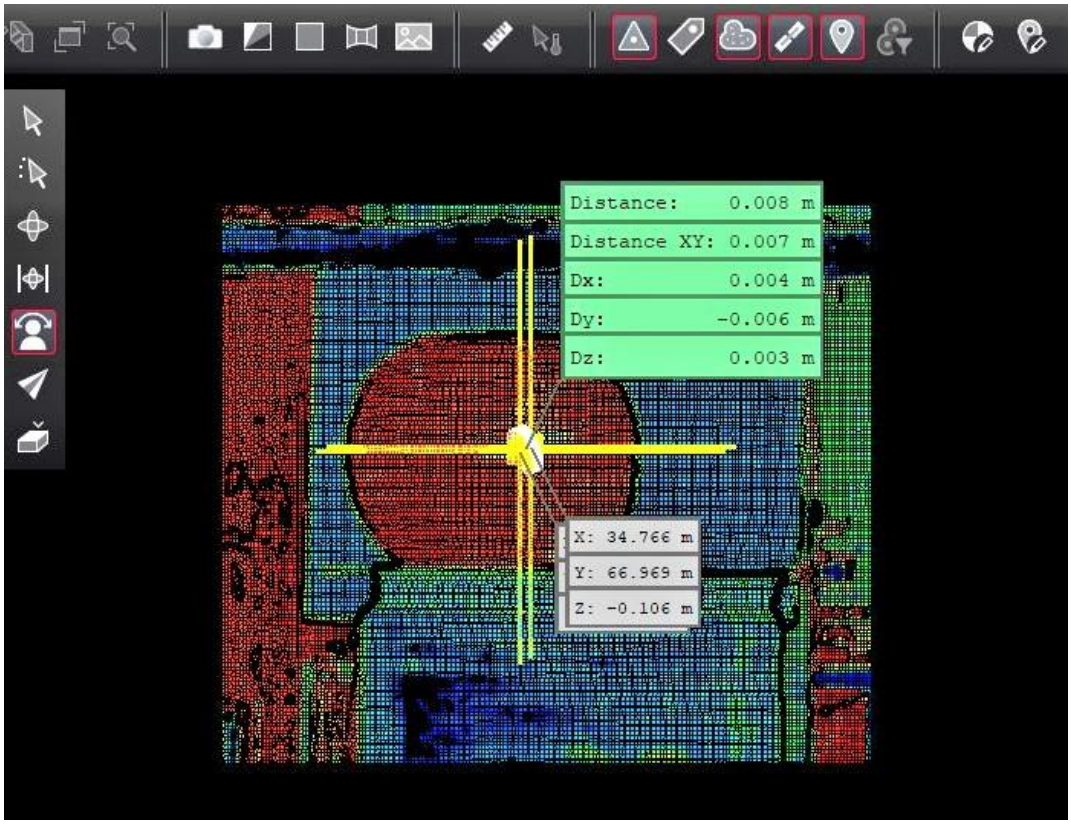

Figure 4.8. Measurement in Software Scan Number 7, Case Study-1, Stage-2

In this stage, a different point from the one selected in the first stage is chosen on the specimen. Accordingly, the relevant focal point's ground-truth value is measured as 7 mm instead of 11 mm. *AEP*s for each scan is then calculated using Equation 1 to bring the acquired data in a comparable form. All calculated *AEP*s in this stage are summarized in Table 4.8.

Table 4.8. *AEP*s in Case Study-1, Stage-2

Scan #	**Scanning Distance (m)**	**Angle of Incidence (°)**	**Scanning Resolution (mm at 10 m)**	**Measured Width (mm)**	**Absolute Error Percent (*AEP*) (%)**
1	10	0	0.8	8	14.29
2	10	0	1.6	8	14.29
3	10	45	0.8	9	28.57
4	10	45	1.6	10	42.86
5	10	30	0.8	9	28.57
6	10	30	1.6	10	42.86
7	7	0	0.8	8	14.29
8	7	0	1.6	8	14.29
9	7	45	0.8	8	14.29
10	7	45	1.6	9	28.57
11	7	30	0.8	8	14.29
12	7	30	1.6	9	28.57
13	5	0	0.8	7	0.00
14	5	0	1.6	7	0.00
15	5	45	0.8	7	0.00
16	5	45	1.6	8	14.29
17	5	30	0.8	7	0.00
18	5	30	1.6	8	14.29

The *AEP*s, summarized in the table above, are carefully examined, and some inferences are made based on this examination. Overall, the findings show a parallel trend with the expected results. The results obtained from the experiments of this stage are summarized in Table 4.9 below to further clarification.

Table 4.9. Results of Case Study-1, Stage-2

Compared Scans	Findings
1 to 18	• As the scanning distances increases, it becomes challenging to measure dimensions, and measurement error percentages increase (H1).
1, 2, 3, 4, 5, 6 7, 8, 9, 10, 11, 12 13, 14, 15, 16, 17, 18	• The increase in incidence angle causes increments in substantial amounts in the error rates regardless of the scanning distance (H1).
3, 4 – 5, 6 9, 10 – 11,12 15, 16 – 17,18	• If the incidence angle is different from 0°, then the error rate increases with a decrease in scanning resolution (i.e., changing resolution settings from 0.8 mm to 1.6 mm).
3, 5 – 4, 6 9, 11 – 10,12 15, 17 - 16, 18	• There was no change observed in the error rates between the 30° and 45° for the same scanning distances and resolution settings, whereas 30° led an increase in the amount of error rate compared with the 0° case.

As understood in Tables 4.5 and 4.9, some critical findings are attained as consequences of these experiments. These findings are capable of guiding future studies in the relevant field. However, it should be noted that they are limited by the number and variety of parameters tested in these experiments. If the findings are to be used for generalization, (1) the number of scans should be increased, and (2) the method should be repeated in different test schemes.

In the experiments carried out in these two stages, it is revealed that change in some scan parameters' values causes severe errors in measurement accuracy of the dimensions, as summarized in Table 4.5 and 4.9. Besides, the use of a specimen with variable crack widths makes it challenging to select the same points for different scans and decreases the tests' overall measurement accuracy.

In this chapter's continuation, a customized test setup is designed by simulating fixed size artificial cracks on foam board and is scanned as a second case study.

4.3 Case Study-2 (Simulated Cracks on Foam Board)

A comparative analysis method is used to verify the device (Leica Scan Station P40) to be used in this study. As a first step, a previously conducted study is selected in literature based on the following criteria:

1) The ability of the current study to answer the research questions of this thesis at the highest rate
2) Repeatability of the test setup used in the study
3) The compatibility ratio between the scan settings of the laser scanner used in Shi & Ergan (2019) and the scan settings of the Leica Scan Station P40

The same experimental test setup used in Shi & Ergan (2019) is designed and prepared as a second step. Subsequently, the experimental setup is tested by following the same methodology, and the results obtained are compared with the ones of the selected study. In the last step, the consistency between the results is discussed, (1) to verify the device before using it in the core experiments, and (2) to better understand the effects of the parameters used in the experiments on the crack measurement error rates.

4.3.1 Overview of the Testbed in the Benchmark Study

In their work, Shi & Ergan (2019) mentioned that many people have complained about the deterioration problems on the building facades in Newyork City (NYC) during the past years. Therefore, they concluded that an effective method for facade inspection is necessary. To this end, they desired to test the use of 3D laser scanners in façade inspection processes. In literature, it is pointed out that the quality of the scan data largely depends on the characteristics of the scan settings. Therefore, the

researchers were motivated to investigate the effects of different scan settings on the detection and measurement accuracy of cracks in building facades due to adjacent construction works. Hence, they simulated cracks on the foam board with different directions, lengths, and widths. Then they performed several laser scans by changing the scan settings each time. Afterward, they compared the acquired scan data to make suggestions on the most appropriate scan settings for similar cases.

The researchers designed their experiments based on the Façade Inspection Safety Program (FISP) guidelines created by the NYC Department of Buildings (DOB) and the suggested crack widths defined by Eschenasy (2016). For the scanning process of cracks, the researchers decided to test two different scan parameters; (1) scanning distance and (2) resolution. The design values of the scan parameters are given in Table 4.10.

Table 4.10. Design Parameters of the Experiment (Shi & Ergan, 2019)

Crack Width (mm)	1, 5, 7
Crack Length (cm)	10, 15
Orientation (°)	0, 90, 45
Scanning Resolution (mm at 10 m)	1.5, 3.1, 6.1
Scanning Distance (m)	3, 5, 7

As illustrated in Figure 4.9 (a) below, the researchers simulated the cracks with different dimensions by cutting the white foam board manually and prepared the related testbed as given in Figure 4.9 (b). They used the Faro Focus S150 terrestrial laser scanner for data acquisition. Furthermore, they used a digital caliper for measuring the ground truth values of the crack dimensions and used a laser meter for arranging the scanning distances Figure 4.10 (a).

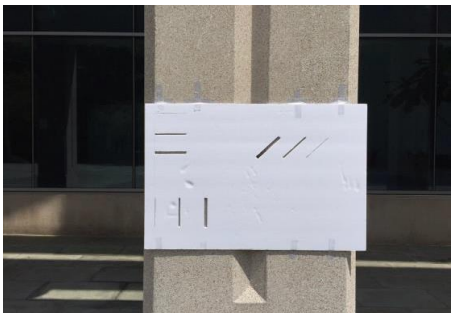

(a) Foam Board for Cracks Simulation

(b) Scanning Set-up

Figure 4.9. The Experiment Setup (Shi & Ergan, 2019)

(a) Digital Caliper & Laser Distance Meter

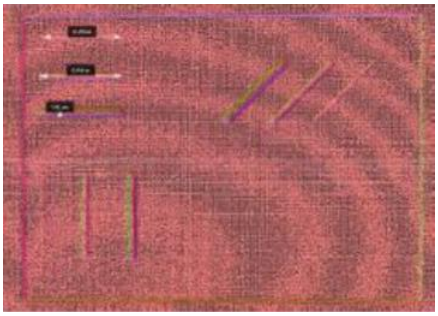

(b) Measurement in Point Cloud Processing Tool

Figure 4.10. The Measurement Process (Shi & Ergan, 2019)

The openings' dimensions are measured with the digital caliper with an accuracy up to 0.01mm, and the results are noted down as ground truth values as shown in Table 4.11. Since the cracks are manually cut, the ground truth values are slightly different from the design ones.

Table 4.11. Ground Truth Values for the Experiment (Shi & Ergan, 2019)

Designed Crack Length (cm)	**Designed Crack Width (mm)**	**Crack Orientation (°)**	**Width (mm)**	**Length (cm)**
10	1	0	1.27	10.06
		45	1.14	10.07
		90	1.27	10.06
	5	0	5.22	10.31
		45	4.86	10.23
		90	4.79	10.11

Table 4.11 (cont'd)

Designed Crack Length (cm)	Designed Crack Width (mm)	Crack Orientation (°)	Width (mm)	Length (cm)
10	10	0	9.75	10.31
		45	9.67	10.27
		90	9.92	10.34
15	1	0	1.52	15.11
		45	1.18	14.86
		90	1.25	14.89
	5	0	4.77	15.06
		45	5.08	14.91
		90	5.17	14.97
	10	0	9.89	15.08
		45	10.11	14.92
		90	9.00	14.84

After performing all the scans with the settings given in Table 4.11, the cracks' dimensions are measured by selecting the edge points of them in the point cloud processing software. The percent error rates of the measured values are calculated by using Equation 1. As a data analysis strategy, the calculated error percentages of three orientations of the same cracks are averaged for each scan (i.e., The three width measurement values (0°, 90°, 45°) of the crack which has 5 mm design width and scanned with 3 m, 3.1 mm scan settings). The calculated averaged error percentages are shown in Table 4.12.

Table 4.12. Average Error Percentage (AEP) (Shi & Ergan, 2019)

AEP	Design	1 mm		5 mm		10 mm	
		10 cm	**15 cm**	**10 cm**	**15 cm**	**10 cm**	**15 cm**
3 m 6.1 mm	Width	70.95%	**100%**	9.25%	16.81%	8.98%	7.04%
	Length	8.07%	39.62%	1.92%	1.76%	1.13%	3.92%
3 m 3.1 mm	Width	**100%**	35.88%	5.16%	10.53%	5.91%	5.41%
	Length	34.86%	5.04%	2.96%	0.91%	1.68%	0.88%

Table 4.12 (cont'd)

AEP	Design	1 mm		5 mm		10 mm	
		10 cm	**15 cm**	**10 cm**	**15 cm**	**10 cm**	**15 cm**
3 m	Width	21.14%	43.78%	4.07%	7.2%	3.21%	7.3%
1.5 mm	Length	3.93%	35.03%	2.73%	2.15%	2.01%	0.45%
5 m	Width	**139.15%**	68.91%	7.36%	8.02%	3.9%	3.67%
6.1 mm	Length	3.73%	5.44%	2.38%	1.74%	1.15%	2.37%
5 m	Width	66.75%	39.63%	4.34%	10.95%	7.39%	6.93%
3.1 mm	Length	7.21%	0.24%	3.82%	0.88%	2.79%	0.59%
5 m	Width	64.01%	**100%**	8.14%	20.33%	2.6%	6.15%
1.5 mm	Length	33%	67.44%	1.93%	0.95%	0.9%	0.72%
7 m	Width	**100%**	**100%**	**100%**	16.14%	**100%**	11.55%
6.1 mm	Length	**100%**	**100%**	1.04%	0.38%	3.86%	2.36%
7 m	Width	85.83%	91.68%	7.76%	15.45%	6.03%	12.81%
3.1 mm	Length	67.76%	67.33%	3.03%	1.47%	36.95%	2.84%
7 m	Width	**109.45%**	**100%**	21.26%	23.65%	8%	4.55%
1.5 mm	Length	7.12%	66.99%	5.2%	1.21%	3.93%	0.7%

Bold in values: Cannot be detected by the given settings

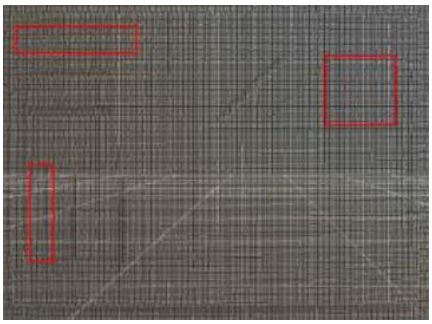

Figure 4.11. The Cracks Captured, Resolution 6.1 mm, Scanning Distance 7 m (Shi & Ergan, 2019)

4.3.2 Overview of the Testbed in this Study

In this case study, the same experiments are repeated with the Leica Scan Station P40 device aiming (1) to verify the laser scanning device before using it in the core experiments and (2) to determine the influence rates of different scan settings on the amount of error in crack detection.

For these purposes, the foam board is carved with the aid of a utility knife. Hence, the cracks are simulated on the foam board with the same dimensions given in the selected study (Figure 4.12 (a)). Then, each of the simulated cracks' dimensions is measured using a digital caliper, and the values are recorded as ground truth values, as given in Table 4.13.

Table 4.13. Ground Truth Values of the Case Study-2

Design Crack Length (cm)	**Design Crack Width (mm)**	**Crack Orientation (°)**	**Measured Crack Width (mm)**	**Measured Crack Length (cm)**
10	1	0	2.6	10.25
		45	2.06	10.25
		90	2.29	10.15
	5	0	5.24	10.15
		45	5.73	10.15
		90	5.98	10.15
	10	0	10.43	9.95
		45	10.3	10
		90	10.28	10

In this phase, it is realized that the actual dimensions slightly differed from the design values since the cracks are simulated by manual operations rather than using automated cutting technologies. Furthermore, the distance profiles along the widths and lengths of the engraved sections showed fluctuations, unlike the planned fixed values, for the same reason. However, these situations did not cause any problems for the execution and analysis of the experiments because the variation rates were

insignificant. After that, the test setup is raised to equalize the laser scanner's and the target's height, as shown in Figure 4.12 (b).

(a) Target View (b) Target Setup

Figure 4.12. Target's Details in Case Study-2

Afterward, the scan settings are specified. In this step, much effort is put to choose settings similar to the scan settings used in the compared study, but the fact that the brands of laser scanners used in these studies differ from each other created limitations in this regard. Still, the study's scan settings are chosen to be highly similar to the ones of the compared study, as shown in Table 4.14.

Table 4.14. Comparison of the Design Parameters in Case Study-2

	Benchmark Study (Shi & Ergan, 2019)	**This Study (Case Study-2)**
Crack Width (mm)	1, 5, 7	1, 5, 10
Crack Length (cm)	10, 15	10
Orientation (°)	0, 90, 45	0, 90, 45
Scanning Resolution (mm at 10 m)	1.5, 3.1, 6.1	1.6, 3.1, 6.3
Scanning Distance (m)	3, 5, 7	3, 5, 7
Scanning Sensitivity	4X*	High, Normal

* The observation time for each scan point is 8μs compared to 1μs at quality 1X.

As given in Table 4.14, the 15 cm crack length is not simulated on the foam board since even the *AEP*s of 10 cm length measurements are within the acceptable limits. On the other hand, the laser scanner's two possible scanning sensitivity options are tested due to considerable differences between data acquisition durations. Hence, (1) the scans' durations are recorded, and (2) the effects of these two options on measurement accuracy are observed.

Later, the experiment setup is installed, as demonstrated in Figure 4.13. During the installation, the laser scanner is calibrated, and then the target setup is located accordingly. To verify the values designed for scanning distances, both the laser scanner's built-in distance measurement tool and laser distance meter are used.

Figure 4.13. The Experiment Setup in Case Study-2

After the laser scanner's calibration and the adjustment of the scanning distances, the laser scanning process started. In this context, 18 laser scans are performed with the scan parameters given in Table 4.15.

Table 4.15. Parameters Used in Case Study-2

Scan #	Scanning Distance (m)	Scanning Resolution (mm at 10 m)	Sensitivity	Scan Durations (s)
1	7	1.6	High	221
2	7	3.1	High	56
3	7	6.3	High	16
4	7	1.6	Normal	56
5	7	3.1	Normal	16
6	7	6.3	Normal	10
7	5	1.6	High	330
8	5	3.1	High	81
9	5	6.3	High	22
10	5	1.6	Normal	81
11	5	3.1	Normal	22
12	5	6.3	Normal	13
13	3	1.6	High	462
14	3	3.1	High	116
15	3	6.3	High	30
16	3	1.6	Normal	116
17	3	3.1	Normal	32
18	3	6.3	Normal	15

Following data acquisition, data processing operations are started. To this end, Leica Cyclone Register 360-point cloud processing software is used, and the procedures described in the data processing part of the first case study are followed.

Since the distance profile of the widths and the lengths of the simulated cracks fluctuate due to manual cutting of the foam board as shown in Figure 4.14, a fixed

point throughout the dimensions is chosen as a point of interest, and five repetitive measurements are taken via digital compass at that place. Then, these repetitive measurements are averaged to obtain a final measurement value for each dimension as given in Table 4.13. The purpose of this process is to minimize the error caused by manual measurement on the foam board.

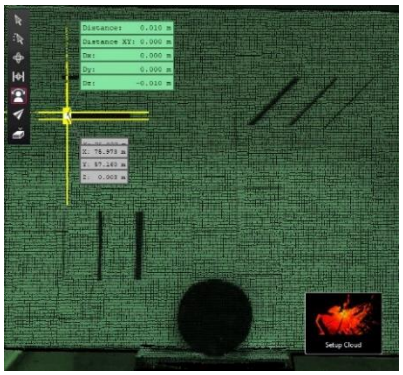

(a). Left End (10 mm)

(b). The Middle (11 mm)

(c). Right End (11 mm)

Figure 4.14. Width Measurements of a Crack in 13th Scan, in Case Study-2

In order to analyze the scan data in the computer environment, the distances between the two edges of the openings at the point of interest are measured three times, and the values are averaged and noted as the final measured values for these sections (Figure 4.15). In this way, it is aimed to minimize the error caused by the manual measurement process in the processing tool.

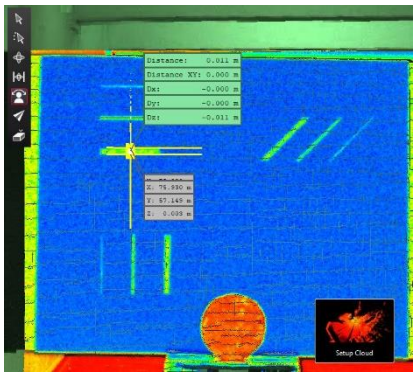

(a). First Trial (11 mm)

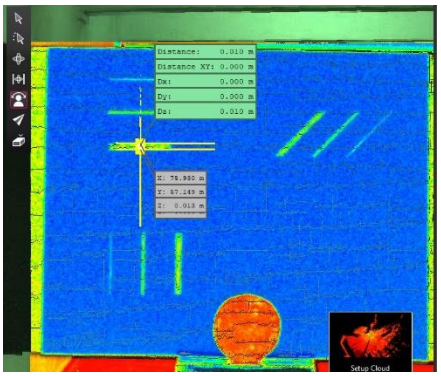

(b). Second Trial (10 mm)

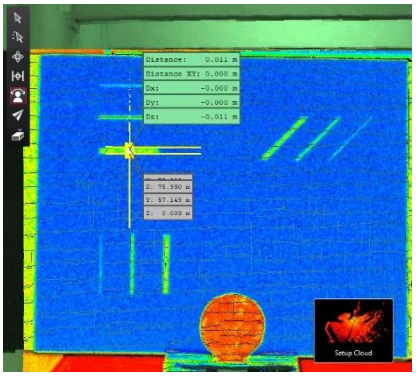

(c). Third Trial (11 mm)

Figure 4.15. Repetitive Width Measurements of a Crack in 13th Scan, in Case Study-2

These distances are measured through the software's distance measurement tool by manually selecting the endpoints of the simulated cracks on the foam board. Since the edges of the simulated cracks are relatively apparent and constant in sizes, the measurement process of these dimensions is easier to perform than the one in the first case study (H3). To attain comparable values from the measurements, *AEP*s of the widths and lengths for each scan are calculated using Equation 3 given below.

$$AEP = \frac{|\, Averaged\ Measured\ Value^{*} - Exact\ Value^{**} \,|}{Exact\ Value^{**}}\ x\ 100 \qquad (Eq.3)$$

*: The cumulative average of the three repetitive measurements of the simulated cracks' widths and lengths.

**: The ground truth values of the width or the length of the simulated cracks.

Consequently, in the second case study, nine width and nine length values are measured for each scan. Thus, a total of 324 measurements are taken, and their corresponding *AEP*s are calculated. Calculated errors revealed that the *AEP* of cracks that have the same width but different orientations (i.e., the three of the cracks designed to have 5 mm crack widths with 0°, 45°, and 90° in orientations) and scanned with the same sensitivity setting (e.g., High or Normal) do not vary significantly. The only exception for this case is the ones that have a 1 mm design crack width. Therefore, for each crack trio in each scan, calculated values at 0°, 45°, and 90° are averaged. Then, this value is noted as the *AEPs* of these cracks. These operations are repeated for the two sensitivity settings.

All the calculated *AEPs* for the high sensitivity setting are demonstrated in Table 4.16, while those for the normal sensitivity setting are given in Table 4.17.

Table 4.16. *AEP*s in Case Study-2 for High Sensitivity Setting

High Sensitivity		**1 mm**	**5 mm**	**10 mm**
3 m, 1/4	Width	31%	8%	7%
	Length	1%	2%	1%
3 m, 1/2	Width	31%	4%	5%
	Length	5%	2%	1%
3 m, 1/1	Width	31%	3%	2%
	Length	2%	1%	1%
5 m, 1/4	Width	39%	14%	18%
	Length	32%	17%	15%
5 m, 1/2	Width	38%	12%	14%
	Length	2%	4%	2%
5 m, 1/1	Width	67%	10%	14%
	Length	2%	2%	2%
7 m, 1/4	Width	147%	51%	26%
	Length	7%	6%	7%
7 m, 1/2	Width	147%	9%	17%
	Length	3%	2%	2%
7 m, 1/1	Width	147%	9%	17%
	Length	2%	2%	1%
Resolution (mm @ 10 m)		**1/4 = 6.3**	**1/2 = 3.1**	**1/1 = 1.6**

Table 4.17. *AEP*s in Case Study-2 for Normal Sensitivity Setting

Normal Sensitivity		**1mm**	**5mm**	**10mm**
3m, 1/4	Width	83%	44%	22%
	Length	3%	2%	1%
3m, 1/2	Width	61%	24%	16%
	Length	3%	2%	1%
3m, 1/1	Width	48%	20%	12%
	Length	3%	2%	1%
5m, 1/4	Width	**N/A**	66%	32%
	Length	**N/A**	4%	3%
5m, 1/2	Width	167%	21%	9%
	Length	**N/A**	2%	2%
5m, 1/1	Width	125%	15%	8%
	Length	1%	3%	1%
7m, 1/4	Width	**N/A**	149%	68%
	Length	**N/A**	4%	6%
7m, 1/2	Width	263%	62%	46%
	Length	**N/A**	3%	9%
7m, 1/1	Width	188%	50%	30%
	Length	**N/A**	3%	1%
Resolution (mm @ 10 m)		**1/4 = 6.3**	**1/2 = 3.1**	**1/1 = 1.6**

N/A: It is not possible to measure the corresponding dimensions for any of the specified cracks' orientations from the scan data in this study.

The given error percentages in Tables 4.16 and 4.17 are compared both within themselves and with each other. Several inferences are made and summarized in Table 4.18 below.

Table 4.18. Results of the Case Study-2

Compared Scans	Findings
1 to 18	• As the scanning distances increases, it becomes challenging to measure dimensions, and measurement error percentages visibly increase (H1).
1, 4 – 2, 5 – 3, 6 7, 10 – 8, 11 – 9, 12 13, 16 – 14, 17 – 15, 18	• Changing the sensitivity settings from High to Normal shortens the scan duration considerably; however, this increases the calculated error percentages. Thus, the Normal option may be suitable for works where approximate calculations are adequate, but it is not for accuracy-related studies (H2).
1, 2 – 2, 3 10, 11 – 11, 12	• The error percentages increase with the decrease in scanning resolution (i.e., changing resolution settings from 1.6 mm to 3.1 mm) (H1).
1 to 18	• Crack widths designed with 1 mm (Ground truth values are around 2 mm) could not be measured with the laser scanner within the 10% acceptable error limit. Therefore, the minimum identifiable size for the cracks with the 10% acceptable error limit is found as 5 mm.
1 to 18 Each Crack Trios in each of the scans	• The calculated *AEP*s of cracks that have the same width but different orientations (e.g., 1 mm, 5 mm, or 10 mm crack widths with 0°, 45°, and 90° in orientations) and scanned with the same sensitivity setting (e.g., High or Normal) do not vary considerably.

Table 4.18 (cont'd)

Compared Scans	Findings
1 to 18 Each Crack Trios in each of the scans	This is because it was observed that for the cracks in different orientations, the highest ratio of the maximum measured width value to the minimum width is 1.3. The specified ratio is considered reasonable for small cracks, such as 2.06 mm, considering the measurement error due to the manual process. Hence, it is concluded that the orientation of the crack does not affect the measurement error rates.

4.3.3 Comparison of the Studies

To verify the laser scanner's representativeness before its usage in the core experiments, the averaged values given in Table 4.16 are compared with the corresponding equivalences in the selected study as follows:

Table 4.19. Difference Between the *AEPs* in Case Study-2 (High Sensitivity) and the Benchmark Study

Comparison of the Studies with Absolute Error Tolerance = 15%				
High Sensitivity & 4X		**1 mm**	**5 mm**	**10 mm**
3 m, 1/4	Width	40%	1%	2%
	Length	7%	0%	0%
3 m, 1/2	Width	**N/A**	1%	1%
	Length	30%	1%	1%
3 m, 1/1	Width	10%	1%	2%
	Length	2%	2%	1%
5 m, 1/4	Width	101%	7%	15%
	Length	28%	15%	14%

Table 4.19 (cont'd)

Comparison of the Studies with Absolute Error Tolerance = 15%				
High Sensitivity & 4X		**1 mm**	**5 mm**	**10 mm**
5 m, 1/2	Width	29%	7%	6%
	Length	5%	1%	1%
5 m, 1/1	Width	3%	2%	11%
	Length	31%	0%	1%
7 m, 1/4	Width	**N/A**	**N/A**	**N/A**
	Length	**N/A**	5%	3%
7 m, 1/2	Width	61%	2%	11%
	Length	65%	1%	35%
7 m, 1/1	Width	38%	12%	9%
	Length	5%	4%	3%
Resolution (mm @ 10 m)		**1/4 = 6.3**	**1/2 = 3.1**	**1/1 = 1.6**
Sensitivity Setting		**High (H)**	**Normal (N)**	**4X**

The values in the above-given Table 4.19 show the difference between the *AEP* values of the identical cases in the studies. In the table, "**N/A**" indicates that it is not possible to measure the corresponding dimension for any of the orientations of the specified crack from the scan data in the benchmarked study. The values in the table were calculated by subtracting the *AEP* values of similar cases in the studies. Then the absolute values of these subtractions are noted as in the table. Throughout the calculations, the absolute error tolerance between the two *AEP* values is considered as a maximum of 15%. Therefore, the deviations of more than 15% are indicated by red fill.

As inferred from Table 4.19, the measurement error percentages for the similar cases are in line with each other in both studies except cracks having 1 mm design width. The reason for this exception can be explained as follows:

- The ground truth values differ from the design values in both cases due to the manual cutting operations.
- The rates of these deviations are different for the studies, as illustrated in Table 4.11 and 4.13 (i.e., in the selected study, the ground truth values are

much closer to the design width value for the 1 mm while in this study, the ground truth values are around 2 mm).

- The measurement error percentages decrease with the increase of crack dimensions.

Moreover, the calculated measurement error for the case of 7 m, and 1/2 (3.1 mm) resolution, is given as 37% in the benchmarked study. Since the same value is calculated as 2% in this study, the error difference has appeared to be 35% in Table 4.19. The value of 37% is much higher than the expected value based on the order of magnitudes for similar cases. The reason may be an unexpected occlusion on the scan data in that specific scan in the benchmarked study, but the exact reasoning has not been known yet since the researchers did not discuss it in their studies. Nevertheless, it is clear that the error value is expected to be around 2-5% under normal conditions.

Apart from these, although the equivalence of the 4X scanning sensitivity setting is the high sensitivity option for the Leica P40, measurements of normal sensitivity and measurements of the selected study (4X) are also compared as follows:

Table 4.20. Difference Between the *AEPs* in Case Study-2 (Normal Sensitivity) and the Benchmark Study

Comparison of the Studies with Absolute Error Tolerance = 15%				
Normal Sensitivity & 4X		**1 mm**	**5 mm**	**10 mm**
3 m, 1/4	Width	12%	34%	13%
	Length	5%	0%	0%
3 m, 1/2	Width	**N/A**	19%	10%
	Length	32%	1%	1%
3 m, 1/1	Width	27%	16%	9%
	Length	1%	0%	1%
5 m, 1/4	Width	**#DIV/0!**	59%	28%
	Length	**#DIV/0!**	1%	2%
5 m, 1/2	Width	100%	17%	2%
	Length	**#DIV/0!**	2%	1%

Table 4.20 (cont'd)

Comparison of the Studies with Absolute Error Tolerance = 15%				
Normal Sensitivity & 4X		**1 mm**	**5 mm**	**10 mm**
5 m, 1/1	Width	61%	7%	5%
	Length	32%	1%	0%
7 m, 1/4	Width	**N/A**	**N/A**	**N/A**
	Length	**N/A**	3%	2%
7 m, 1/2	Width	177%	54%	40%
	Length	**#DIV/0!**	0%	28%
7 m, 1/1	Width	78%	28%	22%
	Length	**#DIV/0!**	2%	3%
Resolution (mm @ 10 m)		**1/4 = 6.3**	**1/2 = 3.1**	**1/1 = 1.6**
Sensitivity Setting		**High (H)**	**Normal (N)**	**4X**

In Table 4.20, the "**#DIV/0!**" implies it is not possible to measure the corresponding dimension for any of the specified crack orientations from the scan data in this study. At the same time, **"N/A"** demonstrates that the same case (the corresponding dimensions for the specified crack in all orientations are undetectable) happens in the selected study.

When Tables 4.19 and 4.20 are compared, it is revealed that the differences between the measured values even for 10 mm cracks with normal sensitivity and the corresponding ground truth values and the error rates of the studies are considerably high (i.e., reach up to 29%). Furthermore, these disparities are understood to be independent of the scanning distance. Therefore, high sensitivity setting should be used in the core experiments, since the main concern is accuracy in this thesis.

The experiments performed in this case study revealed that different combinations of scan parameters cause severe errors in measurement accuracy. Moreover, it is understood that although changing the scanning sensitivity setting from high to normal visibly shortens scan durations, it leads to significant amounts of increase in the *AEP* values. Hence, these measurements are highly sensitive to this setting (H2).

The researchers of the benchmarked study obtained the following findings:

- The measurement error percentages of both width and length measurements show a negative correlation with crack width (H3).
- Using TLS, it is not possible to accurately measure the cracks that are equal to or smaller than 1 mm in width.
- The minimum *AEP*s for the 5 mm cracks are obtained by the best available scanning resolution setting (e.g., 1.5 mm at 10 m scanning distance) at 3 m as 5.63% while, for the 10 mm crack width, it is attained by the scanning resolution of 6.1 mm at 5 m as 3.63%. For the crack lengths, the minimum *AEP* for the 5 mm cracks is acquired with the resolution of 6.1 mm at 7 m as 0.71%, while for the 10 mm ones, it is obtained by the 1.5 mm resolution at 5 m as 0.81%.

In this study, the corresponding findings are as follows:

- The measurement error percentages of both width and length measurements show a negative correlation with crack width as in the benchmarked study (H3).
- Similar to the benchmarked study, using TLS, it was not possible to accurately measure the cracks equal to or smaller than 1 mm width even if the ground truth values were actually larger than 1 mm (on average 2.32 mm) due to handicraft.
- The minimum *AEP*s for the 5 mm and 10 mm cracks are obtained by the best scanning sensitivity setting (e.g., 1.6 mm at 10 m scanning distance) at 3 m as 2.74% and 1.09%, respectively. For the crack lengths, the minimum *AEP* for the 5 mm cracks is acquired with a resolution of 3.1 mm at 7 m as 1.48%, while for the 10 mm ones, it is obtained by the 1.6 mm resolution at 7 m as 1.34%.

Based on the above-given findings, the scan settings which bring minimum *AEPs* in both studies are given in Table 4.21.

Table 4.21. Observed Scan Settings Giving Minimum *AEPs*

		Benchmark Study (Shi & Ergan, 2019)		**This Study (Case Study-2)**	
		Scan Resolution (mm at 10 m)	**Scanning Distance (m)**	**Scan Resolution (mm at 10 m)**	**Scanning Distance (m)**
Crack Width (mm)	5	1.5	3	1.6	3
	10	6.1	5	1.6	3

In the benchmarked study, the researchers assessed the data collection and the analysis processes in terms of time and measurement efficiencies to discuss the effect of scan duration on the data quality. After all, since the researchers realized that changing the scanning resolution from 1.5 mm to 6.1 mm considerably accelerated the data collection process, they suggested that the optimum resolution setting should be 6.1 mm, and the scanning distance should be 5 m for all cases.

Similarly, in this study, it is experienced that scan duration may extensively variate based on the scan settings. For example, for the high sensitivity cases, the difference between the total allocated scan time difference of the scans of 1.6 mm and 6.3 mm was 15 minutes and 45 seconds, whereas the duration for the 6.3 mm was only 1 minute and 8 seconds. Eventually, considering the maximum measurement error as 15% and time-efficiency of laser scanning, it is suggested that the most applicable scanning resolution setting and scanning distance for the cases should be 6.3 mm and 5 m, respectively.

The suggested resolution and scanning distances are given in Table 4.22.

Table 4.22. Suggested Scan Settings According to Scan Duration

	Benchmark Study (Shi & Ergan, 2019)	**This Study (Case Study-2)**
Scanning Resolution (mm at 10 m)	6.1	6.3
Scanning Distance (m)	5	5

Consequently, the laser scanner used in this study (Leica ScanStation P40) is verified for two aspects, (1) the results obtained with it will be representative for the other TLSs in the TOF category, and (2) it can be used for the rest of this thesis without any doubt about the instrument error in data acquisition compared to other TOF laser scanners.

Furthermore, it is verified that the observed scan parameters (e.g., scanning distance and different crack widths and crack orientations) pointedly affect the scan data quality, but we could not have identified the mathematically expressible trend or correlation. Still, based on this verification, it was decided to explore the effects of these variables on scan data quality in different building material types in the next chapter.

CHAPTER 5

CORE EXPERIMENTS ON CRACK IDENTIFICATION

5.1 Introduction

As mentioned before in previous chapters, there is a pressing need to evaluate the material performance on scan data quality of TLS since there is a lack of research and standardization in this subject. The excessive use of TLS, especially for structural health monitoring, has motivated testing the most common building materials used in the buildings in this part of the study. In line with the scope of this study, the specimens with the simulated cracks are used.

Accordingly, this chapter explains the details of the core experiments' design, analysis, and evaluation steps. To this end, (1) the cracks in the specimens of the three most common building materials (RC, wood, and masonry brick) were laser scanned with predetermined scan settings, (2) the acquired scan data were processed to measure the crack dimensions, (3) the corresponding Absolute Error Percentages (*AEP*s) of these measurements were calculated, and (4) these findings were interpreted by various data visualization and comparison methods.

Eventually, the findings obtained in this chapter were used (1) to interpret the individual and the combined effects of different scan parameters (especially those of the target material types) on scan data quality and (2) to define scan data quality as a function of these variables.

5.1.1 Verification of Positioning Methods

As stated in the second part of Chapter 4, two different methods, namely positioning methods, can be used to meet the required incidence angles for the experiments.

In the first method, namely the repositioning method, the target object is moved in the lateral direction, as illustrated in Figure 5.1.

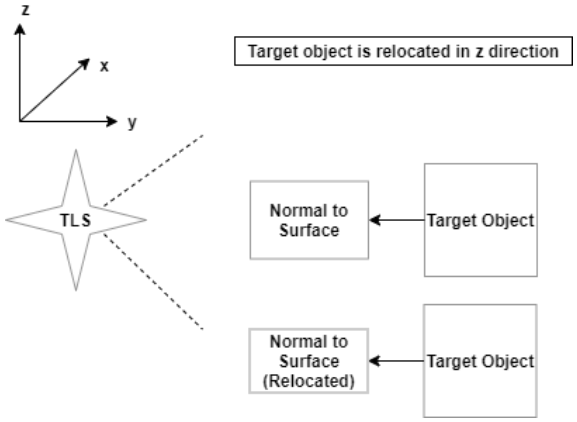

Figure 5.1. Top View of Repositioning Method

In the second method, the target object is rotated instead of repositioning, as shown in Figure 5.2. In this way, the need to have a large area to conduct the experiments is eliminated, and the scanning process is accelerated. For this reason, this method is estimated as superior to the first method, but this estimation should be verified by numerical data analysis.

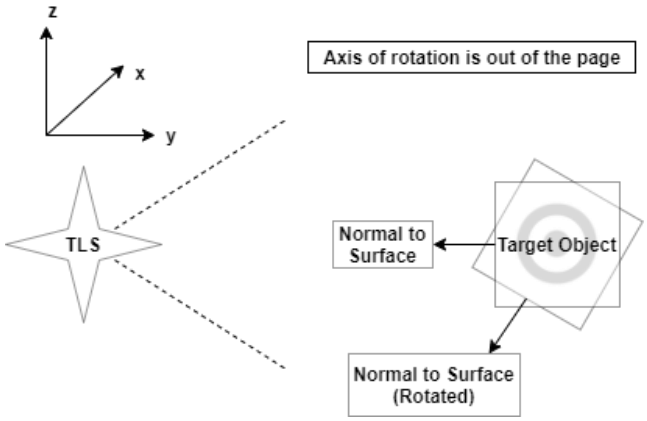

Figure 5.2. Top View of Rotation Method

In theory, these two methods are admitted to be used in crack detection and revealing equally accurate results, but in practice, there is no concrete evidence to prove that (H4). Accordingly, before starting the core experiments, these methods are tested.

Subsequently, two test setups are established. In the first setup, a foam board specimen, which is previously scanned in Chapter 4, is used, as shown in Figure 5.3. In the second one, the RC specimen showed in Figure 5.4 is scanned.

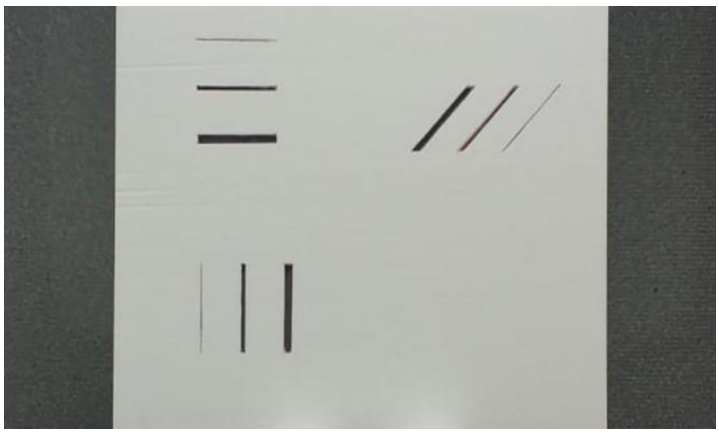

Figure 5.3. Foam Board Specimen*

*The ground truth values of the specimen's crack widths are given in Table 4.13 in Chapter 4.

Figure 5.4. Labeled RC Specimen*

*From top to bottom, the ground truth values of the crack widths on the RC specimen are 11 mm, 7 mm, and 5 mm, respectively.

Both specimens are scanned by deploying the methods mentioned above. Table 5.1 presents the corresponding scan settings for both specimens.

Table 5.1. Parameters Used in Test Setups*

Scan #	Target Material Type	Laser Scanner Location Relative to the Specimen	Method Type	Angle of Incidence (°)
1	RC	Front	Rotation	0
2	RC	Front	Rotation	15
3	RC	Front	Rotation	30
4	RC	Front	Rotation	45
5	Foam Board	Front	Rotation	0
6	Foam Board	Front	Rotation	15
7	Foam Board	Front	Rotation	30
8	Foam Board	Front	Rotation	45
9	RC	Side	Repositioning	15
10	Foam Board	Side	Repositioning	15
11	RC	Side	Repositioning	30
12	Foam Board	Side	Repositioning	30
13	RC	Side	Repositioning	45
14	Foam Board	Side	Repositioning	45

* For all test setups, scanning resolution is set as 0.8 mm at 10 m, scanning distance is held as 5 m, and scanning sensitivity is chosen as high.

In the first setup, simulated cracks on the foam board have constant dimensions, whereas in the RC specimen, the crack width variates through the crack pattern. Hence, to ease the crack widths' measurement by labeling the point of interest on the RC specimen, the Black & White paper targets with a 1 cm diameter given in Figure 5.5 are used.

Figure 5.5. Black & White Target with 1 cm Diameter

After defining the scan setting and labeling the corresponding specimen, scans are conducted following the details given in Table 5.1.

After all, the scan data is imported and analyzed to compare the error performances of the methods. To this end, ten consecutive measurements are taken for each of the widths in each scan. Then, these values are averaged and considered as the measured values of the corresponding widths. Using them and their corresponding ground truth values as input for Equation 4, *AEP* is calculated for each width.

$$AEP_{iy} = \frac{|\, Averaged\ Measured\ Value_{iy} - Exact\ Value_i \,|}{Exact\ Value_i}\ x\ 100 \qquad (Eq.4)$$

Where, AEP_{iy} is the Absolute Error Percentage of the i^{th} crack for the orientation y (y is 1 for 0°, y is 2 for 45°, and y is 3 for 90°), $Averaged\ Measured\ Value_{iy}$ is the cumulative average of the 10 consecutive measurements of the widths at the point of interest, and $Exact\ Value_i$ is the ground truth values of the width of the i^{th} crack.

While calculating these errors in the first setup, the calculated *AEP* of cracks that have the same width but different orientations (i.e., the three of the cracks designed to have 1 mm crack widths with 0°, 45°, and 90° in orientations) the values measured in all orientations are averaged. This is because, based on the measured values, it was observed that for the cracks in different orientations, the highest ratio of the maximum measured width value to the minimum is 1.314 in the worst scenario, which is for the 2.6 mm crack. However, this change does not show a general trend in all cases, and the ratios for wider cracks are lower than 1.314. Hence, the specified ratio is considered reasonable for small cracks, such as 2.6 mm, considering the measurement error due to the manual process. Hence, it is concluded that the width measurement values of cracks in different orientations do not differ considerably.

Therefore, for each crack trio in each scan, their corresponding thirty calculated error percentage values at 0°, 45°, and 90° are averaged using Equation 5. Then, these average values are specified as the *AEP* of these cracks.

$$AEP_i = \frac{AEP_{i1} + AEP_{i2} + AEP_{i3}}{3} \; x \; 100 \qquad (Eq.5)$$

Where, AEP_i is the averaged value for *AEP* values of each simulated crack on the Foam Board having the same width but different orientations.

Since the simulated cracks measurements are performed in only one orientation in the second setup, the average of only ten consecutive measurements is calculated and noted as the *AEP* of the specified width. All the calculated *AEP* are demonstrated in Table 5.2 where **"N/A"** is used to show that the crack width could not be measured for at least one of the orientations (Vertical, Horizontal, or Diagonal).

Table 5.2. *AEPs* in the Comparison of Positioning Method Experiments

Scan #	**Target Material Type**	**Design Crack Widths (mm)**				
		1	**5**	**7**	**10**	**11**
		AEP (%)				
1	RC		7.1	5.7		2.8
2	RC		9.3	6.3		3.8
3	RC		10.1	7.3		2.2
4	RC		11.5	8.3		6.1
5	Foam Board	33.6	11.5		3.9	
6	Foam Board	62.6	13.6		6.4	
7	Foam Board	**N/A**	9.3		5.1	
8	Foam Board	**N/A**	9.4		7.7	
9	RC		10.1	4.9		2.5
10	Foam Board	61.7	8.5		7.6	
11	RC		10.2	6.3		3.2
12	Foam Board	**N/A**	7.3		4.1	
13	RC		13.5	8.3		6.1
14	Foam Board	**N/A**	9.0		7.4	

The **"N/A"** values in the table observed in the smallest possible crack width only. This situation is thought to be due to the inability to perceive the depth on the surface due to the failure of the laser beams to penetrate the crack, depending on the increase in the angle of incidence. For better visualization of the calculated errors, the values are plotted, as shown in Figure 5.6 and 5.7 below.

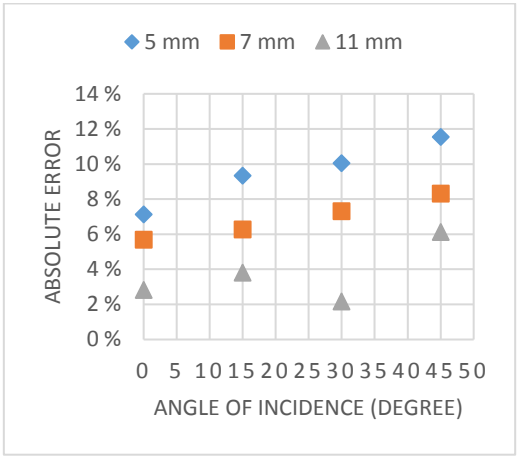

(a) Absolute Error Percentage Plot (Rotation)

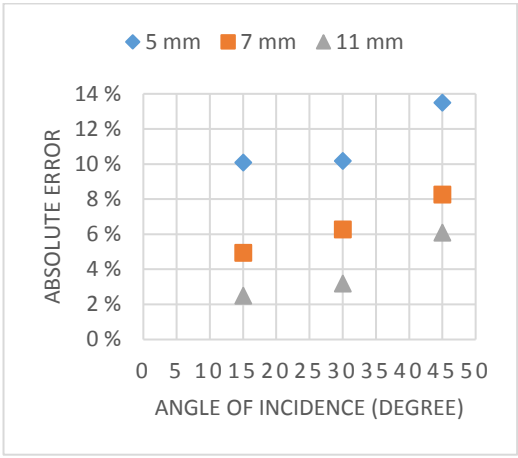

(b) Absolute Error Percentage Plot (Repositioning)

Figure 5.6. *AEP* Plot for RC Specimen

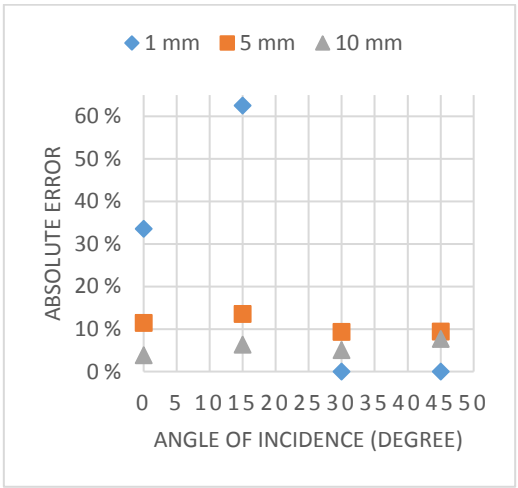

(a) Absolute Error Percentage Plot (Rotation)

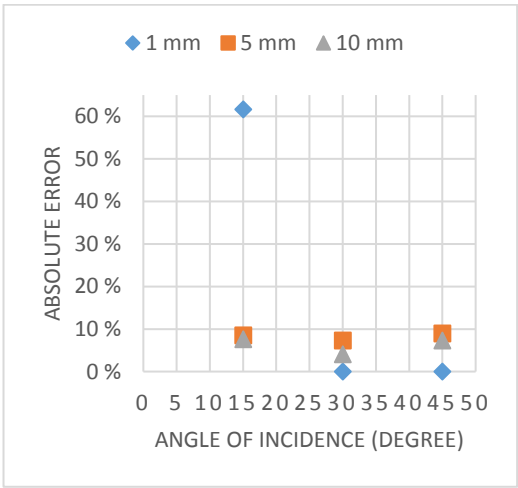

(b) Absolute Error Percentage Plot (Repositioning)

Figure 5.7. *AEP* Plot for Foam Board Specimen

The highest difference between the *AEP*s in the methods deployed under identical scan settings for similar cracks was calculated as 2%, 5.1% in RC, and Foam Board, respectively. Both values appeared in a 5 mm crack (design width). However, when all crack widths and incidence angles are analyzed, the differences are seen to be 1.3% and below. This error percent causes an error of 0.13 mm, even in the largest design width. Moreover, these errors may not be caused by the data, but from the manual labor, as measurements are performed manually. Thus, it is concluded that the calculated errors in both methods are close enough for both material types. Although errors are predicted to occur due to manual labor in crack width measurements, the results are much better than expected. Accordingly, it can be understood that the use of Black & White targets on the RC specimen and the regular and fixed dimensions of the simulated cracks in the Foam Board lead to the minimization of the errors. Still, the simulated cracks of 1 mm width (as a design value) are either identified and measured with errors larger than 30% or could not be identified.

The following observations are also acquired for both test setups:

- The decrease in the crack widths cause an increase in the calculated *AEP*.
- A change in the incidence angle does not cause a substantial increase in the calculated *AEP* within the 5 m range. However, the RC specimen is slightly more sensitive than the Foam Board specimen towards the change in the incidence angle.

Ultimately, it is verified that both methods can be used in meeting the required angle of incidences in the core experiments (H4). Considering the desired scanning ranges up to 10 m, it is decided to use the rotation method in the core experiments.

5.1.2 Selection of Test Environment

After deciding on the positioning method to be utilized, the test environment should be selected appropriately. It is essential because of two conditions; (1) the area must

be free of human action, and the illumination conditions must be constant throughout the scans to reduce the level of noise in the scan data, and (2) there should be enough space to reach 10 m as the maximum scanning distance. The experiments are carried out in a long corridor, illuminated by constant lightning. In this way, the first condition is satisfied. Moreover, particular attention is given to prevent human action while performing scans. The corresponding test atmosphere and the experimental setup are demonstrated in Figure 5.8 (a) and (b).

(a) A Closer Look (b) View from a Distance

Figure 5.8. Test Atmosphere in Core Experiments

5.2 Case Study-1 (Reinforced Concrete)

In this case study, the RC specimen given in Figure 5.9 below, is scanned multiple times with predefined scan settings that will also be used while scanning other building materials.

Figure 5.9. RC Specimen Used in Case Study-1*

*From top to bottom, the ground truth values of the crack widths in the RC specimen are 10.89 mm, 6.92 mm, 5 mm, and 2.98 mm, respectively.

The Black & White target with 1 cm diameter, which is used in the verification of positioning methods, is found inadequate in detecting the crack edges. Therefore, these targets are replaced with those with a diameter of 2 cm. In addition, the number of cracks in the specimen is increased, as shown in Figure 5.9, unlike the setup used in the introduction part of this chapter.

In light of the previous parts' findings, it is decided that the scan settings given in Table 5.3 below are sufficiently appropriate to achieve the objective of the core experiments. The rationale behind the selection of scanning distance and incidence angle values for core experiments are as follows:

- Scanning resolution is defined as 0.8 mm at 10 m, and scanning sensitivity is chosen as high since the study mainly concentrates on crack identification accuracy.
- 0°, 15°, 30°, and 45° are chosen as the angle of the incidence to be tested because values higher than 45° cause a relatively large error amount.

Table 5.3. Parameters Used in Case Study-1, in Core Experiments

Scan #	**Scanning Distance (m)**	**Angle of Incidence (°)**	**Scan Durations (s)**
1	3	0	145
2	3	15	148
3	3	30	131
4	3	45	111
5	5	0	102
6	5	15	100
7	5	30	102
8	5	45	89
9	7	0	85
10	7	15	77
11	7	30	70
12	7	45	65
13	10	0	63
14	10	15	69
15	10	30	63
16	10	45	55

The rest of the case study is carried out in two steps. In the first step, scan data is obtained. Then the data is processed and evaluated.

In the data acquisition part, (1) the instrument is calibrated/leveled up by tightening or loosening the screws to center the built-in bubble indicator to increase the data accuracy, (2) the exact distance to the center of the target object is measured using the device's distance measurement feature to check whether the measured value is the same as the intended value, and (3) the parameters given in the Table 5.3 are employed, and a scan is performed after each modification. At the end of the

experiments performed in this case study, 16 laser scans are obtained: 4 different incidence angles are tested in 4 different scanning distances.

The data processing part is conducted by selecting the edges of the cracked region manually on the point cloud processing software. The procedures in the measurement and selection processes are as follows:

1. Import each scan into the software.
2. Optimize the cloud color by changing the color setting to the Hue/Intensity map. This modification regulates the visual representation of the points according to their normal directions, with different colors. Thus, it eases the selection of the edge points and increases the accuracy of the measurement. The representative change in the view is shown in Figure 5.10.
3. Select the two edges of each crack in the object by providing the maximum amount of zoom-in view.
4. Measure the distances between the chosen points using the software's distance measuring tool with a 2-decimal place precision.

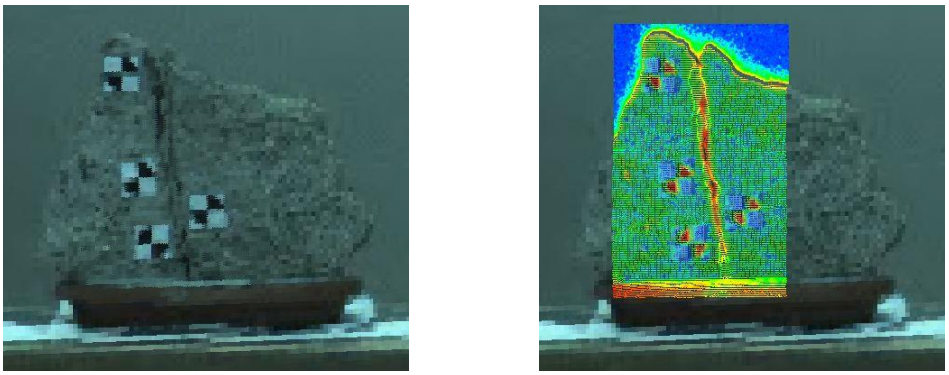

(a) Color from Scanner (b) Hue/Intensity Map Color

Figure 5.10. Representative Change in Colors in Case Study-1

The third and the fourth steps of the procedures repeated ten times in each crack measurement to reduce the manual measurement error to a maximum amount. The total of 10 measured values for each crack width is averaged. At the end of the data processing part, 64 averaged measured values are obtained from 16 laser scans.

Then, the *AEP* of each crack width is calculated using Equation 3. The calculated *AEP* values are noted for later evaluation, as given in Table 5.4.

Table 5.4. *AEPs* in Case Study-1, Core Experiments

RC				***AEP (%)***			
Scan #	**Angle of Incidence (°)**	**Scanning Distance (m)**	**Scan Duration (s)**	**Design Crack Width (mm)**			
				3	**5**	**7**	**11**
1	0	3	145	4.77	3.22	2.24	0.77
2	15	3	148	5.70	3.37	3.42	1.08
3	30	3	131	8.76	5.54	4.71	4.62
4	45	3	111	10.38	8.06	6.25	5.79
5	0	5	102	10.34	7.22	4.27	2.99
6	15	5	100	10.44	8.15	7.26	3.25
7	30	5	102	14.67	9.05	8.91	6.28
8	45	5	89	20.38	13.45	10.32	8.74
9	0	7	85	16.17	11.25	8.23	6.60
10	15	7	77	17.09	10.62	7.90	8.39
11	30	7	70	23.70	14.91	12.23	10.93
12	45	7	65	**#VALUE!**	25.31	14.67	11.71
13	0	10	63	20.14	12.00	8.83	7.07
14	15	10	69	24.83	13.46	9.66	8.39
15	30	10	63	**#VALUE!**	17.86	15.03	11.99
16	45	10	55	**#VALUE!**	28.67	19.69	14.98

#VALUE!: It is not possible to measure the corresponding dimension in the scan data for the specified crack because the crack edges could not be identified in the given configuration. Accordingly, with the given test setup, the detectability ratio for the cracks of RC is calculated as 95.31% (61/64).

In the above-given findings, it is observed that no matter the scan settings are, the cracks are detectable except the 3 mm crack. The maximum error is observed as 28.67%, and it appeared in the 16th scan for the 5 mm crack. The smallest error has arisen in the 1st scan as 0.77% for the 11 mm crack. Further details are presented in Table 5.5.

Table 5.5. Findings of Case Study-1, Core Experiments

Compared Scans	**Findings**
1 to 4 5 to 8 9 to 12 13 to 16	• Regardless of the crack width, as the incidence angle increases, the corresponding *AEP* values also increase (H1). • The *AEP* values of wider cracks are smaller than that of the narrower cracks of the same scan (H3). • The *AEP* values for 0° and 15° of incidence angles are close to each other. The first relatively high increase in the *AEP* values starts while the incidence angle shifts from 15° to 30° for each scanning distance.
1 to 4 (3 m)	• The relative percent increase in the *AEP* value while the incidence angle shifts from 0° to 45° is the highest for the 11 mm crack.
5 to 8 (5 m)	• The relative percent increase in the *AEP* value while the incidence angle shifts from 0° to 45° is the highest for the 11 mm crack, but it has been observed that this rate approaches the average of the relative percent increase of the four crack widths.
9 to 12 (7 m)	• The relative percent increase in the *AEP* value while the incidence angle shifts from 0° to 45° is highest for the 5 mm crack. • The 3 mm crack has become undetectable for the 45° incidence angle.

Table 5.5 (cont'd)

Compared Scans	Findings
13 to 16 (10 m)	• The relative percent increase in the *AEP* value while the incidence angle shifts from 0° to 45° is the highest for the 5 mm crack. • The 3 mm crack has become undetectable for the 30° of incidence angle in addition to the 45°.
1 to 16 (3-10 m)	• *AEP* values increase with increasing scanning distance (H1). • Identifying the edges for the 3 mm and 5 mm cracks becomes challenging, starting from 7 m (H1). Therefore, *AEP* values begin to deviate significantly due to the combined effect of the increase in range and the incidence angle.

In order to further interpret the values given in Table 5.4, a series of dispersion charts covering the whole data set is given in Figure 5.11.

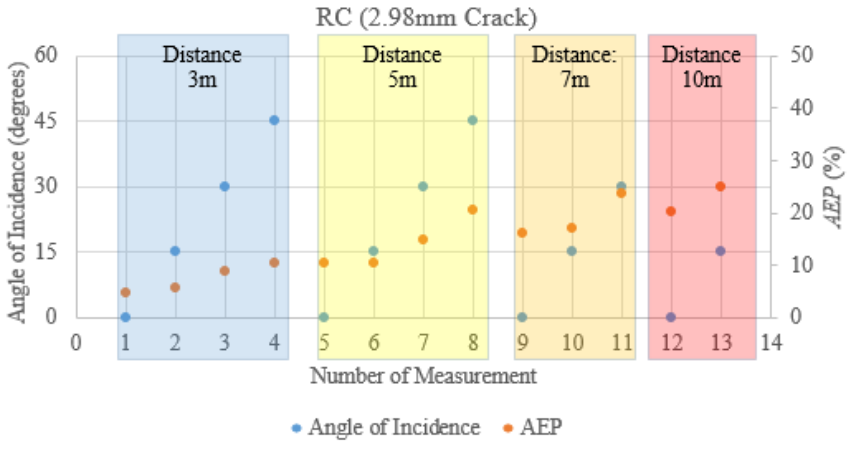

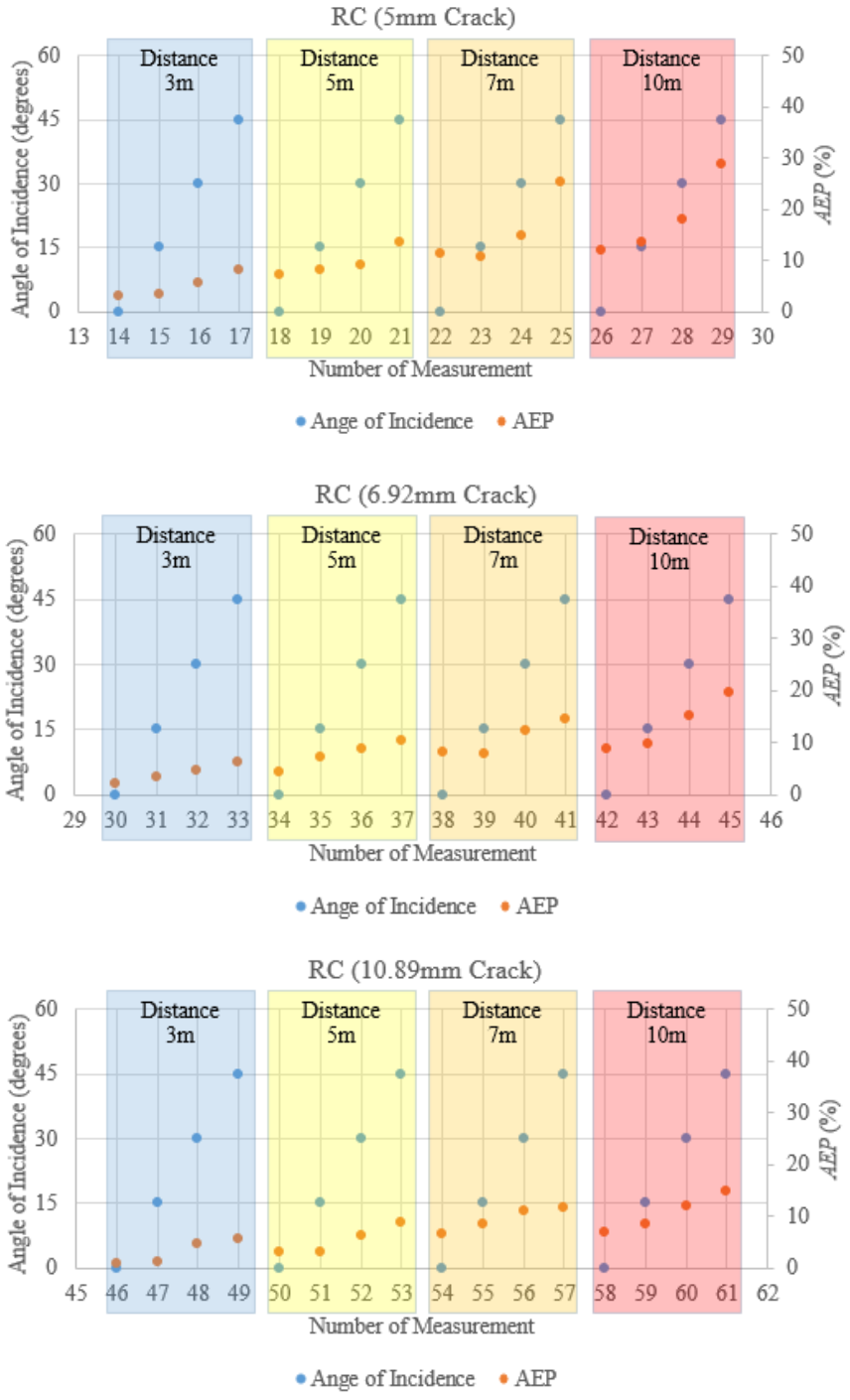

Figure 5.11. Dispersion of Values for RC Specimen

5.3 Case Study-2 (Wooden Material)

In this case study, the wooden specimen given in Figure 5.12 is scanned multiple times following the same scan settings used in the previous section.

Figure 5.12. Wooden Specimen Used in Case Study-2

Two separate wooden parts are assembled using bolts to simulate a crack pattern. Throughout the assembly process, it is intended to simulate the exact design values given in Table 5.6 on the specimen's face. However, they deviated slightly due to manual labor. To quantify these deviations, crack widths are measured with a digital caliper with an accuracy of 0.01 mm. Then, the measurements are noted as the ground truth values, as shown in Table 5.6 below. Moreover, the Black & White targets having 2 cm diameter are used to label the cracks, similar to Case Study-1.

Table 5.6. Design and Ground Truth Values for the Wooden Specimen

Design Crack Width (mm)	**Ground Truth Values (mm)**
6	5.81
4	4.02
2	2.04

Then, the exact data acquisition, data processing, and evaluation steps described in the previous section are followed, respectively.

Consequently, the calculated *AEP* values in this case study are tabulated below.

Table 5.7. *AEPs* in Case Study-2, Core Experiments

Wooden Material				***AEP* (%)**		
Scan #	**Angle of Incidence (°)**	**Scanning Distance (m)**	**Scan Duration (s)**	**Design Crack Width (mm)**		
				2	**4**	**6**
1	0	3	140	1.12	0.78	0.40
2	15	3	123	8.38	1.42	0.91
3	30	3	116	27.77	4.24	3.65
4	45	3	99	34.75	6.64	5.86
5	0	5	80	6.14	4.76	4.10
6	15	5	80	9.79	5.47	4.98
7	30	5	72	24.45	8.58	7.14
8	45	5	72	35.97	10.24	9.10
9	0	7	82	9.31	6.73	4.58
10	15	7	56	16.14	9.67	5.60
11	30	7	67	34.09	16.23	11.06
12	45	7	56	**#VALUE!**	22.14	15.90
13	0	10	53	24.47	17.29	11.03
14	15	10	41	**#VALUE!**	19.37	13.49
15	30	10	47	**#VALUE!**	25.80	17.87
16	45	10	44	**#VALUE!**	30.43	23.01

#VALUE!: It is not possible to measure the corresponding dimension in the scan data for the specified crack because the crack edges could not be identified in the given configuration. Accordingly, with the given test setup, the detectability ratio for the cracks of the wooden material is calculated as 91.67% (44/48).

In the above-given findings, it is observed that no matter the scan settings are, the cracks are detectable except the 2 mm crack. The maximum error is observed as 35.97%, and it appeared in the 8th scan for the 2 mm crack. The smallest error has arisen in the 1st scan as 0.40% for the 6 mm crack. Further details are presented in Table 5.8.

Table 5.8. Findings of Case Study-2, Core Experiments

Compared Scans	**Findings**
1 to 4 5 to 8 9 to 12 13 to 16	• Regardless of the crack width, as the incidence angle increases, the corresponding *AEP* values also increase (H1). • The *AEP* values of wider cracks are smaller than that of the narrower cracks of the same scan (H3). • The *AEP* values for 0° and 15° of incidence angles are close to each other except for the 2 mm crack. The first relatively high increase in the *AEP* values starts while the incidence angle shifts from 15° to 30°.
1 to 4 (3 m)	• The relative percent increase in the *AEP* value while the incidence angle shifts from 0° to 45° is the highest for the 2 mm crack.
5 to 8 (5 m)	• The relative percent increase in the *AEP* value while the incidence angle shifts from 0° to 45° is the highest for the 2 mm crack, but it has been observed that this rate approaches the average of the relative percent increase of the three crack widths.
9 to 12 (7 m)	• The relative percent increase in the *AEP* value while the incidence angle shifts from 0° to 45° is the highest for the 2 mm crack.

Table 5.8 (cont'd)

Compared Scans	**Findings**
9 to 12 (7 m)	• The 2 mm crack has become undetectable for the 45° incidence angle.
13 to 16 (10 m)	• The highest relative percent increase in the *AEP* value while the incidence angle changed from 0° to 45°, has shifted towards the greatest one, 6 mm crack. • The 2 mm crack has become undetectable for the 15°, and 30° of incidence angles in addition to the 45°.
1 to 16 (3-10 m)	• *AEP* values increase with increasing scanning distance (H1). • Identifying the edges for the 2 mm and 4 mm cracks becomes challenging, starting from 7 m (H1). Therefore, *AEP* values begin to deviate significantly due to the combined effect of the increase in range and incidence angle.

In order to further interpret the values given in Table 5.7, a series of dispersion charts covering the whole data set are given in Figure 5.13.

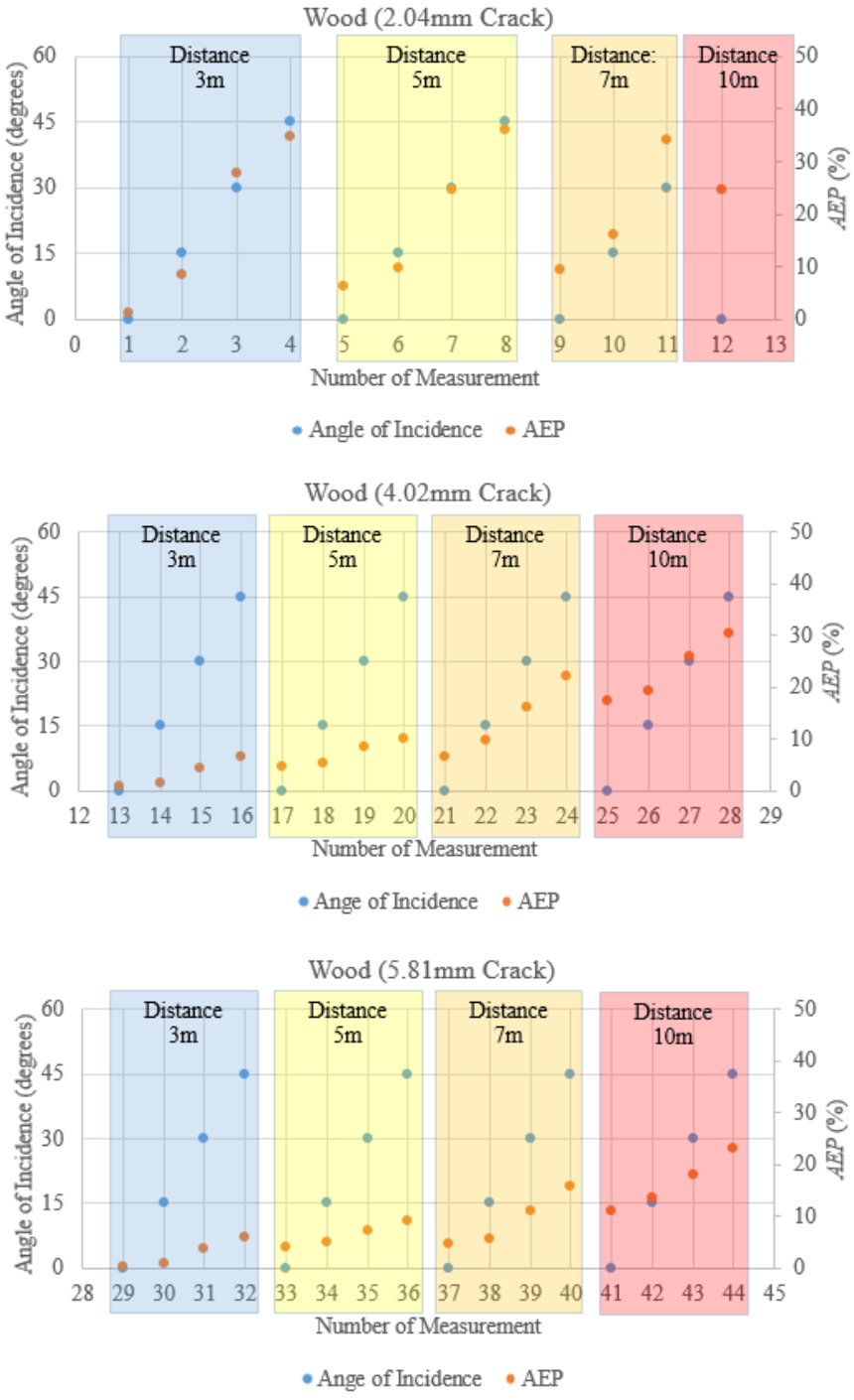

Figure 5.13. Dispersion of Values for Wooden Specimen

5.4 Case Study-3 (Masonry Brick)

In this case study, the masonry brick specimen given in Figure 5.14 is scanned multiple times following the same scan settings used in the previous case studies.

(a) Front Face of the Specimen (b) Back Face of the Specimen

Figure 5.14. Masonry Brick Specimen Used in Case Study-3

Two separate pieces of bricks are put together in a tray, and they are stabilized by using mortar to simulate the desired crack pattern. Throughout the fixation process, it is intended to simulate the exact design values given in Table 5.10 on the specimen's faces, but they deviated slightly due to manual labor. To quantify these deviations, crack widths are measured with a digital caliper with an accuracy of 0.01 mm. Then the measurements are noted as the ground truth values, as shown in Table 5.9 below. Moreover, the Black & White targets having 2 cm diameter are used to label the cracks as similar to the first and second case studies.

Table 5.9. Ground Truth Values for the Wooden Specimen

Design Crack Width (mm)	Ground Truth Values (mm)
11	12.2
7	8
5	5.7

Then, the exact data acquisition, data processing, and evaluation steps described in Case Study-1 are followed, respectively. Consequently, the calculated *AEP* values in this case study are tabulated in Table 5.10.

Table 5.10. *AEPs* in Case Study-3, Core Experiments*

Masonry Brick					***AEP* (%)**		
Scan #	**Angle of Incidence (°)**	**Scanning Distance (m)**	**Scan Duration (s)**		**Design Crack Width (mm)**		
			Front	**Back**	**5**	**7**	**11**
1	0	3	108	109	2.07	1.54	0.22
2	15	3	110	114	2.53	1.72	0.31
3	30	3	106	94	5.05	3.06	2.51
4	45	3	111	112	6.53	4.93	3.56
5	0	5	76	63	5.89	4.53	3.86
6	15	5	64	73	6.43	5.18	4.15
7	30	5	66	72	9.41	6.95	5.35
8	45	5	70	68	11.54	9.06	5.77
9	0	7	65	58	8.68	6.07	5.22
10	15	7	65	55	10.18	10.15	7.06
11	30	7	60	53	13.32	12.19	9.76
12	45	7	53	54	17.90	14.42	11.36
13	0	10	49	44	14.09	10.98	10.55
14	15	10	58	43	16.29	12.26	11.26
15	30	10	47	47	22.41	15.53	14.24
16	45	10	45	48	30.29	25.61	17.70

* With the given test setup, the detectability ratio for the cracks of plaster coated RC material is calculated as 100% (48/48).

In the above-given findings, it is observed that no matter the scan settings are, the cracks are detectable. The maximum error is observed as 30.29%, and it appeared in the 16th scan for the 5 mm crack. The smallest error has arisen in the 1st scan as 0.22% for the 11 mm crack. Further details are presented in Table 5.11.

Table 5.11. Findings of Case Study-3, Core Experiments

Compared Scans	**Findings**
1 to 4 5 to 8 9 to 12 13 to 16	• Regardless of the crack width, as the incidence angle increases, the corresponding *AEP* values also increase (H1). • The *AEP* values of wider cracks are smaller than that of the narrower cracks of the same scan (H3). • The *AEP* values for 0°-15° and 30°-45° of incidence angle are close to each other. The only exception is the 7 mm crack at a 10 m. • The first relatively high increase in the *AEP* values starts while the incidence angle shifts from 30° to 45° at 10 m.
1 to 4 (3 m)	• The relative percent increase in the *AEP* value while the incidence angle shifts from 0° to 45° is the highest for the 11 mm crack.
5 to 8 (5 m)	• The relative percent increase in the *AEP* value while the incidence angle shifts from 0° to 45° is the highest for the 7 mm crack.
9 to 12 (7 m)	• The relative percent increase in the *AEP* value while the incidence angle shifts from 0° to 45° is the highest for the 7 mm crack, but the rates are close to each other for the three cracks. • All the cracks are still detectable.

Table 5.11 (cont'd)

Compared Scans	Findings
13 to 16 (10 m)	• The relative percent increase in the *AEP* value is the highest for the 7 mm crack. • All the cracks are still detectable.
1 to 16 (3-10 m)	• *AEP* values increase with increasing scanning distance (H1). • Identifying the crack edges of 5 mm is compelling only in the 10 m 45° case, but it is still detectable. There was no problem regarding this issue in wider cracks.

To further interpret the values given in Table 5.10, a series of dispersion charts covering the whole data set are given in Figure 5.15.

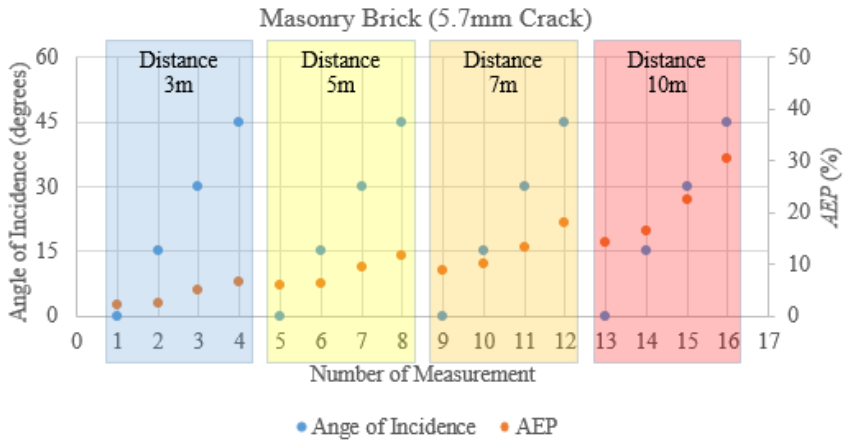

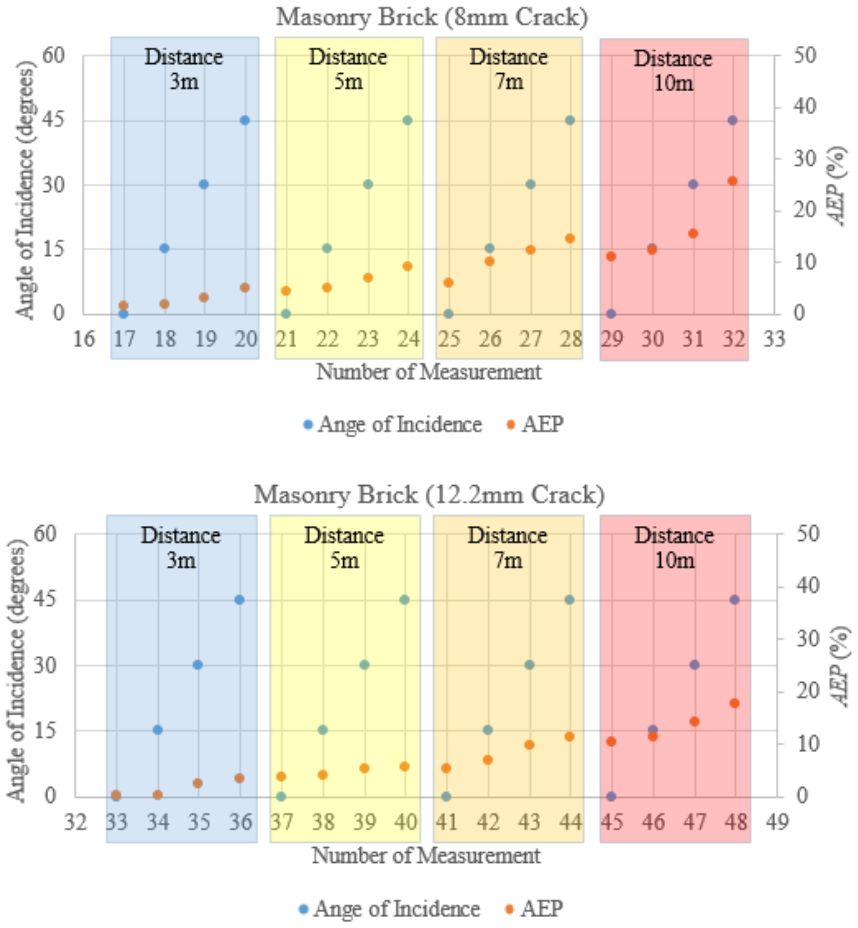

Figure 5.15. Dispersion of Values for Masonry Brick Specimen

5.5 Comparison of the Case Studies

This part of the study is dedicated to comparing the findings obtained in the cases mentioned above. The comparative analysis aims to obtain inferences about the error performance of the material difference in identifying cracks with TLS technology. For this purpose, (1) the order of magnitudes for the calculated error of the measured crack widths are specified for each of the material types, (2) the error performance of each material is discussed by associating it with the materials' error trends given in the first step, (3) the *AEP* values calculated for cracks on different building materials in the previous sections are compared based on the magnitudes, and (4)

inferences about the conditions in which the materials give the best results are presented.

As mentioned in literature review chapter of the study, the adopted crack width limit states differ for each building material. Therefore, cracks on each material are simulated following the recommendations indicated in the specifications (Anagnostopoulos et al., 2004; Baggio et al., 2007). This situation led to the necessity of testing different widths, sometimes identical, and sometimes different from each other in the case studies. For this reason, only the similar/comparable crack widths of different building materials are considered when evaluating the relative performances of them. Besides, the error trend in the crack widths, which are not subjected to comparisons since they are different in magnitudes, is used to assess each material's error performance.

In the first case study in which the RC specimen is scanned, the error performance of four different crack widths (10.89 mm, 6.92 mm, 5 mm, and 2.98 mm) is observed. In the second case study, a wooden sample with 5.81 mm, 4.02 mm, and 2.04 mm of cracks is scanned, and the corresponding measurement errors are examined. In the third case study, a masonry brick's error performance with a crack width of 12.2 mm, 8 mm, and 5.7 mm is scrutinized.

The order of magnitudes of the error in crack width measurements for the RC, wooden, and masonry brick specimens are as follows:

Table 5.12. Order of Magnitudes of Error for the RC Specimen

Crack Width (mm)	**Scanning Distance (m)**			
	3	**5**	**7**	**10**
	Error Percent Average (%)			
10.8	3.06	5.32	9.41	10.61
6.92	4.15	7.69	10.76	13.30
5	5.05	9.47	15.52	18.00
2.98	7.40	13.96	**18.99**	**22.49**

Table 5.13. Order of Magnitudes of Error for the Wooden Specimen

Crack Width (mm)	**Scanning Distance (m)**			
	3	**5**	**7**	**10**
	Error Percent Average			
5.81	2.70	6.33	9.28	16.35
4.02	3.27	7.27	13.69	23.22
2.04	18.01	19.09	**19.85**	**24.47**

Table 5.14. Order of Magnitudes of Error for the Masonry Brick Specimen

Crack Width (mm)	**Scanning Distance (m)**			
	3	**5**	**7**	**10**
	Error Percent Average			
12.2	1.65	4.78	8.35	13.44
8.0	2.81	6.43	10.71	16.10
5.7	4.05	8.32	12.52	20.77

The values in Tables 5.12, 5.13, and 5.14 are calculated by taking the average of the *AEP* values calculated for four different incidence angles at a fixed distance for each of the crack widths. Averaging the values aims to discuss the effect of material type on the scan data quality regardless of the incidence angle by decomposing error margin resulting from angle of incidence. Thus, the error performances are simplified and shown in the above tables. Measurements could not be taken for one or more incidence angles in the cases where the values indicated by bold in the table. Therefore, these values should be higher if the missing ones are also added to the averaging process since they will be calculated for the two farthest possible scanning distances.

While measuring the crack widths in the point cloud software, the crack boundaries can be easily perceived in some of the materials, while in others, the crack edges are quite challenging to detect. Therefore, the error performances of the materials are evaluated from two different aspects: detectability and accuracy.

When the values given in Table 5.12 are analyzed, it is realized that even in the worst scenario for 10.8 mm crack width, the error rates were 10.61%. Likewise, the 6.92

mm crack has a 13.30% error in the worst case. The 5 mm crack's error values were 18%, just above the acceptable limit of 15% error rate, for 10 m range, but up to 7 m, its error rates were still within the acceptable limits. On the other hand, the 2.98 mm crack only has acceptable error rates up to a range of 5 m. This crack's error rates considerably increase with an increase in the scanning range and angle of incidences beyond 5 m.

The crack edges for the 10.8 mm crack could be precisely distinguished in all scans. However, the ones of the 6.92 mm crack were hardly detected in the scans of 10 m 30° and 10 m 45°. The crack edges of 5 mm have become hardly noticeable in the scans of 7 m 45°, 10 m 30°, and 10 m 45°. Moreover, the crack edges of the 2.98 mm crack could not be detected in the same scans.

Examining the values given in Table 5.13, it is understood that even in the worst scenario for 5.81 mm crack width, the error rates were 16.35%. The error values of the 4.02 mm crack were 23.22%, which is above the acceptable limit of 15% error rate for 10 m range, but up to 7 m, its error rates were still within the acceptable limits. On the other hand, the 2.04 mm crack always has an excessive error rate. Its error rate starts with 18.01% and considerably increases with an increase in the range and angle of incidences beyond the closest available distance of 3 m.

The crack edges for the 5.81 mm and 4.02 mm cracks could be precisely distinguished in all scans except for the 10 m 45° case. However, the crack edges of the 2.04 mm crack have become hardly noticeable, starting from the scan of 7 m 30° of the angle of incidence. Furthermore, its crack edges could not be detected in the scans of 7 m 45°, 10 m 15°, 10 m 30°, and 10 m 45°.

Finally, when the values given in Table 5.14 were evaluated, the 12.2 mm crack was found to be 13.44%, even under conditions where the highest error could occur. The error values of the 8 mm crack were slightly above the acceptable limit of 15%. Even the error rates in the smallest alternative, the 5.70 mm crack, were within the acceptable limits up to 7 m range. The rates of this crack raised to 20.77% in the 10 m cases.

The crack edges for the 12.2 mm, 8 mm, and 5.7 mm cracks could be precisely detected in all scans except for the scan of 10 m 45°. In this scan, it became harder to detect the crack edges, but they were still identifiable.

To compare the error performance of the materials, it is necessary to determine the crack widths comparable in magnitude in all materials. A part of the cracks in the RC specimen (10.8 mm, 6.92 mm, 5 mm), the wooden specimen (5.81 mm, 4.02 mm), and the masonry brick specimen (12.2 mm, 8 mm, 5.7 mm) could be compared with each other to make inferences on the material base error performances where the remaining ones in RC specimen (2.98 mm), and the wooden specimen (2.04 mm) could be used in assessing the error performance of the related material only.

Although the design crack widths for the RC specimen and the masonry brick specimen are identical, the cracks in masonry brick are wider than those in the RC. More specifically, the corresponding rates are 14%, 16.71%, and 12.96% for the design widths of 5 mm, 7 mm, and 11 mm, respectively. For this reason, in a scan performed under the same conditions (same scanning distance and angle of incidence), lower error rates are expected for the cracks in masonry brick than those in the RC specimen with the same design width (H3). However, the findings show that the error rates in the RC specimen and the masonry brick specimen are relatively close to each other since the max percent differences between the error rates of the cracks in RC and masonry brick are 2.82%, 2.60%, and 2.87% for 5 mm, 7 mm, and 10 mm cracks. Thus, it is concluded that the RC specimen has lower error rates than the masonry brick under identical scan conditions.

The design crack widths of the wooden specimen are relatively small compared with the masonry brick and RC specimens. Even so, it has cracks (5.81 mm, 4.02 mm) that can be comparable with the ones in the RC specimen (5 mm, 2.98 mm) and the masonry brick specimen (5.7 mm).

In the scans before 7m 30°, the differences between the error rates of the cracks in the RC and wooden specimen go up to 4.52%, in favor of the wooden specimen. However, it is an unexpected consequence since the width of the crack in the wooden

specimen (4.02 mm) is smaller than the one in the RC (5 mm) specimen. These differences revealed that up to this point, the wooden sample has lower error rates. However, starting with the scan at 7 m 30°, the RC specimen started to show up lower error rates, and the difference between the error rates of the cracks of two specimen goes up to 7.94%, in favor of RC, unlike the previous ones. As can be inferred, the crack width in the wooden specimen is 24.38% smaller than the one in the RC. Therefore, it is expected that this crack will be less detectable (H3). This expectation is partially supported by the findings, especially at far distances such as 7 m and 10 m. Nevertheless, having a narrower crack width has not created any detectability issue at relatively closer distances (3 m, 5 m, and partially 7 m) for wooden specimen compared to RC.

When the error values of the 5.81 mm crack in the wooded specimen and the 5.7 mm crack in the masonry brick specimen were compared, lower error rates were observed in the wooded specimen. The findings obtained from comparing the wooden specimen with the RC specimen and the masonry brick specimen are analyzed, and it is concluded that the wooden specimen has lower error rates than the other two specimens. Thus, the pairwise comparisons proved that the scan data quality varies based on the scanned material type (H1). Although the wooden specimen has a complex texture, the surface smoothness is thought to provide a great advantage to this sample regarding the crack edges' detectability when using TLS since the point cloud data is formed relying on the surface depth variations (H5).

Eventually, it is decided to conduct an additional case study to verify whether the surface smoothness is the real cause of the obtained result. In this case study, the RC specimen’s surface is leveled by coating it with satin plaster. Then, this modified specimen is scanned with the scan settings used in the previous case studies, and the findings are compared with those of others. Details of the additional case study are discussed in the next section.

5.6 Case Study-4 (Plaster Coated RC)

In this case study, the satin plaster coated RC specimen given in Figure 5.16 is scanned multiple times following the same scan settings used in the previous case studies.

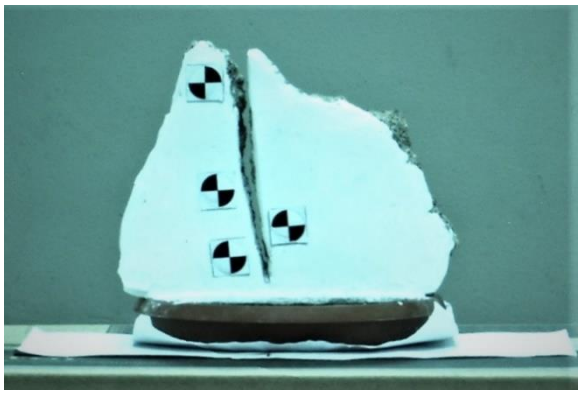

Figure 5.16. Satin Plaster Coated RC Specimen Used in Case Study-4

Based on the inference mentioned in comparing the case studies, the RC specimen is coated with satin plaster to smoothen its surface. By doing so, it is hypothesized that the identification of cracks will become easier, and the calculated *AEP* values will be lower compared to the identical scans of Case Study-1 (H5). The crack widths become relatively narrower than those in the RC specimen without a plaster cover since the satin plaster cover causes thickening around the edges. The corresponding ground truth values of the crack widths are measured with the digital caliper and given in Table 5.15. Moreover, the Black & White paper targets identical to those used in the previous case studies are also used in this case study.

Table 5.15. Ground Truth Values for the Satin Plaster Coated RC specimen

Design Crack Width (mm)	Ground Truth Values (mm)
11	10.80
7	6.85
5	4.98
3	2.94

Then, data acquisition, processing, and evaluation processes described in the first case study are followed precisely in this case study. Consequently, the calculated *AEP* values in this case study are tabulated in Table 5.16.

Table 5.16. *AEPs* in Case Study-4, Core Experiments*

Plaster Coated RC				***AEP (%)***			
Scan #	**Angle of Incidence (°)**	**Scanning Distance (m)**	**Scan Duration (s)**	**Design Crack Width (mm)**			
				3	**5**	**7**	**11**
1	0	3	144	6.13	5.47	1.20	0.45
2	15	3	130	9.16	6.08	2.11	0.72
3	30	3	133	12.32	10.75	3.48	3.95
4	45	3	125	15.63	11.70	4.65	3.97
5	0	5	95	13.71	7.84	3.06	0.83
6	15	5	92	14.40	9.89	4.23	1.46
7	30	5	81	16.49	11.91	5.84	3.23
8	45	5	70	22.56	14.64	6.87	3.95
9	0	7	62	17.47	11.53	4.46	4.50
10	15	7	72	19.33	11.92	6.73	5.10
11	30	7	64	23.18	13.35	7.63	8.15
12	45	7	64	30.25	16.63	11.40	8.30
13	0	10	65	20.79	14.99	7.35	5.55
14	15	10	59	23.29	16.35	8.56	6.10
15	30	10	59	32.62	19.63	10.72	8.61
16	45	10	59	41.74	22.07	11.28	9.95

***** With the given test setup, the detectability ratio for the cracks of plaster coated RC material is calculated as 100% (64/64).

In the above-given findings, it is observed that no matter the scan settings are, the cracks are detectable. The maximum error is observed as 41.71%, and it appeared in the 16th scan for the 3 mm crack. The smallest error has arisen in the 1st scan as 0.45% for the 11 mm crack. Further details are presented in Table 5.17.

Table 5.17. Findings of Case Study-4, Core Experiments

Compared Scans	**Findings**
1 to 4 5 to 8 9 to 12 13 to 16	• Regardless of the crack width, as the incidence angle increases, the corresponding *AEP* values also increase (H1). • The *AEP* values of wider cracks are smaller than that of the narrower cracks of the same scan (H3). • The *AEP* values for 0°-15° and 30°-45° of incidence angle are close to each other. The only exception is the 3 mm crack, especially at 7 m and 10 m. • The first relatively high increase in the *AEP* values starts while the incidence angle shifts from 30° to 45° at 10 m.
1 to 4 (3 m)	• The relative percent increase in the *AEP* value while the incidence angle shifts from 0° to 45° is the highest for the 11 mm crack.
5 to 8 (5 m)	• The relative percent increase in the *AEP* value while the incidence angle shifts from 0° to 45° is the highest for the 11 mm crack.
9 to 12 (7 m)	• The relative percent increase in the *AEP* value while the incidence angle shifts from 0° to 45° is the highest for the 7 mm crack.

Table 5.17 (cont'd)

Compared Scans	Findings
13 to 16 (10 m)	• The relative percent increase in the *AEP* value while the incidence angle changed from 0° to 45°, has shifted towards the smallest one, 3 mm crack.
1 to 16 (3-10 m)	• *AEP* values increase with increasing scanning distance (H1). • All the cracks stand identifiable through the test range. However, for the 3 mm and 5 mm cracks, the *AEP* values significantly deviate due to the combined effect of the range and incidence angle increase.

As mentioned earlier, this case study aims to confirm the predicted cause of the findings from comparisons of previous case studies. For this purpose, the *AEP* values obtained in this case study are compared with those obtained in the first case study.

As a result of the comparison, two outcomes have been obtained: (1) coating the specimen's surface with satin plaster makes cracks more identifiable (H5) as in Figure 5.17, and (2) it considerably reduces the calculated *AEP* values of the cracks especially of the relatively larger ones such as the cracks of 7 mm and 11 mm.

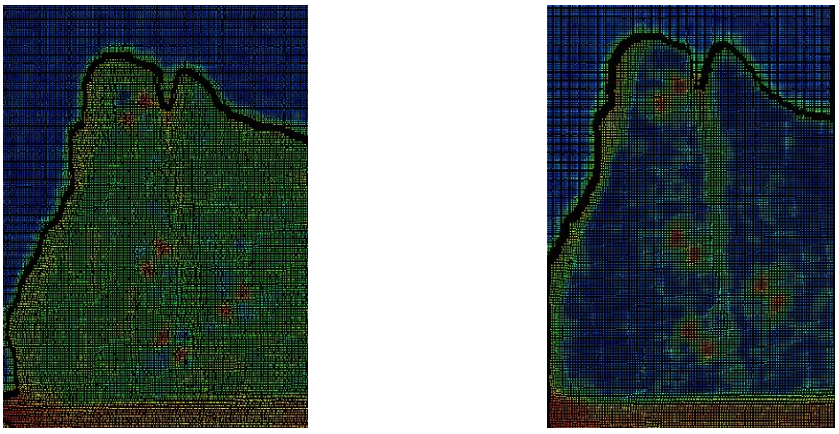

(a) View from RC specimen (b) View from coated RC specimen

Figure 5.17. Crack Views at 10 m and 30° Incidence Angle

Nevertheless, in the specimen coated with satin plaster, the *AEP* value of the 3 mm crack is measured relatively higher at 3 m and 5 m compared to the RC specimen. The maximum percent difference between the *AEP* values of the two materials' cases is noted as 5.26% at the 3 m 45° case. Furthermore, the average *AEP* value for the cases of 3 m and 5 m is noted as 3.12%. Since the crack width measurements are performed via manual operations, these findings are considered as outliers, and they do not affect the general trend of plaster coating on error performance. Thus, it is concluded that coating the specimen with a rough/irregular surface with satin plaster provides benefits on the measurement accuracy and detectability (H5).

In order to further interpret the values given in Table 5.16, a series of dispersion charts covering the whole data set are given in Figure 5.18.

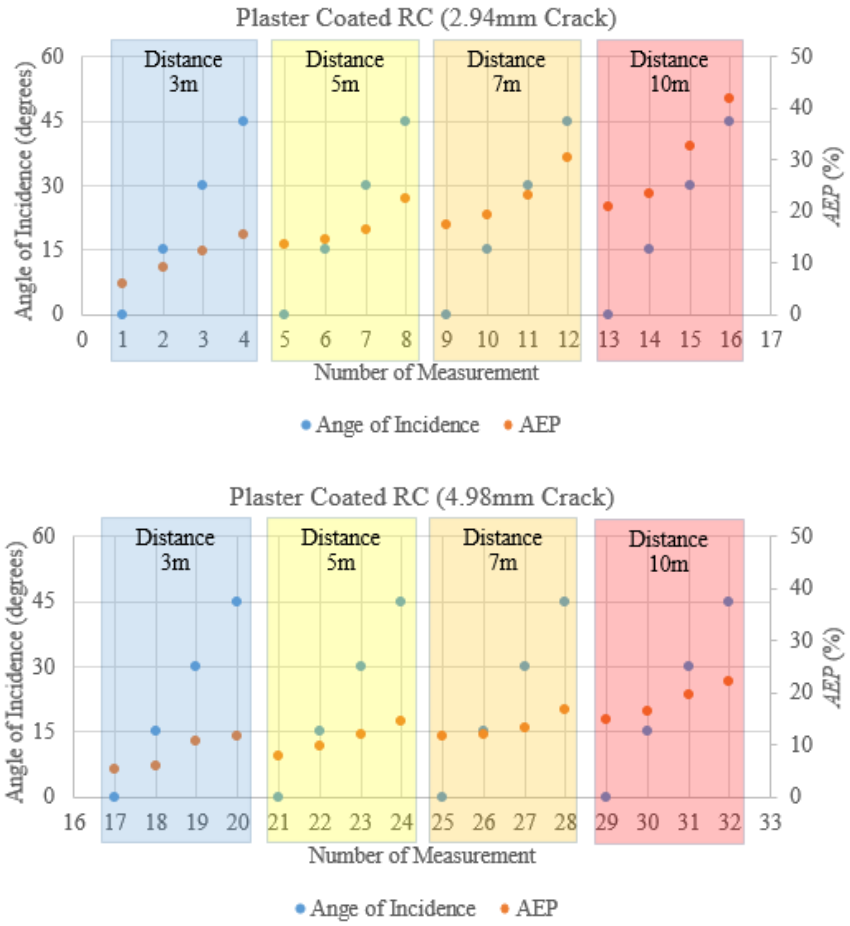

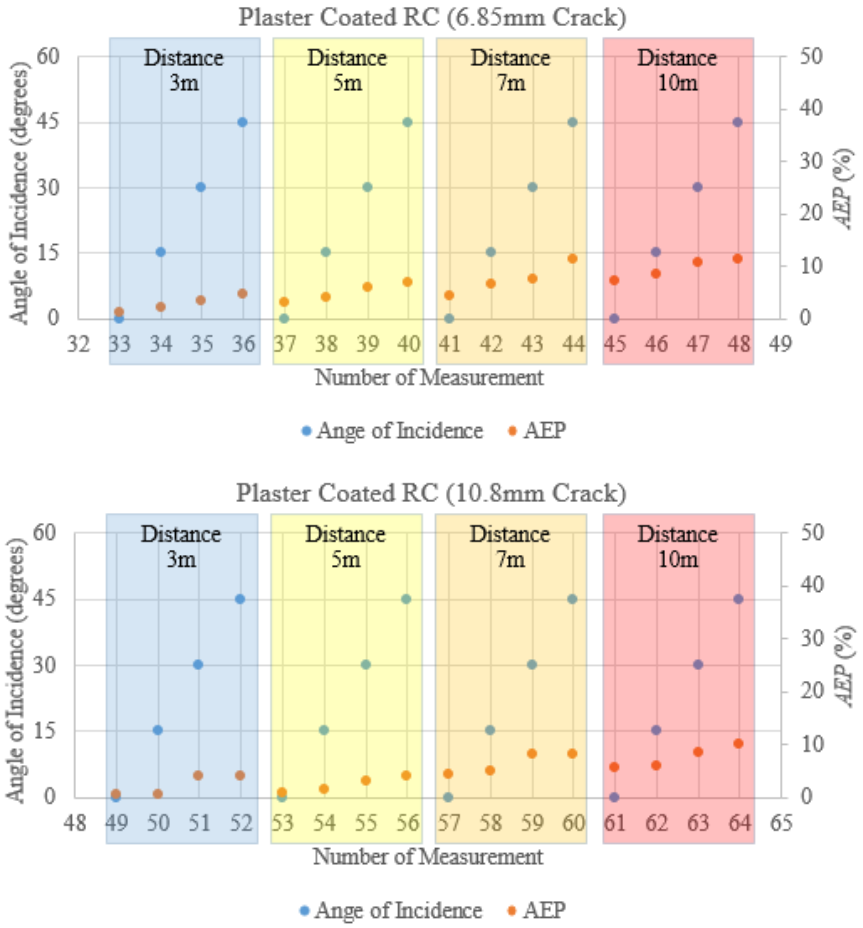

Figure 5.18. Dispersion of Values for Plaster Coated RC Specimen

5.7 Prediction of Unidentified Values and Derivation of Error Estimation Equations

As mentioned in the previous parts, in several cases, the detection of the crack edges and, therefore, the calculation of the corresponding *AEP* values was not possible using the data analysis method described in this thesis. Nevertheless, it is believed that these values can be measured with the help of computer-based automatic data processing algorithms since the data is not thoroughly corrupted.

Although the *AEP* values calculated for the rest are sufficient to conclude on each material's error tendency, the imputation of the missing data could still be possible through statistical data analysis methods.

To this end, in this part, (1) the error estimation equation for each of the material types is derived as a function of crack width, scanning distance, and incidence angles by employing Multiple Linear Regression (MLR), (2) the missing *AEP* values are estimated using the derived equations, and (3) the goodness of fit of the scan data to the derived equations is discussed.

Even though the volume of scan data seems inadequate to conduct an MLR, the data quality (showing a particular trend) enables the process. Therefore, it was deemed appropriate to perform the analysis.

The analysis is carried out in four steps:

- The whole data set is cleared of data related to the parts where the measurement could not be taken.
- The analysis is carried out, and the corresponding error equation is derived.
- The previous two steps are repeated for each specimen used in the case studies.
- The significance of the variables included in the equation is discussed by conducting p-value based hypothesis testing.

Before conducting the regressing analysis, the following null hypothesis (H_0) and the alternative hypothesis (H_1) are developed to be tested:

Null Hypothesis (H_0): For each building material, the *AEP* estimation equation cannot be derived as a function of crack width, scanning distance, and angle of incidence.

Research/Alternative Hypothesis (H_1): For each building material, the *AEP* estimation equation can be derived as a function of crack width, scanning distance, and angle of incidence.

The regression statistics obtained from the MLR on the dataset of each material are given in Table 5.18.

Table 5.18. Regression Statistics Obtained by MLR for Each Material Type

Material Type	Multiple R	R Squared	Adjusted R Squared	Standard Error	Observations
RC	0.898	0.806	0.796	2.802	61
Wood	0.871	0.758	0.740	5.096	44
Masonry Brick	0.950	0.903	0.896	2.083	48
Plaster Coated RC	0.888	0.789	0.778	3.831	64

Based on the attained results of the analyses, the derived error prediction equations are given below in the following format $EP_{XX} = f(W, D, \theta)$:

Where,

- XX stands for the material type
- W stands for the crack width (mm)
- D stands for the scanning distance (m)
- θ stands for the incidence angle (°)

$$EP_{RC} = |3.973 - 1.074 * \mathrm{W} + 1.633 * \mathrm{D} + 0.166 * \theta| \quad \textit{(Eq.6)}$$

$$EP_{Wood} = |7.586 - 3.693 * \mathrm{W} + 2.21 * \mathrm{D} + 0.336 * \theta| \quad \textit{(Eq.7)}$$

$$EP_{Masonry\ Brick} = |-1.34 - 0.645 * \mathrm{W} + 1.997 * \mathrm{D} + 0.16 * \theta| \quad \textit{(Eq.8)}$$

$$EP_{Coated\ RC} = |10.273 - 1.892 * \mathrm{W} + 1.471 * \mathrm{D} + 0.157 * \theta| \quad \textit{(Eq.9)}$$

Since the error values can be calculated in all cases for coated RC and masonry brick, only the unidentified error values of RC and wooden specimen are estimated using

Equations 6 and 7, respectively. The corresponding absolute error values and scan details are given in Table 5.19.

Table 5.19. Estimated Error Values for RC and Wooden Specimen

Material Type	**Crack Width (mm)**	**Scanning Distance (m)**	**Angle of Incidence (°)**	**Estimated *AEP* *(%)***
RC	2.98	7	45	19.67
	2.98	10	30	22.08
	2.98	10	45	24.57
Wood	2.04	7	45	30.64
	2.04	10	15	27.19
	2.04	10	30	32.23
	2.04	10	45	37.27

Finally, it is necessary to discuss (1) to what extent the derived equations represent the dataset, (2) the ranges in which they are valid, (3) how significant the variables are in the equation, and (4) whether the null hypothesis is rejected or accepted based on the findings.

Statistically, R-squared (R^2) value is defined as the rate of change in the dependent variable that can be predicted through independent variables. This value is one of the goodness-of-fit measures on how well the model (the equations for our case) derived following a regression analysis fits the data (Joseph F. Hair et al., 2017). Typically, the higher R^2 values indicate higher model accuracy. Authorities state that deciding the goodness-of-fit based on the adjusted R^2 value rather than the R^2 value itself is more appropriate (Joseph F. Hair et al., 2017). Moreover, acceptable R^2 values vary according to the research scope and the purpose of the analysis (Joseph F. Hair et al., 2013). For example, Chin (1998) labels R^2 values of 0.67, 0.33, and 0.19 as substantial, moderate, and weak, respectively. Haaland (1989) states that R^2 value should be at least 0.75 or higher to be acceptable and if the values above 0.90 are

preferable. Still, Joe F. Hair et al. (2011) mentions that R^2 values of 0.75, 0.50, and 0.25 can be defined as substantial, moderate, and weak as a rule of thumb.

Considering that all of the R^2 related values given in Table 5.18 are above 0.75 and referring to the abovementioned rule of thumb R^2 values, it is concluded that the derived equations well fit the data.

The range of raw data used in the derivation of the equations is given in Table 5.20.

Table 5.20. Validity Intervals of Each Equation

Material Type	**Crack Width Interval (mm)**	**Scanning Distance Interval (m)**	**Incidence Angle Interval (°)**
RC	2.98-10.89	3-10	0-45
Wood	2.04-5.81	3-10	0-45
Masonry Brick	5.7-12.2	3-10	0-45
Coated RC	2.94-10.80	3-10	0-45

The accuracy rate of the given equations for extrapolation may be low. To clarify this issue, additional data acquisition and analysis should be carried out for the cases lying outside the valid intervals. Nevertheless, for the observed cases, the error performances of the equations are visualized as follows:

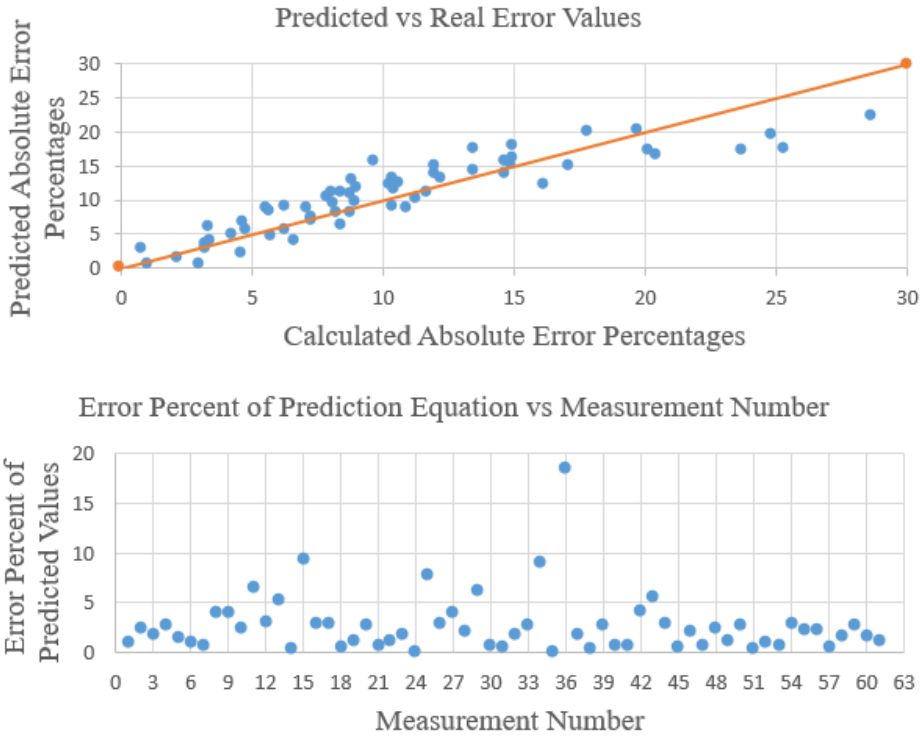

Figure 5.19. Error Performance of the Equation Derived (RC Specimen)

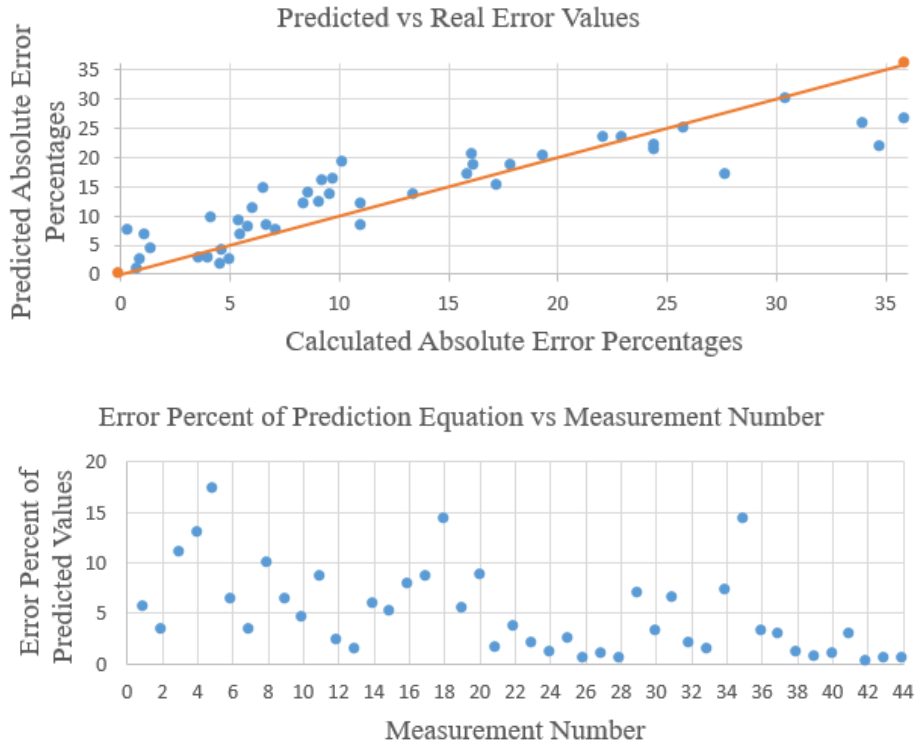

Figure 5.20. Error Performance of the Equation Derived (Wooden Specimen)

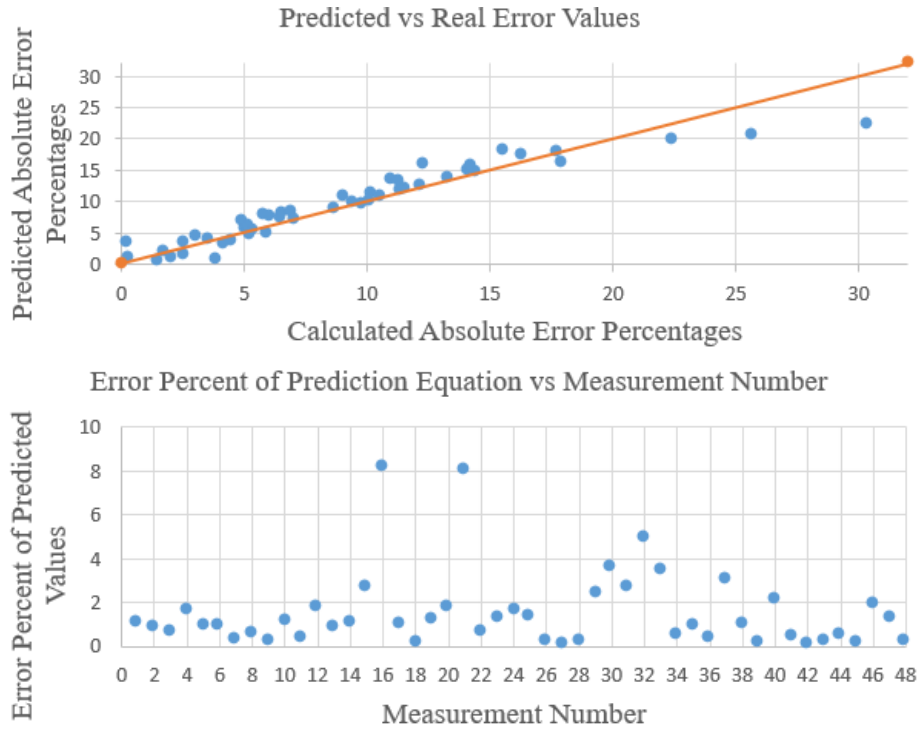

Figure 5.21. Error Performance of the Equation Derived (Masonry Brick Specimen)

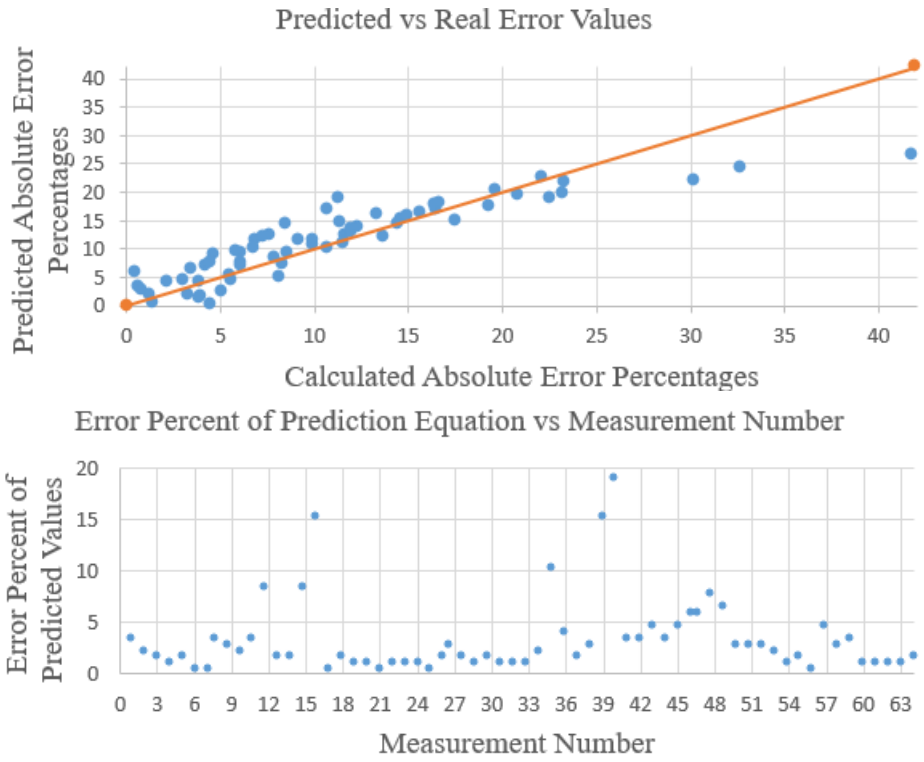

Figure 5.22. Error Performance of the Equation Derived (Coated RC Specimen)

Beyond the high error rates (20% - 25%), all the equations predict lower error rates than the actual measured values. This situation is thought to occur due to the existence of an inadequate number of measurements related to high error rates in our raw data. Moreover, it has been observed that the error percent of predicted values rises to 20% in all building materials except the masonry brick. For the masonry brick, these values appear to be around 10%. The smaller cracks in materials other than masonry brick cause a deviation from the linear trend of the *AEP* values. Thus, the equations derived based on the MLR become more erroneous. Even so, the above-given figures reveal that the 98.36%, 88.64%, 100%, and 95.31% of the values respectively for RC, wood, masonry brick, and plaster coated RC have less than 10% of prediction deviations. Thus, it is concluded that (except for few outliers), the derived equations operate with sufficient accuracy in error prediction (H6).

Furthermore, the data set is used to perform a significance test to understand the variables' significance and test the hypothesis. Biau et al. (2010) defines P-value as one of the most usually used statistical measures of indication against the null hypothesis. Hung et al. (1997) adds on the definition by mentioning that by itself, P-value is a uniform distribution between the interval [0, 1] under the null hypothesis. P-value's numerical value can give invaluable insights to the researchers (Biau et al., 2010). The smaller the P-value emerges as a reliable indicator to reject the null hypothesis. Moreover, a P-value of less than α=5% (i.e., 95% confidence interval) is accepted to be statistically significant (W. Zhu, 2016). Accordingly, α=5% (i.e., 95% confidence interval) is designated as the typical threshold of significance in the testing. Likewise, the P-values of each variable in the equations are used to quantify the observed results' statistical significance.

The following four tables show the P-values and confidence intervals corresponding to the variables in the derived equation of each building material type.

Table 5.21. P-Values and Confidence Intervals of RC

RC			
		Confidence Level	
Variable	**P-Value**	**Lower 95%**	**Upper 95%**
Intercept	0.003	1.39	6.56
Crack Width	7.24E-12	-1.32	-0.82
Scanning Distance	1.31E-16	1.35	1.91
Angle of Incidence	2.57E-10	0.12	0.21
ANOVA			
	Df	**F**	**P-Value**
Regression	3	79.1	2.65E-20
Residual	57		

Table 5.22. P-Values and Confidence Intervals of Wood

Wood			
		Confidence Level	
Variable	**P-Value**	**Lower 95%**	**Upper 95%**
Intercept	0.012	1.76	13.41
Crack Width	1.60E-08	-4.75	-2.63
Scanning Distance	1.43E-08	1.58	2.84
Angle of Incidence	7.98E-09	0.24	0.43
ANOVA			
	Df	**F**	**P-Value**
Regression	3	41.78	2.13E-12
Residual	40		

Table 5.23. P-Values and Confidence Intervals of Masonry Brick

Masonry Brick			
		Confidence Level	
Variable	**P-Value**	**Lower 95%**	**Upper 95%**
Intercept	0.311	-3.98	1.30
Crack Width	7.15E-07	-0.87	-0.42
Scanning Distance	3.91E-21	1.76	2.23
Angle of Incidence	2.14E-11	0.12	0.20
ANOVA			
	Df	**F**	**P-Value**
Regression	3	135.93	2.86E-22
Residual	44		

Table 5.24. P-Values and Confidence Intervals of Plaster Coated RC

Plaster Coated RC			
		Confidence Level	
Variable	**P-Value**	**Lower 95%**	**Upper 95%**
Intercept	2.309	6.75	13.79
Crack Width	1.02E-16	-2.22	-1.56
Scanning Distance	6.12E-11	1.10	1.84
Angle of Incidence	8.12E-07	0.10	0.21
ANOVA			
	Df	**F**	**P-Value**
Regression	3	74.77	3.01E-20
Residual	60		

Based on the fact that all of the P-values of crack width, scanning distance, and angle of incidence given in the tables are relatively small (almost zero), the null hypothesis (H_0) is rejected, and the research/alternative hypothesis (H_1) is accepted for each

material type (H6). Moreover, the same conclusion is observed to be drawn by the F-test using the F values in the Analysis of Variance (ANOVA) results.

CHAPTER 6

SUMMARY, CONTRIBUTIONS, AND FUTURE WORK

6.1 Introduction

Buildings are designed to be safer and more robust than before; however, they can still suffer much damage under the earthquake loads. Over the years, the necessity of the post-earthquake structural damage assessment, which aims (1) to identify structural damage type and severities, and (2) assess the buildings' serviceability, has been further understood.

To date, various methods have been used to assess structural damage of buildings. Some of these methods can be considered outdated, while others are still promising.

The oldest method, visual inspection, is a set of procedures in which manual inspection is conducted. In this method, experts who have advanced structural engineering knowledge, both academically and practically, are expected to reach the judiciary on buildings' current condition by visually inspecting the structural elements. This method is mostly criticized for being subjective, time-consuming, and error-prone. To overcome the drawbacks of this method, with the development of technology and modern tools, several alternative tools and methods have emerged (e.g., remote sensing, image-based, and laser technologies).

In recent years, a laser-based technology, TLS, has garnered great attention due to its high accuracy and reliability rates. Notably, its usage in post-earthquake structural damage identification and crack detection is still an unexplored study area. Therefore, an efficient base should be advanced in using Terrestrial Laser Scanners (TLSs).

The following sections discuss the summary, practical, empirical, and theoretical contributions of the research and suggested future research directions.

6.2 Summary and Lessons Learned

In this study, the main goal was to systematically analyze the measurement error rates in the three most common building materials' crack identification process by performing a series of scans via TLS. In this way, it is aimed to obtain information about the effects of different building materials on the scan data quality and accuracy, which are not yet mentioned in the previous studies. To perform the core experiments efficiently, and since the number of studies conducted on the post-earthquake structural crack identification is inadequate, several preliminary experiments have been carried out to determine the parameters affecting the scan data quality within the scope of this study. Hence, it can be concluded that the study proceeds in a learning curve and has emerged as a compilation of individual lessons.

To better understand which scan parameters affect the scan data quality and the extent of these effects, a cracked asphalt specimen was observed as the first case study. As the first lesson learned, (1), it was realized that marking the boundaries of the crack on the specimen with the help of chalk provided an absolute advantage during the analysis of the obtained scan data. This case study was carried out in two stages. In the first stage, the effects of three different scanning distances, two different scanning resolutions, three different angles of incidence, and two different sensitivity values on the scan data quality were observed. As a result of comparing the Absolute Error Percentages (*AEP*s) calculated for different scan settings, the second and third inferences were made: (2), angle of incidence significantly affects the scan data quality, and (3), scanning with the normal sensitivity setting shortens the scan durations. However, it causes measurement error even at relatively close distances up to 5 m. In the second stage, the same sample was re-scanned by differentiating the scan parameters considering that the normal sensitivity setting would not be sufficient for studies where the measurement accuracy is the priority.

Moreover, scanning distances should be increased to practically feasible values (i.e., higher than the ones observed in the first stage). As a result of the scans performed in this stage, the fourth and fifth conclusions were drawn, which are as follows: (4)

the scanning distance visibly affects calculated error rates, and (5) 15° angle of incidence should also be tested due to the existence of the remarkable difference between the calculated error rates of the scans at 0° and 30°. Although the conclusions mentioned above from the first case study are quite precious, as a new case study, it was envisaged to observe cracks having more certain widths with similar scan settings, since the width of the crack measured in the first case study varies along the crack line (i.e., crack width was not constant).

In the second case study, several crack types having different widths and orientations were simulated on a Foam Board. The goals were to verify the representativeness of the TLS for other Time-of-Flight (TOF) based TLSs before using it in the core experiments and to understand the effects of the scan parameters better. For this purpose, a study investigating subjects similar to this thesis' research topics, but conducted with a different TLS, was chosen to benchmark. In this case study, the effects of several scan parameters, including crack width, crack orientation, scanning distance, resolution, and sensitivity, were observed. The same scans with the selected study were re-performed, and corresponding AEP values were calculated based on the goals. During the calculations, (6) it was understood that the crack widths could not provide sufficient accuracy when measured only once, and therefore their values should be calculated by taking the average of the measurements repeated at least three times even in measuring relatively constant crack width profiles. Based on the findings, (7) it was discerned that if it is desired to measure surface deformations in crack width like small dimensions, the highest scanning resolution setting (e.g., 0.8 mm at 10 m) of the TLS should be used. Then, these values are compared to the ones obtained in the selected study. Based on the comparison, (8) it was observed that the error values calculated in both studies were approximately equal, and therefore it was concluded that possibly similar results would be obtained for different TLSs. Moreover, (9) it was noticed that the crack widths and the *AEP* values are negatively correlated. After exploring the effects of different scanning parameters on scan data quality and verifying that the TLS to be used is adjusted, the core experiments were

initiated to examine the effects of different building materials on the scan data quality, which is the main research focus of the study.

The core experiments were designed based on the lesson learned from the previous parts. Before conducting the experiments, two different methods, namely positioning methods, were used to provide the required incidence angle values. Following, the error performances of these methods were examined with identical test settings in two different testbeds. In this way, the claim that both methods reveal equally accurate results could be proved with numbers. Accordingly, the results of the tests have verified that. During the experiments for verification, (10) it is noted that 1 cm diameter of Black and White targets are too small to be identified even from 5 m range; therefore, it is concluded that larger ones should be used for farther distances. Subsequently, the three testbeds of the most commonly used building materials (e.g., RC, wood, and masonry brick) were prepared based on the suggested crack width intervals in the post-earthquake damage and safety assessment guidelines for each material type. These specimens were explored in Case Study-1,2 and 3, respectively, to interpret the effects of the target material types and other scan parameters on scan data quality and to define scan data quality as a function of these variables. For these purposes, a set of scan parameter settings was designed to be used in all case studies.

In the first case study, the concentration was on measuring the cracks in the RC specimen (10.89 mm, 6.92 mm, 5 mm, and 2.98 mm). The wooden sample with cracks of 5.81 mm, 4.02 mm, and 2.04 mm was examined in the second one. The cracks in the masonry brick specimen (12.2 mm, 8 mm, and 5.7 mm) were scanned several times in the third one. Subsequently, the *AEP* values of these cracks were calculated one by one. The calculated values for all crack widths belong to each material type were compared among themselves. After all, regardless of the material type, the above-given second and the fourth inferences were numerically verified. Likewise, the calculated *AEP* of the cracks having similar widths in each material type were compared pairwise, aiming to comprehend the scan data quality variations based on the material type.

Consequently, (11) it was concluded that wood's error performance is better than the others, while RC shows a better performance than the masonry brick. Based on the findings, it was decided to re-perform the scans for the RC specimen by covering its surface with satin plaster since (12) it was thought that smooth surfaces might reduce the calculated *AEP* values. Afterward, the satin plaster coated RC specimen was scanned, and its corresponding *AEP* values were calculated. Then, these values were compared to those calculated for the RC, and the hypothesis regarding smooth surfaces was verified.

Lastly, error estimation equations for building materials in the four case studies mentioned above were obtained by applying multiple linear regression analysis to each data set. Likewise, these equations' reliability was discussed through the visuals created based on the raw and estimated data values besides performing a significance test to understand the level of significance of the variables used in these equations and to test the proposed hypotheses in the regression analysis.

To sum up, some prominent findings of the study are as follows: (1) If the area of interest is marked, then the measurement accuracy is expected to increase, (2) If the primary purpose of a study is measurement accuracy, the highest possible scanning sensitivity setting should be preferred for data acquisition, (3) If a distance between two points in point cloud data is aimed to be measured by manual methods, a value closer to the ground truth should be obtained by taking an average of multiple measurements instead of one measurement, (4) If a Time of Flight TLS will be decided to be used in a study, the findings of this thesis study should be considered to estimate the scan data quality because the results are representative for these type of scanners, (5) If measurements are to be taken at distances of more than 5 m in a study, targets with a diameter of more than 1 cm should be used as a reference point, (6) Regardless of the target material type, the effects of the increase in incidence angles in the measurement of cracks larger than ~ 3 mm are at a minimal level up to 7 m, (7) Regardless of the scanning distance, the effects on scan data quality of the incidence angle increase from 30° to 45° are much remarkable than those of 15° to 30° and 0° to 15°.

Moreover, (8) If a length of ~3 mm on a reinforced concrete surface is to be measured in a study, scanning distance more than 7 m and angles greater than 45° should not be preferred because the relevant length becomes undetectable beyond these limits. The ones recommended for wooden surfaces as 10 m and 45°, (9) If a size of ~5 mm on a reinforced concrete surface is to be measured in a study, it is possible to obtain measurements with ~1 mm of error up to a scanning distance of 10 m for the incidence angle interval, 0°-45° except for 10 m 45° case. The same is valid for both wood and masonry brick. Still, the masonry brick has an additional exception of 10 m 30° case, (10) If a length of ~7 mm on a reinforced concrete surface is to be measured in a study, it is possible to obtain measurements with ~1 mm of error up to a scanning distance of 10 m for the incidence angle interval, 0°-45° except for 10 m 45° case. The same is valid for masonry brick with an additional exception of 10 m 30° case, (11) If a length of ~10 mm on a reinforced concrete surface is to be measured in a study, it is possible to obtain measurements with ~1 mm of error up to a scanning distance of 10 m for the incidence angle interval, 0°-45° except for 10 m 45° case. The same is valid for masonry brick with an additional exception of 10 m 30° case.

6.3 Contributions

This research tried to answer the following research questions:

- What are the salient parameters that affect scan data quality?
- What is the combined effect of several scan parameters on scan data quality?
- What is the effect of building material type on scan data quality?

As discussed in the previous section, experimental studies have been conducted in this context, and critical findings have been obtained. Based on these findings, all of the hypotheses given in Chapter 1 and proposed by considering the above-given research questions are accepted.

This thesis study's contributions can be examined from three perspectives: theoretical, empirical, and practical.

6.3.1 Theoretical Perspective

In literature, several studies concentrate on the geometric accuracy based on the effects of the color or reflection properties of different materials on the scan data quality (Derek D. Lichti & Harvey, 2002; Thomas Voegtle et al., 2008). Likewise, studies investigate the effects of different building materials on scan data quality obtained by TLSs (Hassan et al., 2017; Suchocki & Katzer, 2018; Yuan et al., 2020). In all of them, researchers have stated that the scan data's quality varies from material to material. While many of them provided these conclusions, they either obtained results based on observational data of one material type or conducted their studies in line with the focuses other than crack widths. Thus, although theoretical results have been obtained from the studies in this context, particular findings have not been fully supported by the numerical data, mainly from the perspective of earthquake-induced crack identification. In this sense, this study differentiates from the existing ones because its boundaries, methodological steps, and focus were fully defined, and its findings were based on numerical data besides the points mentioned above. The study supported the observations mentioned in theory with numerical data. Similarly, by numerically analyzing the measurement error rates regarding the post-earthquake cracks in different building materials, it helped to concretize the statements regarding the effects of different building materials on the scan data quality obtained by TLS.

6.3.2 Empirical Perspective

It is possible to come across studies investigating the scan parameters affecting the scan data quality and how effective these parameters are in literature (Boehler & Marbs, 2003; M. K. Kim et al., 2015; Thomas Voegtle et al., 2008; Zaimovic-Uzunovic & Lemes, 2010). In these studies, mostly focused on geometric quality

assessment, the effect of each parameter on scan data quality has been discussed separately. In contrast, this thesis has discussed the individual and combined effects of scan parameters on scan data quality. Furthermore, it is the first study to reveal the effects of different building materials on the error in crack identification and crack width measurement. The statement that the type of material affects the scan data quality has been addressed and tested based on surface reflectivity, roughness, and color in several studies (Clark & Robson, 2004; Godin et al., 2001). However, none have empirically investigated this inference for the analysis of post-earthquake cracks. In this regard, this thesis is the first experimental study to explain the effects of different building materials numerically.

6.3.3 Practical Perspective

As described in detail in the previous section, numerous scans have been carried out with different experimental setups designed considering the information mentioned in literature throughout the study. As a result, a comprehensive experimental study was carried out in which the theoretical knowledge mentioned in pieces from previous studies was tested in practice. In previous studies, laser scanning's main disadvantage has been heavily mentioned as it can be time-consuming and ineffective, depending on whether redundant data collection is performed or not (Tang & Alaswad, 2012; Cheng Zhang et al., 2016). For this reason, researchers have worked on methods to shorten scan durations. Thus, several studies aim to create and optimize the scanning plan, as it will save a considerable amount of time from obtaining scan data by performing the least number of scans. As it is essential to comprehend which scan parameters affect scan data quality and how much they affect it, the results of this study that answers these questions will be quite beneficial in practice. In other words, understanding the scan characteristics will undoubtedly facilitate scan plan optimization and shorten the scan durations.

Another result of the study that can be applied in practice is the derived equations to estimate the measurement error rates for different building materials. These

equations will help scan plan establishment in areas where the primary building material is one of those discussed in this study. The error rates to be obtained from the designed scan plan can be estimated with the help of equations, and accordingly, relevant revision can be made at the very first phases. In this way, the extra time and resource allocation can be prevented, the scan process can be expedited, and more refined scan data can be obtained.

6.4 Future Work

The following research directions are recommended to be explored in future studies:

- The experiments should be repeated with different TLSs than the one used in this study to verify that the calculated error values are equipment independent. Furthermore, measurement error rates due to multiple scans registration should be studied in future studies since, in this study, only single-point scan station data is used.
- In this study, only the performance of the elements constructed with a monotype material was evaluated, and findings were obtained accordingly. Moreover, there are other building materials such as steel and natural stone in which detecting cracks are also vital. Today, considering the demand for a transition to hybrid materials due to aesthetic concerns in construction, the research should be extended towards this direction in future studies. Furthermore, the performance of non-explored common building materials (i.e., other than the ones examined in this study) should be assessed by conducting experiments with the same methodology in order to concretize the findings.
- The experiments focused entirely on crack widths in this study. However, there are other prominent damage indicators, such as crack depths. Therefore, although crack depth assessment relies heavily on expert judgment and is expressed in practice by perceptions rather than numbers, future studies should investigate error trends regarding these damage indicators. Also,

although building materials without reflection problem were used in the experiments in the study, the effects of material-dependent variables such as surface roughness, color, and reflection characteristics were examined indirectly. Nevertheless, it is recommended to investigate the effect of building materials with reflection problems such as glass on scan data quality in future studies.

- In the MLR, the adjusted R-squared values were calculated as 0.8, except for the masonry brick. It means the confidence interval of the equations was 80%. The value is within acceptable limits, but a better error estimation model can be obtained by increasing this value. For this reason, in future studies, diversity and limits of scanning parameters should be increased, and error estimation equations should be optimized by managing more data. The derived error estimation equations have a distinct validity interval. Therefore, their accuracy rate for extrapolation may be low. To test this issue, additional data acquisition and analysis should be carried out for the cases lying outside the given validity intervals for each equation in future studies. Consequently, (1) the reliability of the derived error estimation equations should be tested by conducting additional experiments, and (2) the equations should be verified in real case studies, and the results should be compared with those of this study.
- The findings have revealed that errors occurred in the identification of cracks solely based on the TLS data. Therefore, it is envisaged that hybrid systems that use 2D and 3D photographic technologies, together with point cloud data, should be designed to attain more accurate results. Moreover, developing sets of novel algorithms to automate the crack identification, width based crack classification, and building material based error prediction in crack width measurement processes from point clouds is suggested to expedite the data processing step since the data processing was conducted in a semi-automated way, which was relatively time-consuming.

REFERENCES

Abdel-Qader, I., Abudayyeh, O., & Kelly, M. E. (2003). Analysis of edge-detection techniques for crack identification in bridges. *Journal of Computing in Civil Engineering*, *17*(4), 255–263. https://doi.org/10.1061/(ASCE)0887-3801(2003)17:4(255)

Adam-Carr, C. (2010). Nelson Science Perspectives 10. In *Nelson Science Perspectives 10*. Nelson Education.

Adams, S., Friedland, C., & Levitan, M. (2010). Unmanned Aerial Vehicle Data Acquisition for Damage Assessment in Hurricane Events. *8th International Workshop on Remote Sensing for Disaster Management, September 2014*, 1–7. http://www.enveng.titech.ac.jp/midorikawa/rsdm2010_pdf/13_adams_paper.pdf

Ahmed, F., Amir, M., & Anwar, N. (2018). Construction monitoring and reporting using drones and unmanned aerial vehicles (UAVs). *The Tenth International Conference on Construction in the 21st Century (CITC-10), July*, 1–8.

Ajmar, A., Boccardo, P., & Tonolo, F. G. (2011). Earthquake damage assessment based on remote sensing data. The Haiti case study. *Italian Journal of Remote Sensing / Rivista Italiana Di Telerilevamento*, *43*(2), 123–128. https://doi.org/10.5721/ItJRS20114329

Alkan, R. M., & Karsidag, G. (2012). Analysis of The Accuracy of Terrestrial Laser Scanning Measurements. *FIG Working Week 2012 - Knowing to Manage the Territory, Protect the Environment, Evaluate the Cultural Heritage, May 2012*, 16.

Alshawabkeh, Y., & Haala, N. (2004). Integration of digital photogrammetry and laser scanning for heritage documentation. *International Archives of the Photogrammetry, Remote Sensing and Spatial Information Sciences - ISPRS Archives*, *35*, 424–429.

Altan, O., Toz, G., Kulur, S., Seker, D., Volz, S., Fritsch, D., & Sester, M. (2001). Photogrammetry and geographic information systems for quick assessment, documentation and analysis of earthquakes. *ISPRS Journal of Photogrammetry and Remote Sensing*, *55*(5–6), 359–372. https://doi.org/10.1016/S0924-2716(01)00025-9

Anagnostopoulos, S. A., Moretti, M., Panoutsopoulou, M., Panagiotopoulou, D., & Thoma, T. (2004). *Post earthquake damage and usability assessment of buildings: Further development and applications. Final report*. 166. http://ec.europa.eu/echo/files/civil_protection/civil/act_prog_rep/peadab.pdf

Anil, E. B. (2015). *Utilization of As-is Building Information Models Obtained from Laser Scan Data for Evaluation of Earthquake Damaged Reinforced Concrete Buildings*.

Anil, E. B., & Akinci, B. (2013). *Characterization of Laser Scanners for Detecting Cracks for Post-Earthquake Damage Inspection*.

Anil, E. B., Akinci, B., & Huber, D. (2011). Representation requirements of as-is building information models generated from laser scanned point cloud data. In *Proceedings of the 28th International Symposium on Automation and Robotics in Construction, ISARC 2011* (pp. 355–360). https://doi.org/10.22260/isarc2011/0063

Applied Technology Council (ATC). (1989). *Procedures for postearthquake safety evaluation of buildings*.

Baggio, C., Bernardini, A., Colozza, R., Corazza, L., Bella, M., Di Pasquale, G., Dolce, M., Goretti, A., Martinelli, A., Orsini, G., Papa, F., & Zuccaro, G. (2007). Field Manual for post-earthquake damage and safety assessment and short term countermeasures (AeDES). *JRC Scientific and Thechnical Reports*, 1–100.

Barazzetti, L., & Scaioni, M. (2009). Crack measurement: Development, testing and applications of an automatic image-based algorithm. *ISPRS Journal of Photogrammetry and Remote Sensing*, *64*(3), 285–296. https://doi.org/10.1016/j.isprsjprs.2009.02.004

Becker, N. K., Ireland, D., Kennedy, N., Nathwani, R., Ross, B., & Teron, W. (2016). Structural Condition Assessments of Existing Buildings and Designated Structures Guideline. *Professional Engineers*. http://www.peo.on.ca/index.php/ci_id/31399/la_id/1.htm

Bendea, H., Boccardo, P., Dequal, S., Giulio Tonolo, F., Marenchino, D., & Piras, M. (2008). Low cost UAV for post-disaster assessment. *International Archives of the Photogrammetry, Remote Sensing and Spatial Information Sciences - ISPRS Archives*, *37*, 1373–1380.

Benz, H. M., Herman, M., Tarr, A. C., Hayes, G. P., Furlong, K. P., Villaseñor, A., Dart, R. L., Rhea, S., Papua, W., Sea, S., Sea, A., & Sea, C. (2010). Seismicity of the Earth 1900 – 2010. *Usgs*, *1311*, 170.

Bernardini, F., Rushmeier, H., Martin, I. M., Mittleman, J., & Taubin, G. (2002). Building a Digital Model of Michelangelo's Florentine Pieta. *IEEE Computer Graphics and Applications*, *22*(1), 59–67. https://doi.org/10.1109/38.974519

Biau, D. J., Jolles, B. M., & Porcher, R. (2010). P value and the theory of hypothesis testing: An explanation for new researchers. *Clinical Orthopaedics and Related Research*, *468*(3), 885–892. https://doi.org/10.1007/s11999-009-1164-4

Boehler, W., & Marbs, A. (2003). Investigating Laser Scanner Accuracy. *The International Archives of Photogrammetry Remote Sensing and Spatial Information Sciences*, *34*, 696–701. https://doi.org/10.1002/pbc.ABSTRACT

Bryan, H., Heng, W., Michael, L., Tim, R., Tamara, L., & Sarah, H. (2015). Feasibility Study of UAV use for RFID Material Tracking on Construction Sites. *51st ASC Annual International Conference Proceedings*, *1995*, 669–676.

Cheng, T., & Teizer, J. (2013). Real-time resource location data collection and visualization technology for construction safety and activity monitoring applications. *Automation in Construction*, *34*, 3–15. https://doi.org/10.1016/j.autcon.2012.10.017

Cheok, G. S., Lytle, A. M., & Saidi, K. S. (2006). Status of the NIST 3D imaging system performance evaluation facility. *Laser Radar Technology and Applications XI*, *6214*, 62140F. https://doi.org/10.1117/12.665833

Cheok, G. S., Saidi, K. S., & Scott, N. A. (2011). *Nist TN 1695*.

Chin, W. W. (1998). The partial least squares approach for structural equation modeling. *Modern Methods for Business Research*, *April*, 295–336.

Clark, J., & Robson, S. (2004). Accuracy of measurements made with a Cyrax 2500 laser scanner against surfaces of known colour. *Survey Review*, *37*(294), 626–638. https://doi.org/10.1179/sre.2004.37.294.626

Costa-Jover, A., Lluis i Ginovart, J., Coll-Pla, S., & López Piquer, M. (2019). Using the terrestrial laser scanner and simple methodologies for geometrically assessing complex masonry vaults. *Journal of Cultural Heritage*, *36*, 247–254. https://doi.org/10.1016/j.culher.2018.10.003

Dai, F., Rashidi, A., Brilakis, I., & Vela, P. (2013). Comparison of image-based and time-of-flight-based technologies for three-dimensional reconstruction of infrastructure. *Journal of Construction Engineering and Management*, *139*(1), 69–79. https://doi.org/10.1061/(ASCE)CO.1943-7862.0000565

Dandoulaki, M., Panoutsopoulou, M., & Ioannides, K. (1998). An overview of post-earthquake building inspection practices in Greece and the introduction of a rapid building usability evaluation procedure after the 1996 Konitsa earthquake. *11th Europe an Conferen Ce on Ear Thqua Ke Engin Eering*, *May*, 1–11. http://nisee.berkeley.edu/response/greece.pdf

Dominici, D., Alicandro, M., & Massimi, V. (2017). UAV photogrammetry in the post-earthquake scenario: case studies in L'Aquila. *Geomatics, Natural Hazards and Risk*, *8*(1), 87–103. https://doi.org/10.1080/19475705.2016.1176605

Donduren, M. S., & Kollu, M. S. (2018). DAMAGES AND CAUSES OF MASONRY BUILDINGS DURING EARTHQUAKES IN THE LAST 15 YEARS IN TURKEY. *Journal of Selcuk-Technic*, *17*(2), 59–66.

Ellenberg, A., Kontsos, A., Bartoli, I., & Pradhan, A. (2014). Masonry Crack Detection Application of an Unmanned Aerial Vehicle. *2014 International Conference on Computing in Civil and Building Engineering*, 1788–1795.

Ersöz, A. B. (2016). *Development of UAV-Based Pavement Crack Identificaiton System Using Artificial Intelligence* (Issue September).

Eschenasy, D. (2016). *Facade Conditions - An Illustrated Glossary of Visual Symptoms*. [PowerPoint Slides]. https://www1.nyc.gov/assets/buildings/images/content/misc/FacadePresentation.pdf

Farmer, M. C. (2004). Building Facade Maintenance, Repair, and Inspection. In *Building Facade Maintenance, Repair, and Inspection* (pp. 162–173). https://doi.org/10.1520/stp1444-eb

Federal Emergency Management Agency (FEMA). (2000). *New FEMA Study Estimates U.S. Losses From Earthquakes At $4.4 Billion Per Yearo Title*. https://www.fema.gov/news-release/2000/09/20/new-fema-study-estimates-us-losses-earthquakes-44-billion-year#

Forkuo, E. K., & King, B. (2004). Automatic fusion of photogrammetric imagery and laser scanner point clouds. *International Archives of the Photogrammetry, Remote Sensing and Spatial Information Sciences - ISPRS Archives*, *35*.

Fraser, C. S. (1998). Some thoughts on the emergence of digital close range photogrammetry. *Photogrammetric Record*, *16*(91), 37–50. https://doi.org/10.1111/0031-868X.00112

Fu, G. (2005). Inspection and monitoring techniques for bridges and civil structures. In *Inspection and Monitoring Techniques for Bridges and Civil Structures*. https://doi.org/10.1533/9781845690953

Gagg, C. R. (2014). Cement and concrete as an engineering material: An historic appraisal and case study analysis. *Engineering Failure Analysis*, *40*, 114–140. https://doi.org/10.1016/j.engfailanal.2014.02.004

Gavilán, M., Balcones, D., Marcos, O., Llorca, D. F., Sotelo, M. A., Parra, I., Ocaña, M., Aliseda, P., Yarza, P., & Amírola, A. (2011). Adaptive road crack detection system by pavement classification. *Sensors*, *11*(10), 9628–9657. https://doi.org/10.3390/s111009628

Gheisari, M., Irizarry, J., & N. Walker, B. (2014). UAS4SAFETY: The Potential of Unmanned Aerial Systems for Construction Safety Applications. *Construction Research Congress 2014*, *2008*, 140–149.

Godin, G., Beraldin, J., Rioux, M., Levoy, M., & Cournoyer, L. (2001). An assessment of laser range measurement of marble surfaces. *Proceedings of the 5th Conference on Optical 3-D Measurement Techniques. Vienna, Austria*, 49–56.

Golparvar-Fard, M., Bohn, J., Teizer, J., Savarese, S., & Peña-Mora, F. (2011). Evaluation of image-based modeling and laser scanning accuracy for emerging automated performance monitoring techniques. *Automation in Construction*, *20*(8), 1143–1155. https://doi.org/10.1016/j.autcon.2011.04.016

González-Aguilera, D., Gómez-Lahoz, J., & Sánchez, J. (2008). A new approach for structural monitoring of large dams with a three-dimensional laser scanner. *Sensors*, *8*(9), 5866–5883. https://doi.org/10.3390/s8095866

Graybeal, B. A., & Washer, G. (2015). *Reliability of Visual Inspection for Highway Bridges , Volume I : Final Report*. *March*.

Guldur Erkal, B., & Hajjar, J. F. (2017). Laser-based surface damage detection and quantification using predicted surface properties. *Automation in Construction*, *83*(August), 285–302. https://doi.org/10.1016/j.autcon.2017.08.004

Hair, Joe F., Ringle, C. M., & Sarstedt, M. (2011). PLS-SEM: Indeed a silver bullet. *Journal of Marketing Theory and Practice*, *19*(2), 139–152. https://doi.org/10.2753/MTP1069-6679190202

Hair, Joseph F., Black, W. C., Babin, B. J., & Anderson, R. E. (2017). Multivariate Data Analysis (MVDA). In *Pharmaceutical Quality by Design: A Practical Approach*. https://doi.org/10.1002/9781118895238.ch8

Hair, Joseph F., Ringle, C. M., & Sarstedt, M. (2013). Partial Least Squares Structural Equation Modeling: Rigorous Applications, Better Results and Higher Acceptance. *Long Range Planning*, *46*(1–2), 1–12. https://doi.org/10.1016/j.lrp.2013.01.001

Hassan, M. U., Akcamete-Gungor, A., & Meral, C. (2017). *Investigation of Terrestrial Laser Scanning Reflectance Intensity and RGB Distributions to Assist Construction Material Identification*. *July*, 507–515. https://doi.org/10.24928/jc3-2017/0312

Hirosawa, M., Sugano, S., & Kaminosono, T. (1994). *Seismic evaluation method and restoration techniques for existing and damaged buildings developed in Japan.*

Hung, H. M. J., O'Neill, R. T., Bauer, P., & Kohne, K. (1997). The Behavior of the P-Value When the Alternative Hypothesis is True. *Biometrics*, *53*(1), 11. https://doi.org/10.2307/2533093

Hutchinson, T. C., & Chen, Z. (2010). Image-based framework for concrete surface crack monitoring and quantification. *Advances in Civil Engineering*, *2010*. https://doi.org/10.1155/2010/215295

Indirabai, I., Nair, M. V. H., Jaishanker, R. N., & Nidamanuri, R. R. (2019). Terrestrial laser scanner based 3D reconstruction of trees and retrieval of leaf area index in a forest environment. *Ecological Informatics*, *53*(December 2018), 100986. https://doi.org/10.1016/j.ecoinf.2019.100986

Irizarry, J., Gheisari, M., & Walker, B. N. (2012). Usability assessment of drone technology as safety inspection tools. *Electronic Journal of Information Technology in Construction*, *17*(September), 194–212.

Japan Council for Quick Inspection of Earthquake Damaged Buildings, J. C. for Q. I. of E. D. B. (2002). *Postearthquake Quick Inspection of Damaged Buildings*.

Kaasalainen, S., Jaakkola, A., Kaasalainen, M., Krooks, A., & Kukko, A. (2011). Analysis of incidence angle and distance effects on terrestrial laser scanner intensity: Search for correction methods. *Remote Sensing*, *3*(10), 2207–2221. https://doi.org/10.3390/rs3102207

Kaasalainen, S., Niittymäki, H., Krooks, A., Koch, K., Kaartinen, H., Vain, A., & Hyyppä, H. (2010). Effect of target moisture on laser scanner intensity. *IEEE Transactions on Geoscience and Remote Sensing*, *48*(4 PART 2), 2128–2136. https://doi.org/10.1109/TGRS.2009.2036841

Kashani, A. G., Crawford, P. S., Biswas, S. K., Graettinger, A. J., & Grau, D. (2015). Automated Tornado Damage Assessment and Wind Speed Estimation Based on Terrestrial Laser Scanning. *Journal of Computing in Civil Engineering*, *29*(3), 04014051. https://doi.org/10.1061/(asce)cp.1943-5487.0000389

Kashani, A. G., & Graettinger, A. J. (2015). Cluster-Based Roof Covering Damage Detection in Ground-Based Lidar Data. *Automation in Construction*, *58*, 19–27. https://doi.org/10.1016/j.autcon.2015.07.007

Kempton, J., Nichol, S., Anumba, C., & Dickens, J. (2001). Surveyor variability in large-scale house condition surveys. *Structural Survey*, *19*(4), 156–162. https://doi.org/10.1108/02630800110406658

Kerle, N. (2015). Disasters: Risk Assessment, Management, and Post-Disaster Studies Using Remote Sensing. In *Remote Sensing of Water Resources, Disasters, and Urban Studies* (Issue October 2015, pp. 455–482). https://doi.org/10.1201/b19321-39

Kerle, N., Nex, F., Gerke, M., Duarte, D., & Vetrivel, A. (2019). UAV-based structural damage mapping: A review. *ISPRS International Journal of Geo-Information*, *9*(1), 1–23. https://doi.org/10.3390/ijgi9010014

Kersbergen, D. (2018). *Automated Building Damage Classification using Remotely Sensed Data Case study: Hurricane Damage on St. Maarten*. Delft University of Technology.

Kersten, T, Mechelke, K., Lindstaedt, M., & Sternberg, H. (2008). Geometric accuracy investigations of the latest terrestrial laser scanning systems. *FIG Working Week*, *June*, 1–16. http://fig.net/pub/fig2008/papers/ts02d/ts02d_01_mechelke_etal_2785.pdf

Kersten, TP. (2005). Investigations into the accuracy behaviour of the terrestrial laser scanning system Mensi GS100. *Proceedings of 7th Conference in Optical 3D Measurement Techniques, I*, 122–131. http://archive.cyark.orarchive.cyark.org/temp/hcuhamburgkerstenetal2005.pdf

Kim, H., Sim, S. H., & Cho, S. (2015). Unmanned aerial vehicle (UAV)-powered concrete crack detection based on digital image processing. *International Conference on Advances in Experimental Structural Engineering*, *2015-Augus*.

Kim, Hyunjun, Lee, J., Ahn, E., Cho, S., Shin, M., & Sim, S. H. (2017). Concrete crack identification using a UAV incorporating hybrid image processing. *Sensors (Switzerland)*, *17*(9), 1–14. https://doi.org/10.3390/s17092052

Kim, M. K., Sohn, H., & Chang, C. C. (2014). Automated dimensional quality assessment of precast concrete panels using terrestrial laser scanning. *Automation in Construction*, *45*, 163–177. https://doi.org/10.1016/j.autcon.2014.05.015

Kim, M. K., Sohn, H., & Chang, C. C. (2015). Localization and Quantification of Concrete Spalling Defects Using Terrestrial Laser Scanning. *Journal of Computing in Civil Engineering*, *29*(6), 1–12. https://doi.org/10.1061/(ASCE)CP.1943-5487.0000415

Kim, M. K., Wang, Q., & Li, H. (2019). Non-contact sensing based geometric quality assessment of buildings and civil structures: A review. In *Automation in Construction* (Vol. 100, pp. 163–179). Elsevier B.V. https://doi.org/10.1016/j.autcon.2019.01.002

Kim, S. W., & Kim, N. S. (2011). Multi-point displacement response measurement of civil infrastructures using digital image processing. *Procedia Engineering*, *14*, 195–203. https://doi.org/10.1016/j.proeng.2011.07.023

Koch, C., Paal, S., Rashidi, A., Zhu, Z., König, M., & Brilakis, I. (2014). Achievements and challenges in machine vision-based inspection of large concrete structures. *Advances in Structural Engineering*, *17*(3), 303–318. https://doi.org/10.1260/1369-4332.17.3.303

Laefer, D. F., Gannon, J., & Deely, E. (2010). Reliability of crack detection methods for baseline condition assessments. *Journal of Infrastructure Systems*, *16*(2), 129–137. https://doi.org/10.1061/(ASCE)1076-0342(2010)16:2(129)

LeBoeuf, R. A., & Shafir, E. (2006). The long and short of it: Physical anchoring effects. *Journal of Behavioral Decision Making*, *19*(4), 393–406. https://doi.org/10.1002/bdm.535

Lee, J., Son, H., Kim, C., & Kim, C. (2013). Skeleton-based 3D reconstruction of as-built pipelines from laser-scan data. *Automation in Construction*, *35*, 199–207. https://doi.org/10.1016/j.autcon.2013.05.009

Leica Geosystems AG. (2017). *Leica ScanStation P30 / P40 Because every detail matters*. 2.

Leica Geosystems AG. (2018). *Leica ScanStation P50/P40/P30 User Manual*. 1–66. https://surveyequipment.com/assets/index/download/id/457/

Liang, X., Hyyppä, J., Kaartinen, H., Lehtomäki, M., Pyörälä, J., Pfeifer, N., Holopainen, M., Brolly, G., Francesco, P., Hackenberg, J., Huang, H., Jo, H. W., Katoh, M., Liu, L., Mokroš, M., Morel, J., Olofsson, K., Poveda-Lopez, J., Trochta, J., … Wang, Y. (2018). International benchmarking of terrestrial laser scanning approaches for forest inventories. *ISPRS Journal of Photogrammetry and Remote Sensing*, *144*(December 2017), 137–179. https://doi.org/10.1016/j.isprsjprs.2018.06.021

Lichti, D D, Stewart, M. P., Tsakiri, M., & Snow, A. J. (2000). Calibration and Testing of a Terrstrial Laser Scanner. *Int. Arch. of Photogrammetry and Remote Sensing*, *33*(Part B5), 485–492.

Lichti, Derek D., & Harvey, B. . (2002). The Effects of Reflecting Surface Material Properties on Time-of-Flight Laser Scanner Measurements. *Geospatial Theory, Processing and Applications*, *2001*.

Liu, P., Chen, A. Y., Huang, Y. N., Han, J. Y., Lai, J. S., Kang, S. C., Wu, T. H., Wen, M. C., & Tsai, M. H. (2014). A review of rotorcraft unmanned aerial vehicle (UAV) developments and applications in civil engineering. *Smart Structures and Systems*, *13*(6), 1065–1094. https://doi.org/10.12989/sss.2014.13.6.1065

Lizundia, B., Durphy, S., Griffin, M., Hortacsu, A., Kehoe, B., Porter, K., & Welliver, B. (2014). Rapid visual screening of buildings for potential seismic hazards: FEMA 154 and FEMA 155 updates. *NCEE 2014 - 10th U.S. National Conference on Earthquake Engineering: Frontiers of Earthquake Engineering*, *January*. https://doi.org/10.4231/D3M90238V

Maeda, M., Matsukawa, K., & Ito, Y. (2014). Revision of guideline for post-earthquake damage evaluation of RC buildings In Japan. *NCEE 2014 - 10th U.S. National Conference on Earthquake Engineering: Frontiers of Earthquake Engineering*. https://doi.org/10.4231/D3959C81P

Maffei, J., Comartin, C. D., Kehoe, B., Kingsley, G. R., & Lizundia, B. (2000). Evaluation of Earthquake-Damaged Concrete and Masonry Wall Buildings. *Earthquake Spectra*, *16*(1), 263–283. https://doi.org/10.1193/1.1586111

Mancini, F., Dubbini, M., Gattelli, M., Stecchi, F., Fabbri, S., & Gabbianelli, G. (2013). Using unmanned aerial vehicles (UAV) for high-resolution reconstruction of topography: The structure from motion approach on coastal environments. *Remote Sensing*, *5*(12), 6880–6898. https://doi.org/10.3390/rs5126880

Mandriota, C., Nitti, M., Ancona, N., Stella, E., & Distante, A. (2004). Filter-based feature selection for rail defect detection. *Machine Vision and Applications*, *15*(4), 179–185. https://doi.org/10.1007/s00138-004-0148-3

Marks, E. D., Cheng, T., & Teizer, J. (2013). Laser Scanning for Safe Equipment Design That Increases Operator Visibility by Measuring Blind Spots. *Journal of Construction Engineering and Management*, *139*(8), 1006–1014. https://doi.org/10.1061/(asce)co.1943-7862.0000690

Meier, P., & Soesilo, D. (2015). Using Drones for Disaster Damage Assessments in Vanuatu. *Drones in Humanitarian Action*, *10*(10), 5. http://delair.aero/wp-content/uploads/2017/05/CASE_STUDY_Using-Drones-for-Disaster-Damage-Assessments.pdf

Menches, C. L., Markman, A. B., & Jones, R. J. (2008). Innovative method for investigating the facility damage assessment process. *Proceedings of the AEI 2008 Conference - AEI 2008: Building Integration Solutions*, *328*, 1–10. https://doi.org/10.1061/41002(328)53

Mitomi, H., Saita, J., Matsuoka, M., & Yamazaki, F. (2001). Automated damage detection of buildings from aerial television images of the 2001 Gujarat, India earthquake. *International Geoscience and Remote Sensing Symposium (IGARSS)*, *1*(May 2014), 147–149. https://doi.org/10.1109/igarss.2001.976085

Monserrat, O., & Crosetto, M. (2008). Deformation measurement using terrestrial laser scanning data and least squares 3D surface matching. *ISPRS Journal of Photogrammetry and Remote Sensing*, *63*(1), 142–154. https://doi.org/10.1016/j.isprsjprs.2007.07.008

Moore, E. (2018). *Practical Considerations for Façade Inspections*.

Moore, G. K. (1979). What is a picture worth? a history of remote sensing. *Hydrological Sciences Bulletin*, *24*(4), 477–485. https://doi.org/10.1080/02626667909491887

Motawa, I., & Kardakou, A. (2018). Unmanned aerial vehicles (UAVs) for inspection in construction and building industry. *16th International Operation & Maintenance Conference (OMAINTEC 2018), 18-20th November 2018, Cairo, Egypt.*, *November*, 18–20.

Nakano, Y., Maeda, M., Kuramoto, H., & Murakami, M. (2004). Guideline for post-earthquake damage evaluation and rehabilitation of RC buildings in Japan. *13th World Conference on Earthquake Engineering*, *124*, 15.

Nisser, T., & Westin, C. (2006). Human factors challenges in unmanned aerial vehicles (uavs): A literature review. *School of Aviation of the Lund University, Ljungbyhed*. http://www.lusa.lu.se/upload/Trafikflyghogskolan/HumanFactorsChallengesUnmannedAerialVehicles.pdf

Obradović, R., Vasiljević, I., Kovačević, D., Marinković, Z., & Farkas, R. (2019). Drone Aided Inspection during Bridge Construction. *2019 Zooming Innovation in Consumer Technologies Conference, ZINC 2019*, 1–4. https://doi.org/10.1109/ZINC.2019.8769345

Olsen, M. J., Kuester, F., Chang, B. J., & Hutchinson, T. C. (2010). Terrestrial laser scanning-based structural damage assessment. *Journal of Computing in Civil Engineering*, *24*(3), 264–272. https://doi.org/10.1061/(ASCE)CP.1943-5487.0000028

Oskouie, P., Becerik-Gerber, B., & Soibelman, L. (2016). Automated measurement of highway retaining wall displacements using terrestrial laser scanners. *Automation in Construction*, *65*, 86–101. https://doi.org/10.1016/j.autcon.2015.12.023

Park, H. S., Lee, H. M., Adeli, H., & Lee, I. (2007). A new approach for health monitoring of structures: Terrestrial laser scanning. *Computer-Aided Civil and Infrastructure Engineering*, *22*(1), 19–30. https://doi.org/10.1111/j.1467-8667.2006.00466.x

Pfeifer, N., Dorninger, P., Haring, A., & Fan, H. (2007). Investigating terrestrial laser scanning intensity data: Quality and functional relations. *8th Conference on Optical 3-D Measurement Techniques, March 2014*, 328–337.

Phillips, S., & Narasimhan, S. (2019). Automating Data Collection for Robotic Bridge Inspections. *Journal of Bridge Engineering*, *24*(8), 1–13. https://doi.org/10.1061/(ASCE)BE.1943-5592.0001442

Puri, N., & Turkan, Y. (2020). Bridge construction progress monitoring using lidar and 4D design models. *Automation in Construction*, *109*(September 2019), 102961. https://doi.org/10.1016/j.autcon.2019.102961

Ramage, M. H., Burridge, H., Busse-Wicher, M., Fereday, G., Reynolds, T., Shah, D. U., Wu, G., Yu, L., Fleming, P., Densley-Tingley, D., Allwood, J., Dupree, P., Linden, P. F., & Scherman, O. (2017). The wood from the trees: The use of timber in construction. *Renewable and Sustainable Energy Reviews*, *68*(October 2015), 333–359. https://doi.org/10.1016/j.rser.2016.09.107

Rens, K. L., Wipf, T. J., & Klaiber, F. W. (1997). Review of nondestructive evaluation techniques of civil infrastructure. *Journal of Performance of Constructed Facilities*, *11*(4), 152–160. https://doi.org/10.1061/(ASCE)0887-3828(1997)11:4(152)

Reshetyuk, Y. (2006). Investigation of the influence of surface reflectance on the measurements with the terrestrial laser scanner Leica HDS 3000. *ZFV - Zeitschrift Fur Geodasie, Geoinformation Und Landmanagement*, *131*(2), 96–103.

Rönnholm, P., Honkavaara, E., Litkey, P., Hyyppä, H., & Hyyppä, J. (2007). Integration of Laser Scanning and Photogrammetry. *Iaprs*, *XXXVI*(Sep.), 355–362.

Safa, M., Shahi, A., Nahangi, M., Haas, C., & Noori, H. (2015). Automating measurement process to improve quality management for piping fabrication. *Structures*, *3*, 71–80. https://doi.org/10.1016/j.istruc.2015.03.003

Salvatore Cafiso, A. D. G., & Battiato, S. (2006). Evaluation of Pavement Surface Distress Using Digital Image Collection and Analysis. *Seventh International Congress on Advances in Civil Engineering. Istanbul, Turkey, January*, 1–10. http://iplab.dmi.unict.it/download/Elenco Pubblicazioni (PDF)/International Conferences/IC50 ACE 2006 Pavement.pdf

San José Alonso, J. I., Martínez Rubio, J., Fernández Martín, J. J., & García Fernández, J. (2012). Comparing Time-of-Flight and Phase-Shift. the Survey of the Royal Pantheon in the Basilica of San Isidoro (León). *ISPRS - International Archives of the Photogrammetry, Remote Sensing and Spatial Information Sciences*, *XXXVIII-5/*(October 2015), 377–385. https://doi.org/10.5194/isprsarchives-xxxviii-5-w16-377-2011

Sankarasrinivasan, S., Balasubramanian, E., Karthik, K., Chandrasekar, U., & Gupta, R. (2015). Health Monitoring of Civil Structures with Integrated UAV and Image Processing System. *Procedia Computer Science*, *54*, 508–515. https://doi.org/10.1016/j.procs.2015.06.058

Schabowicz, K. (2019). Non-destructive testing of materials in civil engineering. *Materials*, *12*(19), 1–13. https://doi.org/10.3390/ma12193237

Sepasgozar, S. M. E., Wang, C. C., & Shirowzhan, S. (2016). Challenges and opportunities for implementation of laser scanners in building construction. *ISARC 2016 - 33rd International Symposium on Automation and Robotics in Construction, June 2018*, 742–751. https://doi.org/10.22260/isarc2016/0090

Shanmugamani, R., Sadique, M., & Ramamoorthy, B. (2015). Detection and classification of surface defects of gun barrels using computer vision and machine learning. *Measurement: Journal of the International Measurement Confederation*, *60*, 222–230. https://doi.org/10.1016/j.measurement.2014.10.009

Sharma, A., & Mehta, N. (2016). Structural Health Monitoring Using Image Processing Techniques-A Review. *International Journal of Modern Computer Science*, *4*(4), 2320–7868. http://ijmcs.info/current_issue/IJMCS160832.pdf

Shi, Z., & Ergan, S. (2019). Leveraging Point Cloud Data for Detecting Building Façade Deteriorations Caused by Neighboring Construction. *Tamap Journal of Engineering*, *2018*(DOB 2018). https://doi.org/10.29371/2018.3.66

Shih, N. J., Wang, H. J., Lin, C. Y., & Liau, C. Y. (2007). 3D scan for the digital preservation of a historical temple in Taiwan. *Advances in Engineering Software*, *38*(7), 501–512. https://doi.org/10.1016/j.advengsoft.2006.09.014

Son, H., & Kim, C. (2016). Automatic segmentation and 3D modeling of pipelines into constituent parts from laser-scan data of the built environment. *Automation in Construction*, *68*, 203–211. https://doi.org/10.1016/j.autcon.2016.05.010

Son, H., Kim, C., & Kim, C. (2015). Fully Automated As-Built 3D Pipeline Extraction Method from Laser-Scanned Data Based on Curvature Computation. *Journal of Computing in Civil Engineering*, *29*(4), 1–9. https://doi.org/10.1061/(asce)cp.1943-5487.0000401

Soudarissanane, S., Van Ree, J., Bucksch, A., & Roderik, L. (2007). Error budget of terrestrial laser scanning: infuence of the incidence angle on the scan quality. *3D-NordOst*, 1–8.

Spencer, B. F., Hoskere, V., & Narazaki, Y. (2019). Advances in Computer Vision-Based Civil Infrastructure Inspection and Monitoring. *Engineering*, *5*(2), 199–222. https://doi.org/10.1016/j.eng.2018.11.030

Suchocki, C. (2020). Comparison of time-of-flight and phase-shift TLS intensity data for the diagnostics measurements of buildings. *Materials*, *13*(2). https://doi.org/10.3390/ma13020353

Suchocki, C., & Katzer, J. (2018). TLS Technology in Brick Walls Inspection. *Proceedings - 2018 Baltic Geodetic Congress, BGC-Geomatics 2018*, 359–363. https://doi.org/10.1109/BGC-Geomatics.2018.00074

Sunohara, H. (2018). *Post-earthquake building damage assessment and new technologies in Japan*.

Tang, P., & Alaswad, F. S. (2012). *Sensor Modeling of Laser Scanners for Automated Scan Planning on Construction Jobsites*. 1021–1031. https://doi.org/10.1061/9780784412329.103

Teizer, J., Allread, B. S., & Mantripragada, U. (2010). Automating the blind spot measurement of construction equipment. *Automation in Construction*, *19*(4), 491–501. https://doi.org/10.1016/j.autcon.2009.12.012

Terabee. (2019). *Time of flight Principle*. https://www.terabee.com/time-of-flight-principle/

Teza, G., Galgaro, A., & Moro, F. (2009). Contactless recognition of concrete surface damage from laser scanning and curvature computation. *NDT and E International*, *42*(4), 240–249. https://doi.org/10.1016/j.ndteint.2008.10.009

The Applied Technology Council, T. A. T. C. (1998). *Evaluation of earthquake damaged concrete and masonry wall buildings. basic procedures manual. Applied Technology Council, Federal Emergency Management Agency (FEMA)*.

Torok, M. M., Golparvar-Fard, M., & Kochersberger, K. B. (2014). Image-based automated 3D crack detection for post-disaster building assessment. *Journal of Computing in Civil Engineering*, *28*(5), 1–13. https://doi.org/10.1061/(ASCE)CP.1943-5487.0000334

Tsakiri, M, Lichti, D., & Pfeifer, N. (2006). Terrestrial Laser Scanning For Deformation Monitoring. *3rd IAG / 12th FIG Symposium, Baden, May 22-24*, 1–10. https://doi.org/10.3305/nh.2014.30.1.7485

Tsakiri, Maria, Ioannidis, C., & Carty, A. (2002). *Laser Scanning Issues for the Geometrical Recording of a Complex Statue*. 1–8.

Turkan, Y., Bosche, F., Haas, C. T., & Haas, R. (2011). Automated progress tracking of erection of concrete structures. *Proceedings, Annual Conference - Canadian Society for Civil Engineering*, *4*, 2746–2756.

U.S. Geological Survey. (2006). Earthquake hazards: a national threat. *Fact Sheet*, 2. https://doi.org/10.3133/fs20063016

Union of Chambers of Turkish Engineers and Architects, U. of C. of T. E. and A. (2016). *Depremin Etkiledigi Betonarme ve Yıgma Binalarda Hasar Tespiti*.

United States Geology Survey (USGS). (n.d.). *Earthquake Lists, Maps, and Statistics*. Retrieved December 1, 2020, from https://www.usgs.gov/natural-hazards/earthquake-hazards/lists-maps-and-statistics

Valero, E., Adán, A., & Bosché, F. (2016). Semantic 3D Reconstruction of Furnished Interiors Using Laser Scanning and RFID Technology. *Journal of Computing in Civil Engineering*, *30*(4), 04015053. https://doi.org/10.1061/(asce)cp.1943-5487.0000525

Voegtle, T, & Wakaluk, S. (2009). Effects on the Measurements of the Terrestrial Laser Scanner HDS 6000 (Leica) caused by Different Object Materials. *IAPRS, Vol. XXXVIII Part 3/W8*, *XXXVIII*(2003), 68–74.

Voegtle, Thomas, Schwab, I., & Landes, T. (2008). Influences of different materials on the measurements of a terrestrial laser scanner (TLS). *International Archives of the Photogrammetry, Remote Sensing and Spatial Information Sciences*, *XXXVII*(B5), 1061–1066.

Wang, P., Li, R., Bu, G., & Zhao, R. (2019). Automated low-cost terrestrial laser scanner for measuring diameters at breast height and heights of plantation trees. *PLoS ONE*, *14*(1), 1–26. https://doi.org/10.1371/journal.pone.0209888

Wang, Q., & Kim, M. K. (2019a). Applications of 3D point cloud data in the construction industry: A fifteen-year review from 2004 to 2018. *Advanced Engineering Informatics*, *39*(September 2018), 306–319. https://doi.org/10.1016/j.aei.2019.02.007

Wang, Q., & Kim, M. K. (2019b). Applications of 3D point cloud data in the construction industry: A fifteen-year review from 2004 to 2018. *Advanced Engineering Informatics*, *39*(September 2018), 306–319. https://doi.org/10.1016/j.aei.2019.02.007

Wang, Q., Kim, M. K., Cheng, J. C. P., & Sohn, H. (2016). Automated quality assessment of precast concrete elements with geometry irregularities using terrestrial laser scanning. *Automation in Construction*, *68*, 170–182. https://doi.org/10.1016/j.autcon.2016.03.014

Wang, Q., Sohn, H., & Cheng, J. C. P. (2016). Development of a mixed pixel filter for improved dimension estimation using AMCW laser scanner. *ISPRS Journal of Photogrammetry and Remote Sensing*, *119*, 246–258. https://doi.org/10.1016/j.isprsjprs.2016.06.004

Wilkinson, M. W., Jones, R. R., Woods, C. E., Gilment, S. R., McCaffrey, K. J. W., Kokkalas, S., & Long, J. J. (2016). A comparison of terrestrial laser scanning and structure-frommotion photogrammetry as methods for digital outcrop acquisition. *Geosphere*, *12*(6), 1865–1880. https://doi.org/10.1130/GES01342.1

Xiong, X., Adan, A., Akinci, B., & Huber, D. (2013). Automatic creation of semantically rich 3D building models from laser scanner data. *Automation in Construction*, *31*, 325–337. https://doi.org/10.1016/j.autcon.2012.10.006

Yamaguchi, T., & Hashimoto, S. (2010). Fast crack detection method for large-size concrete surface images using percolation-based image processing. *Machine Vision and Applications*, *21*(5), 797–809. https://doi.org/10.1007/s00138-009-0189-8

Yamaguchi, T., Nakamura, S., Saegusa, R., & Hashimoto, S. (2008). Image-based crack detection for real concrete surfaces. *IEEJ Transactions on Electrical and Electronic Engineering*, *3*(1), 128–135. https://doi.org/10.1002/tee.20244

Ye, X. W., Dong, C. Z., & Liu, T. (2016). A Review of Machine Vision-Based Structural Health Monitoring: Methodologies and Applications. *Journal of Sensors*, *2016*. https://doi.org/10.1155/2016/7103039

Yokoyama, H., Date, H., Kanai, S., & Takeda, H. (2010). Automatic 3D modelling of indoor Manhattan-world scenes from laser data. *International Archives of the Photogrammetry, Remote Sensing and Spatial Information Sciences - ISPRS Archives*, *38*(5W12), 115–120. https://doi.org/10.5194/isprsarchives-XXXVIII-5-W12-115-2011

Yon, B., Sayin, E., & Onat, O. (2017). Earthquakes and Structural Damages. In *Earthquakes - Tectonics, Hazard and Risk Mitigation* (pp. 319–339). https://doi.org/http://dx.doi.org/10.5772/57353

Yu, S. N., Jang, J. H., & Han, C. S. (2007). Auto inspection system using a mobile robot for detecting concrete cracks in a tunnel. *Automation in Construction*, *16*(3), 255–261. https://doi.org/10.1016/j.autcon.2006.05.003

Yuan, L., Guo, J., & Wang, Q. (2020). Automatic classification of common building materials from 3D terrestrial laser scan data. *Automation in Construction*, *110*(November 2019), 103017. https://doi.org/10.1016/j.autcon.2019.103017

Zaimovic-Uzunovic, N., & Lemes, S. (2010). Influences of surface parameters on laser 3D scanning. *10th International Symposium on Measurement and Quality Control 2010, ISMQC 2010*, *September 2010*, 408–411.

Zhang, Cheng, Kalasapudi, V. S., & Tang, P. (2016). Rapid data quality oriented laser scan planning for dynamic construction environments. *Advanced Engineering Informatics*, *30*(2), 218–232. https://doi.org/10.1016/j.aei.2016.03.004

Zhang, Chengyi, & Arditi, D. (2013). Automated progress control using laser scanning technology. *Automation in Construction*, *36*, 108–116. https://doi.org/10.1016/j.autcon.2013.08.012

Zheng, P. (2014). *Crack Detection and Measurement Utilizing Image-Based Reconstruction*. 1–41. https://vtechworks.lib.vt.edu/bitstream/handle/10919/48963/crack_detection_and_measurement_utilizing_image_based_reconstruction.pdf?sequence=1

Zhou, Z., Gong, J., & Guo, M. (2016). Image-Based 3D Reconstruction for Posthurricane Residential Building Damage Assessment. *Journal of Computing in Civil Engineering*, *30*(2), 04015015. https://doi.org/10.1061/(asce)cp.1943-5487.0000480

Zhu, W. (2016). P < 0.05, < 0.01, < 0.001, < 0.0001, < 0.00001, < 0.000001, or t... *Journal of Sport and Health Science*, *5*(1), 77–79. https://doi.org/10.1016/j.jshs.2016.01.019

Zhu, Z., German, S., & Brilakis, I. (2011). Visual retrieval of concrete crack properties for automated post-earthquake structural safety evaluation. *Automation in Construction*, *20*(7), 874–883. https://doi.org/10.1016/j.autcon.2011.03.004

Zulkipli, M. A., & Tahar, K. N. (2018). Multirotor UAV-Based Photogrammetric Mapping for Road Design. *International Journal of Optics*, *2018*. https://doi.org/10.1155/2018/1871058